SKRIFTER NR. 169

Results from Norwegian Antarctic Research 1974–1977

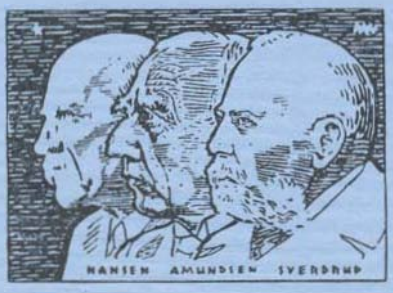

NORSK POLARINSTITUTT
OSLO 1978

DET KONGELIGE DEPARTEMENT FOR INDUSTRI OG HÅNDVERK

NORSK POLARINSTITUTT

Rolfstangveien 12, Snarøya, 1330 Oslo Lufthavn, *Norway*

SALG AV BØKER

Bøkene selges gjennom bokhandlere, eller bestilles direkte fra:

SALE OF BOOKS

The books are sold through bookshops, or ay be ordered directly from:

UNIVERSITETSFORLAGET

Postboks 307
Blindern, Oslo 3
Norway

Global Book Resources Limited
109 Great Russel Street
London WC1B 3ND
England

Columbia University Press
136 South Broadway
Irvington-on-Hudson
NY 10038
USA

Publikasjonsliste, som også omfatter land- og sjøkart, kan sendes på anmodning.

List of publications, including aps and charts, may be sent on request.

SKRIFTER NR. 169

Results from Norwegian Antarctic Research 1974—1977

NORSK POLARINSTITUTT
OSLO 1978

Utgitt ved TORE GJELSVIK, direktør

Redaksjonssekretær: ANNEMOR BREKKE

Fagkomité:
VIDAR HISDAL, THOR LARSEN, ØRNULF LAURITZEN,
PETER HAGEVOLD

Trykt desember 1978

ISBN 82-90307-02-0

Fra *Nimbusryggen*, en liten nunatak i Vestfjella (73°44'S — 14°52'V). Deltagere i Den norske Antarktisekspedisjonen 1976/77, YNGVAR GJESSING, JOHN SNUGGERUD og TORGNY VINJE, setter opp en Nimbus-satellitt automatstasjon.

From Nimbusryggen *(Nimbus Ridge), a small nunatak in Vestfjella (73°44'S — 14°52'W). Participants in the Norwegian Antarctic Research Expedition 1976/77,* YNGVE GJESSING, JOHN SNUGGERUD, and TORGNY VINJE, *are establishing a Nimbus satellite automatic station.*

Photo: AUDUN HJELLE

Contents

Stratigraphy and igneous petrology of Southern Heritage Range, Ellsworth Mountains, Antarctica

BY AUDUN HJELLE, YOSHIHIDE OHTA AND THORE S. WINSNES

Abstract

Sedimentary and magmatic rocks of Late Proterozoic to Late Paleozoic age, from the southern half of Ellsworth Mountains (c. 80°S — 82°W) are described. Basic volcanic rocks, mainly agglomeratic, occur abundantly in the lower part of the succession, in the Minaret Group, and in the lower part of the Heritage Group of CRADDOCK (1969), but are not recorded in the upper part of his Heritage Group. Due to this lithostratigraphic contrast a new classification is proposed: the Heritage Group including the Middle Horseshoe Formation (500 m+, the upper part of the Minaret Group of CRADDOCK) and the Edson Hills Formation (3500 m, the lower part of the Heritage Group of CRADDOCK). A stratigraphic gap is evident above the Edson Hills Formation and a separate unit — the Dunbar Ridge Formation (1200 m, the upper part of the Heritage Group of CRADDOCK) — is proposed. This formation is of Middle-Upper Cambrian age, with trilobite-bearing limestones.

The structure is governed by a major anticline with a NW plunge in the north but almost horizontal in the south. Contrast of fold intensity and fold style below the youngest exposed unit, the Whiteout Conglomerate and a weathered surface above the Crashsite Quartzite suggests a late Paleozoic deformation phase.

Two phases of magmatism are distinguished. The pre-Middle Cambrian magmatism is dominantly K-alkalic and suggests the beginning of block subsidence at the early stage of a rift tectonics on a continental crust. The presumptive Late Paleozoic magmatism is Na-alkalic and tholeiitic, and occurred after the main deformation; however the rocks were regionally metamorphosed in the actinolite-greenschist facies probably in late Paleozoic time. This magmatism is considered to represent an advanced stage of block tectonics.

Introduction

The Ellsworth Mountains are located as a geographic bridge between the East Antarctic shield and the Antarctic Peninsula; it is thus very important to consider the relationship between these two geologic units. It is thought that a more comprehensive description is required, although a short summary

is presented by us in an article in Antarctic Geology and Geophysics, Madison, Wis. (in press).

Three expeditions from the University of Minnesota established a general stratigraphy of the folded sedimentary rock sequence which ranges from Late-Cambrian to Permian with a total thickness of about 13 km. The area covered by the present study, the Heritage Range, includes most stratigraphic units already known, except for the lowest calcareous succession and the uppermost Permian Polarstar Formation. The study has been focused on the structures and on the petrography and chemistry of magmatic rocks. No discussion on large-scale tectonics is included. The name Middle Horseshoe Ridge is used for the mountain ridge extending c. 15 km from Linder Peak towards the SSE.

Stratigraphy

Owing to limited occurrences of fossils, the grouping of stratigraphic units in this area is essentially based on the lithologic characteristics. Four among the five units distinguished by previous authors (Craddock et al. 1964; Craddock 1969) have been observed: the Minaret Group, the Heritage Group, the Crashsite Quartzite and the Whiteout Conglomerate (Fig. 1).

The Minaret Group was defined by its dominant carbonate rocks and the Heritage Group by its clastic rocks with some calcareous and volcanic rocks. Our mapping shows that the upper part of the Heritage Group contains dominantly shaly-slaty rocks with only a few carbonate beds, and has no magmatic and coarse-grained clastic rocks. The lower part of the Minaret Group, which we did not observe, was described as a wholly calcareous succession (Craddock et al. 1964).

The succession containing volcanigenic rocks is clearly defined between the lower calcareous and the upper shaly-slaty successions. The grouping proposed by Craddock is based on rocks other than the volcanigenic ones, as calcareous beds. However, calcareous beds occur both in his Minaret and Heritage Group; it seems reasonable therefore to define the volcanigenic-bearing succession as an independent group, and a new grouping is proposed as shown in Table 1.

THE HERITAGE GROUP

This Group includes 1) the lower volcanic-calcareous succession: the Middle Horseshoe Formation, and 2) the upper volcanic-clastic one: the Edson Hills Formation.

The Middle Horseshoe Formation

This formation constitutes the upper part of the Minaret Group of Craddock, including the middle silty limestone with oolite and pisolite (150 m) and the

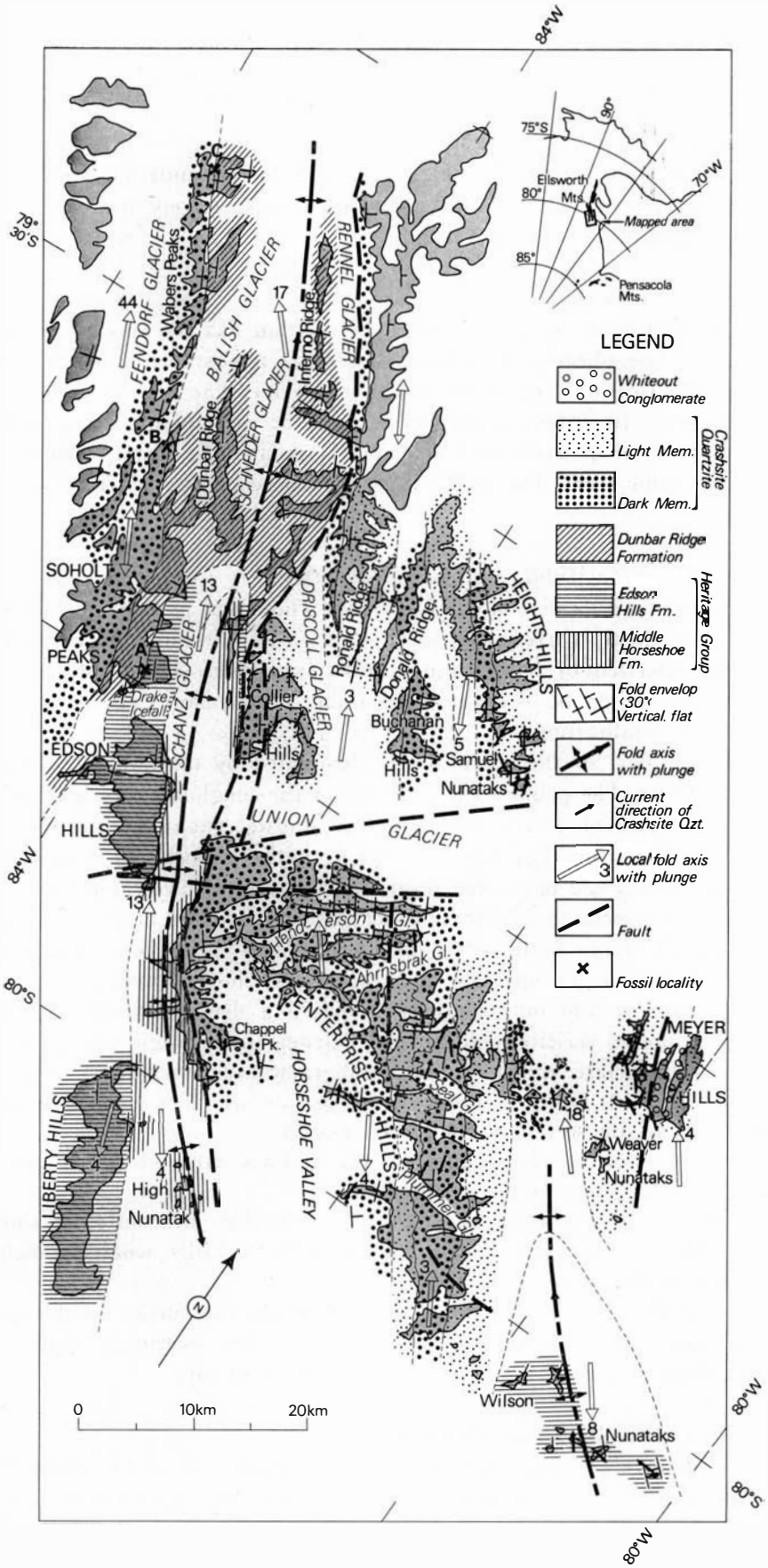

Fig. 1. *Geological map of southern Heritage Range, Ellsworth Mountains.*

youngest unit of calcareous rocks (610 m) of Craddock et al. (1964). The rocks are distributed along the axial zone of the major anticline, south of the Schanz Glacier. Below, (E) and (W) refer, to respectively the eastern and western limbs of the anticline (Fig. 2).

High Nunatak area (E):

This southernmost occurrence of the formation has the succession shown in Table 2. The siliceous shale has a hornfelsic appearance and might have suffered silicification from later volcanic activity. The breccia body which occurs slightly discordant to the bedding of the surrounding rocks and has angular blocks of quartzite and volcanics is assumed to be an eruptive vent of later volcanic rocks. The oolitic limestone bed characterizes the top of this formation.

Southern end of the Middle Horseshoe Ridge (E):

This is the type locality of the formation. The upper part of the succession (Table 3) evidently corresponds to Craddock's middle and upper carbonate units, characterized by oolitic and pisolitic limestones. The pisolitic ovoids, 1—2 cm long, might be of organic origin, but the primary details are obliterated by recrystallization.

The lower part of the succession is dominated by dark coloured coarse-grained clastics. The pebbles and boulders of the conglomerate horizons have a maximum size of 15 cm, and comprise diorite, gabbro, basic volcanics, quartzite and marble. The marble is white with distinct purple-weathered crust. The matrix is a black, coarse-grained sandstone of volcanic origin. The agglomerates associated with these rocks have varicoloured blocks up to 50 cm across, mostly dense basic rocks, porphyrites, and tuffbreccias. The matrix is strongly stained by opaques and commonly shows phyllitic cleavages. Fresh plagioclase and quartz are scattered in a dense mixture of opaque, sphene, actinolite, sericite, chlorite and calcite. Small fragments of dolerite with lath plagioclase and hornblende, subgreywacke, black chert, and shale are also included. Garnet, zircon or tourmaline which are common in the Crashsite Quartzite, were not found in the matrix.

The pillow lava is inpersistent, and the pillows are deformed into flat ovoids with pale green epidote-rich cores.

This volcanic-clastic unit also crops out on the discontineous ridge connecting the Middle Horseshoe Ridge and the Liberty Hills, where it includes some white marble beds.

Some cracks a few centimetres deep occur at the top surface of the uppermost pink limestone, being filled by red clay of the overlying shale. This contact, however is conformable and shows no trace of slip.

NW corner of the Horseshoe Valley (E):

The Middle Horseshoe Formation was observed east of Guarcello Peak, where a white limestone 50 m thick and a banded limestone 60 m thick, sand-

wich a 10 m thick dark green shale. The shale is strongly phyllitic and crenulated, and the banded limestone shows small-scale, tight interlayer foldings. A dark agglomeratic rock more than 100 m thick underlies this succession. The upper limit of this calcareous succession is cut by a reverse fault against the dark member of the Crashsite Quartzite to the east.

A distinct white limestone bed, 30—50 m(?), was seen from a distance at the Rhodes Bluff, the SE corner of the Union Glacier, with a continuation along the ridge from the Guarcello Peak.

W side of the Collier Hills (E):

A schistose grey limestone 30 m thick, which occurs here, has oolitic-pisolitic textures, and is commonly brecciated. The upper side of this bed gradationally changes into a brown muddy limestone 20 m thick with conformably overlying grey sandy shale, 50 m thick. The oolitic limestone defines the top of the Middle Horseshoe Formation.

The nunataks just SSW of Mt. Rodger are composed of dark phyllittic sandstone, shale and green schist. The exposed thickness is about 100 m and the stratigraphical position a few hundred metres below the oolitic limestone bed.

NW slopes of the Liberty Hills (W):

The oolitic limestone and the underlying basic rocks occur in this area; the upper calcareous unit is shown in Table 4.

A few hundred metres south, massive volcanic rocks occur below the calcareous succession. The rocks have partly amygdaloidal and pillow structures, and a dyke cuts the limestone in one place, associating a narrow zone of hornfels. Most of these volcanic rocks are older than the calcareous rocks, but the dyke may be an eruptive vent of a later volcanic activity.

The eastern slope of the Edson Hills (W):

A distinct limestone bed 50—100 m thick occurs along the eastern foothills from the Elvers Peak to the Hyde Glacier.

The succession obtained from the ridge between the Hyde Glacier and the Drake Ice Fall is shown in Table 5. The upper calcareous unit disappears under the Schanz Glacier in the north of the Drake Ice Fall. Although no oolitic rock was observed, this unit is correlated to the upper calcareous succession of the Middle Horseshoe Formation. No stratigraphic gap was detected at the top of this unit.

The volcanic-clastic succession below consists mostly of dark-coloured conglomerate and agglomerate. The pebbles and cobbles, maximum sizes about 50 cm across, are red shale, grey limestone, epidote rock, diabase and green sandstone. The intrusive sheets in the calcareous unit are related to the later igneous activity.

Summary (Fig. 2):

Maximum observed thickness of the Middle Horseshoe Formation is about 500 m. The upper limit is defined by the oolitic-pisolitic limestone bed, and the transition upwards is gradational. The lower boundary was not observed. The Upper Unit is dominantly calcareous and includes a few beds of argillaceous rocks. The primary textures of limestone are preserved better in the eastern than in the western limb of the major anticline. Clastic rocks interbed in the north.

In the Lower Unit, the amount of volcanigenic rocks varies very much from place to place. Agglomerates are dominant in association with deformed pillow lava. The conglomerates are polymictic, including a large proportion of basic igneous rocks, beside sedimentary rocks. These coarse-grained clastic rocks suggest high local relief caused by the volcanic activity. The associated sandstones are also coarse-grained and probably of volcanic origin. A later shallow sea sedimentary environment is suggested by the Upper Unit with oolitic-pisolitic limestone.

The Edson Hills Formation

A volcanic-clastic succession occurring above the oolitic limestone is defined as the Edson Hills Formation. It constitutes the lower part of the Heritage Group of Craddock et al. (1964) and is distributed mainly along the western side of the major anticline outside the area of the Middle Horseshoe Formation.

Liberty Hills (W):

A thick succession of interbedded shale and sandstone about 800 m thick occurs on the eastern foothills of the Liberty Hills above the oolitic limestone (to the west of High Nunatak). The alternation is very frequent and consists of green and red coloured beds. Above this occurs a 700 m thick alternation of dark green, coarse-grained, commonly conglomeratic sandstone and grey shale, showing well sorted and graded structures. The pebbles in the conglomeratic beds, less than 5 cm across, are red quartzite, limestone, diabase and porphyrite. Thin schistose amphibolite beds a few metres thick are rarely intercalated.

A similar alternation was seen from a distance on the eastern slopes of Mt. Rosenthal, the calculated thickness being about 1,700 m. The total thickness of the clastic successions is about 3,200 m.

E-slope of the Edson Hills and the Soholt Peaks (W):

The succession observed in the lower part of the hills north of the Hyde Glacier is shown in Table 6. A rhombporphyry is included in the green agglomerate. The green phyllite which might be derived from a tuff, contains many large volcanic blocks, some of which are impregnated by green Cu-minerals. The volcanic succession in the middle to upper parts of the

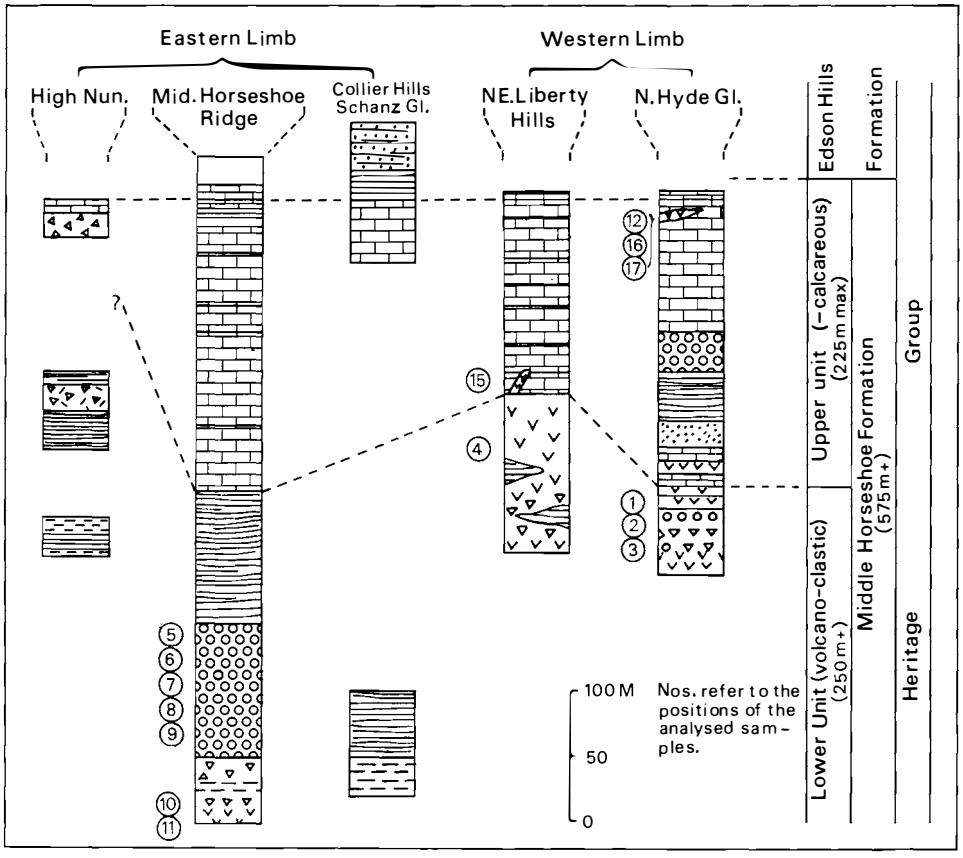

Fig. 2. *Observed successions of the Middle Horseshoe Formation. Legend: see Fig. 3.*

mountain slope, by the binocular observations, is assumed to include at least two lava beds 30—50 m thick in frequent alternation with sandstones. At the top of the Hyde Glacier, two white marble beds are seen separated by a hard, dark bed. The total estimated and calculated thickness of the Edson Hills Formation here is about 3,100 m.

The white marbles at the top of the Hyde Glacier extend northwards, forming a small nunatak in the upper stream of the Drake Ice Fall, and make a smooth ridge on the northern side of the ice fall, showing tight folds of a hundred metres' wave length. This marble bed is covered by a black slate with Middle Cambrian trilobites.

Southernmost nunatak of the Middle Horseshoe Ridge (E):

A 2.5 m thick green and red shale alternation with 20—50 cm units, occurs above the pink limestone of the Middle Horseshoe Formation. Above this occurs an about 50 m thick fine-grained green sandstone with a dark shale bed of up to 3 m in thickness. These beds are almost vertical in position. A few hundred metres east of the nunatak, regularly banded quartzite of the

light member of the Crashsite Quartzite crops out with a moderate eastern dip. A large strike fault separates these two localities.

SW edge of the Collier Hills (E):

The succession shown in Table 7 overlies the oolitic limestone on the western slope of a small nunatak at the south-western edge of the Collier Hills. The eastern side of this nunatak is composed of the dark member of the Crashsite Quartzite, and the large strike fault passes across the middle of the nunatak.

The Wilson Nunataks (at the SE end of the Heritage Range):

The sedimentary unit characterized by conglomerates, arkosic sandstone, and thin limestone beds crops out in six scattered nunataks. The observed thickness is 300 m, but the total thickness, including the ice-covered area, may reach a few thousands of metres after the simplest assumption of the structure. The northwesternmost nunatak (the 837 m point on the map) contains the thickest succession, 152 m, as shown in Table 8. The pebbles and boulders of the arkosic conglomerate are well rounded and comprise quartz diorite, gneisses, quartzite, grey limestone, conglomerate, and sandstone; the maximum size is 50 cm across. In the middle nunataks, dark shale prevails with a maximum thickness of about 100 m, being intruded and partly hornfelsed by gabbro and porphyrite.

The arkosic matrix of the conglomerate is a feldspar-quartzite or a feldspar-greywacke (Pettijohn 1949), including granite decomposed in-situ in the fine-grained sericite-quartz matrix of 10—30 volume %. Very coarse-grained, fractured quartz grains, microcline perthite (15—20%), and a small amount of plagioclase are main granular constituents. Small lithic fragments detected are chert, sericite shale, chlorite-sericite phyllite, gneiss and migmatites, hornblende porphyrite, quartzite and graphite shale. No garnet or sphene were seen. The source area of the arkosic conglomerate is inferred to be a migmatite-gneiss area with a cover of sediments and low grade metamorphic rocks, intruded by porphyrite.

Two nunataks in the SE include the succession shown in Table 9. The southeasternmost nunatak is composed of a conglomerate 50 m thick, with 8—15 cm pebbles of limestone and dolomite (60—65%), and shale.

These rocks of the Wilson Nunataks are independent from those of any neighbouring areas. From the interpretation of regional structures, this clastic succession is assumed to be of the Edson Hills Formation. Lack of volcanigenic rocks indicates that the sedimentary conditions here were different from those of the major anticline area. Abundance of arkosic sandstone and granite-gneiss pebbles in the conglomerates suggests that this area was closer to the crystalline source area than the major anticline area in the west where volcanism might be localized.

Table 1. Correlation of the new and the old stratigraphic grouping in the Ellsworth Mountains.

Craddock 1969	This paper		
Whiteout Congl.	Whiteout Congl.		
Crashsite Qzt.	Crashsite Qzt.		
	Dunbar Ridge Fm.		Paleoz.
Heritage Group	Edson Hills Fm.	Heritage Gr.	
	Middle Horseshoe Fm.		
Minaret Group		Minaret Gr.	Proteroz.

Table 2. The Middle Horseshoe Formation observed in the High Nunatak area, central Horseshoe Valley.

Oolitic limestone	10 m
Agglomerate	20 m
(Unexposed 50 m)	
Siliceous shale	10 m
Breccia bed	20 m
Siliceous shale	30 m
(Unexposed 50 m)	
Black shale with thin white limestone	35 m
Total exposed	125 m

Table 3. The Middle Horseshoe Formation at the southern tip of the Middle Horseshoe Ridge (the type locality).

Sharp contact to overlying green and chocolate coloured shale alternation.

Pink and white banded limestone	8 m	
Massive grey oolitic limestone	10 m	
Thin dolomite bed	0.2 m	
Massive grey oolitic limestone	2 m	Upper Calcareous unit
Grey slate	5 m	
Pisolitic limestone with oolitic matrix	20 m	
Mylonitic grey limestone (cave filling breccia)	40 m	
White limestone (orange-yellow weathering)	20 m	
Dark grey, sheared banded limestone	70 m	
White limestone of very consistent thickness	50 m	
Dark shale, slaty and partly conglomeratic	50-100 m	Lower volc.clastic unit
Dark polymictic congl. of varying thickness	100 m	
Agglomerate, pillow lava and green phyllite	50 m	
Total observed	425-475 m	

Table 4. The Upper Calcareous unit of the Middle Horseshoe Formation at the northern slopes of the Liberty Hills.

(Unexposed 120 m)	
White-pink banded limestone	5 m
Dense grey oolitic limestone	15 m
Grey schistose banded limestone	30 m
White massive marble	20 m
Banded limestone	15 m
White massive marble	30 m
Grey banded limestone	20 m
White massive marble	15 m
Total exposed	150 m

Table 5. The Middle Horseshoe Formation on the northern side of the Hyde Glacier, Edson Hills.

(Contact to green agglomerate above)		
White marble with a sheet of dacite (Purple laminated shale on both sides)	5 m	
Schistose conglomeratic marble (with varicoloured blocks and white matrix)	100 m	Upper Calcareous unit
Brown conglomerate	30 m	
Purple-brown shale with congl. at the top	40 m	
Coarse-grained sandstone	20 m	
White limestone conglomerate with a basic intrusive sheet of 10 m	30 m	
Congl. and aggl., both polymictic	5 m	Lower Volcano-clastic unit
Grey lava and tuff breccia	10 m	
Congl. and aggl., both polymictic	50 m	
Total observed	290 m	

Table 6. The Edson Hills Formation along the Hyde Glacier, Edson Hills.

White limestone	150 m	calculated
Sandstones and some lavas	2500 m	calculated
Varicoloured phyllitic agglomerates (With malachite-stained volcanic blocks)	250 m	
Green phyllite with chlorite spots	20 m	observed
Dark agglomerates	30 m	thickness
Green aggl. with glassy dacite lavas	150 m	455 m
Purple shale	5 m	
Total observed and calculated	3105 m+	

Table 7. The Edson Hills Formation at the SW edge of the Collier Hills.

Coarse-grained laminated sandstone	50 m
Grey shale and sandstone alternation	40 m
Brown muddy limestone	20 m
Total observed	110 m

Table 8. The largest succession observed in the Wilson Nunataks, presumptive Edson Hills Formation.

Dark conglomerate	10 m
Arkosic conglomerate	50 m
(Unexposed 50 m)	
Sandstone and conglomerate alternation	20 m
Conglomerate	10 m
Sandstone	10 m
Sandstone and conglomerate alternation	7 m
Conglomerate	15 m
Sandstone	10 m
Sandstone and conglomerate alternation	20 m
Total observed	152 m

Table 9. The succession seen in one of the nunataks in the southern part of the Wilson Nunataks (NNE of 787 m point).

Quartzite and shale alternation	35 m
Quartzitic sandstone	25 m
Arcosic sandstone	30 m
Grey limestone	10 m
Total observed	100 m

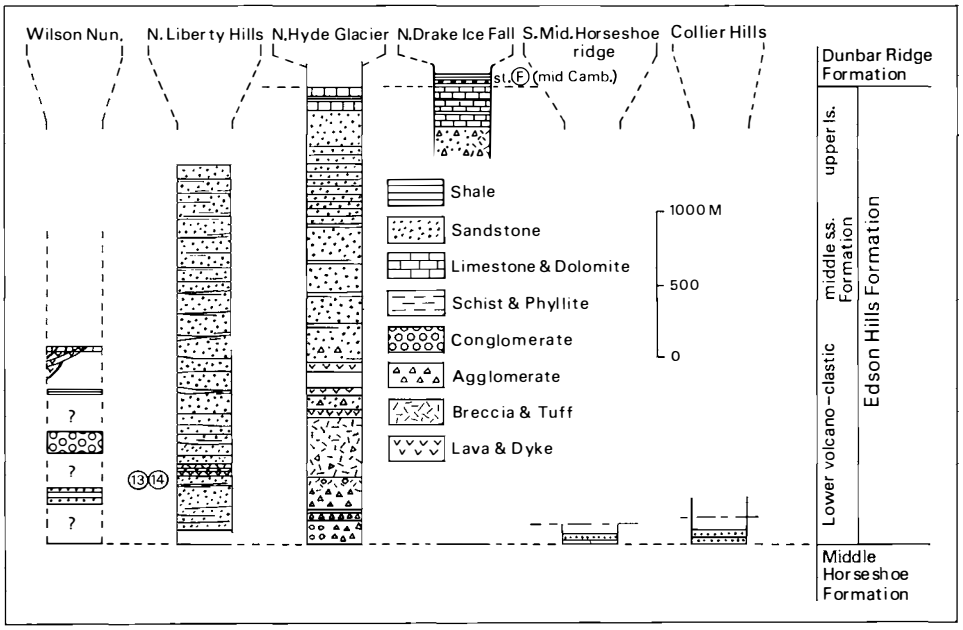

Fig. 3. *Observed successions of the Edson Hills Formation. Nos. along the columns refer to the analysed samples (Table 12).*

Summary (Fig. 3):

The transition from the underlying succession is gradational and the uppermost unit is the marble bed below the slate including Middle Cambrian trilobites, thus the age of this formation is Middle Cambrian or older. The volcanigenic sediments dominate in the Edson Hills area, while clastic rocks constitute the main part of the succession in the Liberty Hills. The volcanism was localized around the present Edson Hills area and a rough relief of volcanic topography existed. The arkosic conglomerate in the Wilson Nunataks indicates that the source area was to the SE and not too far away. The total thickness of the Edson Hills Formation is about 3,500 m.

THE SUCCESSION ABOVE THE HERITAGE GROUP

The Dunbar Ridge Formation

This formation corresponding to the upper part of the Heritage Group of Craddock et al. (1964), is mainly composed of monotonous slate and black calcareous shale and shows strong contrast of lithology to the underlying succession. It occupies the northern part of the axial zone of the major anticline which plunges gently north.

SE part of the Soholt Peaks:

This southernmost occurrence of the Dunbar Ridge Formation is composed of about 200 m slate and 500 m grey-green sandstone and limestone. Three limestone beds occur; the middle one, 50 m, associates conglomeratic limestone, the other two are about 10 m in thickness. Weak impregnation of Cu mineral was seen in the sandstone. The slate is weathered into very soft mud on the surface and includes many calcareous nodules, 10—20 cm across, with numerous trilobite fragments in the core. The trilobites were examined by Webers (pers. comm. 1976) and a Middle Cambrian age was suggested.

E and W of the Dunbar Ridge:

A quartzite with intercalated black shale occurs at the western tip of the ridge extending westwards from Mt. Sporli, and a muddy limestone-bearing succession crops out at the western end of the Mhire Spur. These represent the lower part of the Dunbar Ridge Formation near the core of the major anticline.

A 70 m thick grey limestone occurs on the ridge extending north from the Eley Peak, Soholt Peaks, having a good fauna of trilobites. This is the southern extension of the fossil-bearing limestone on the eastern flank of the Springer Peak, Webers Peaks. The fossils form a thick accumulated mass and include probable Upper Cambrian trilobites, inarticulated brachiopods, and pelmatozoan columnals (Webers, pers. comm. 1976). This fauna is perhaps slighly older than that of the Springer Peak reported by Webers (1972) and this locality presents a good succession of the Upper Cambrian fauna.

Webers Peaks and Inferno Ridge:

The upper few hundred metres of the Dunbar Ridge Formation crop out in these ridges.

On the eastern foothill of the Springer Peak, 6 m of a grey, partly brecciated and oolitic-pisolitic limestone occurs. The Upper Cambrian fauna reported by Webers (1972) was from this bed. Our collections include two *Knightoconus*, eight *«Maclurites»* and one *Matherella* (Yochelson pers. comm. 1975). Above the limestone occur varicoloured shale and sandstone about 10 m thick, which are overlain conformably by the Crashsite Quartzite. Below the fossiliferous limestone is a monotonous succession of black slate, partly sandy, about 500 thick.

Similar slaty succession occurs at the Orheim Point, north of the Inferno Ridge, with 30 m of muddy nodular limestone above. The middle part of the Dunbar Ridge Formation crops out along the Inferno Ridge and is composed in the upper part of a few hundred metres of slate and in the lower part of a quartzite intercalating shaly succession 200—300 m thick.

The slaty rocks have well sorted matrix with 50—60% calcite, and quartz and plagioclase grains of 0,1 mm size. The plagioclase which is a clear albite comprises about 10 volume % and 0.5% potash feldspar is associated. Minor amounts of detrital micas, garnet, and zircon are included and idiomorphic pyrite grains are distinct.

Summary:

This formation is defined by the fossils to be of Middle to Upper Cambrian age. The successions are dominantly slaty; quartzite beds are intercalated in the lower part and sandy facies are dominant in the upper part. The thickness decreases towards the south from 1,200 m to 700 m. Although no discontinuity has been observed at the base, the complete extinction of volcanic activity is noteworthy. The lithology suggests closed quiet shallow sea conditions.

The Crashsite Quartzite

This formation occupies more than two-thirds of the mapped area, mainly in a large synclinorium to the east of the major anticline. The rocks are white-green quartzites, commonly alternating with green and red sandstone and shale beds, a few centimetres to a few metres thick. These rocks are so intensely folded in small-scale that an estimation of thickness is almost impossible to make in the field. The calculated thickness from the profile is about 1,800 m.

The base of this formation had been observed along the eastern flank of the Webers Peaks and is conformable with the underlying Dunbar Ridge Formation. In the eastern limb of the major anticline, it is separated from the underlying formation by a large strike fault in the whole length of the mapped area.

Thin conglomeratic sandstone beds are intercalated just above the base in the Springer Peak. The pebbles, well rounded and a few centimetres in size, are white and black cherts, calc-siliceous phyllites, sericite-quartz schist, felsic gneiss, and fractured microcline granite. The matrix is arkosic sandstone with 50% subangular quartz, 20—30% microcline commonly interlocked with albite and quartz, about 10% garnet and 1% biotite. The interstitial material in the arkose is a fine-grained quartz-calcite-sericite mixture. The calc-argillaceous matrix might be inherited from the underlying Dunbar Ridge Formation, while the coarse-grained components suggest a reactivation of uplift in the provenance area which was composed of a series of metamorphic rocks and granites.

The succession of this formation is divided into two members; the lower Dark Member and the upper Light Member, based on the amount of intercalated sandy-shaly beds. Fig. 4 shows the percentages of the quartzite

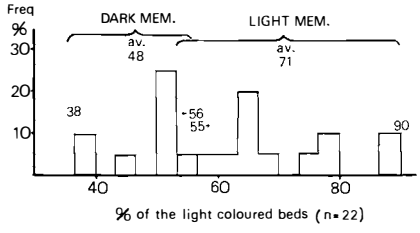

Fig. 4. *Percentages of the light coloured beds at different localities in the Crashsite Quartzite and the frequency of occurrences.*

(light-coloured bed) observed on large cliff faces. Although the ratios are gradational between the two members, the transitions are always very sharp in actual exposures. The Light Member occurs around the middle of the Enterprise Hills along the synclinorium axis and in the Meyer Hills (Fig. 1). The calculated thickness of the Dark and Light Members are 750 m and 1,000 m, respectively.

Cross bedding, ripple marks, and slumping structures are common in this formation, and some worm-tracks were also seen. The paleocurrent direction was estimated as shown in Fig. 1. The current was roughly parallel to the regional fold trend and this may mean that some topographic reliefs existed during this period, roughly parallel to the present major anticline trend, controlling the current direction.

Megascopic lithic fragments are mostly quartzite, phyllite-schists and contemporaneous breccias of shale. The volcanic fragments derived from the Heritage Group below are not distinct, contrasting to the description of Craddock et al. (1964) in the Sentinel Range. The conglomeratic sandstone beds, rarely interbedded, have mainly quartzite pebbles.

Craddock (1969) divided the Crashsite Quartzite into three members and a dark member was distinguished in the upper part. A thin succession, 10—20 m thick, at the top of the Holt Peak, probably corresponds to his Upper Dark Member, while this lacks on the Seaquist Peak, both in the Meyer Hills. At the latter locality, a reddish-brown layer a few metres thick develops at the top of the Crashsite Quartzite and is covered by the Whiteout Conglomerate. This coloured layer is considered to be an old weathered surface and the lack of the Upper Dark Member here may suggest a clino-unconformity.

A strange black nodular rock occurs in the south-middle part of the Meyer Hills in a fault zone separating the Crashsite Quartzite from the Whiteout Conglomerate. The rock shows bituminous luster and includes many small nodules of less than 1 cm across, which are composed of radial fibrous fluor-apatite. The matrix is a very fine-grained, opaque-rich shale. The stratigraphic position of this rock is not clear, but it possibly belongs to the upper Crashsite Quartzite. Similar sedimentary phosphate was reported from the Middle Paleozoic of the Pensacola Mts. (Cathcart & Schmidt 1977).

Although no fossil was found by us in the mapped area, the Middle Paleozoic age of this formation is certain (Craddock et al. 1964; Craddock 1969). A steady subsidence of a shallow sea basin is conceivable during the period of this formation.

Fifty modal analyses were made on the rocks of this formation, the average values being shown in Table 10. The rocks from both the Dark and the Light Members are generally similar and range from pelite to quartzite (Fig. 5, Pettijohn 1949). Three groups are distinguishable on account of their amounts of intergranular detritals (I.D.): shaly subgreywacke + pelite (I.D. $> 60\%$), subgreywacke ($60 > $I.D. > 33), and quartzitic subgreywacke + quartzite (I.D. < 33). Quartzites tend to be dominant in the Light Member. The quartz grains in quartzites include rutile, apatite, blue tourmaline, zir-

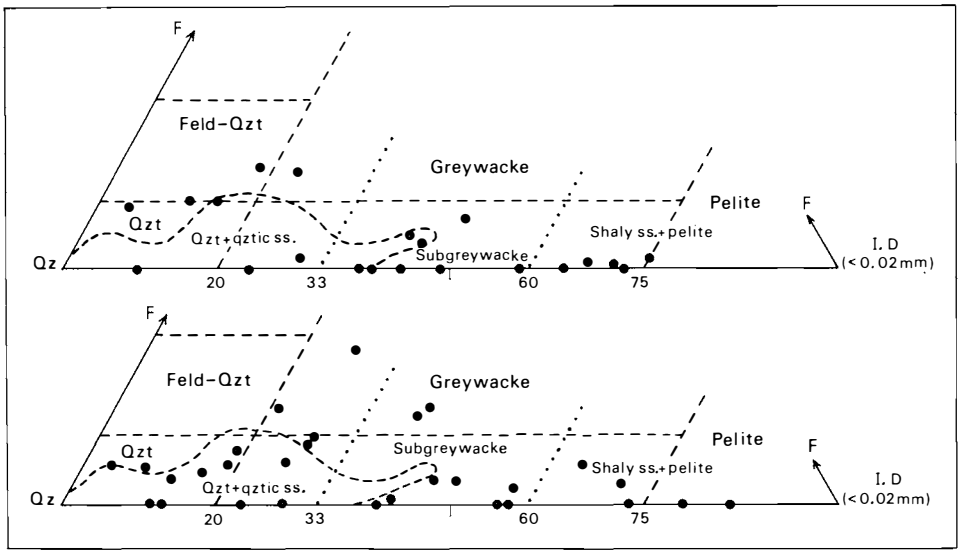

Fig. 5. *Modal composition of the Crashsite Quartzite (the classification after Pettijohn 1949). Above: the Dark Member. Below: the Light Member. I.D.: interstitial detrials. Dotted lines: border of the present divisions. Broken curve: lower-middle Paleozoic sandstones of Pensacola Mts. (Williams 1969).*

con, biotite, and vermiculite. The feldspar components of the feldspar-quartzites and greywackes are mainly microcline perthite and small amounts of albitic plagioclase. Association of relatively large amounts of lithic fragments with the feldsphatic rocks, is characteristic (Table 10). These rocks occur in limited areas: from the Collier Hills to the Ronald Ridge and in the Meyer Hills. More than 35% of the analysed rocks are less matured than the Middle Paleozoic clastic rocks of the Pensacola Mts. (Williams 1969). Four calcareous rocks (calcite matrix >15%) were detected from the lower and the upper part of the Light Member.

According to the classification of Dott (1964), arenites (matrix < 15%) are common in the quartzites. Lithic sandstones tend to be distinct in the Dark Member, while the Light Member contains more feldspathic sandstones. The lithic fragments comprise chert, quartzite with sericite and chlorite, sericite shale, graphite shale, phyllite, and mylonitic quartzite. Some siliceous volcanic fragments were found in the sandstones of the Meyer Hills. Comparing with the rocks of the Polarstar Formation, representing relatively rapid uplift of the provenance area (Castle and Craddock 1975), the rocks of the Crashsite Quartzite are dominated by quartzite. This suggests a quiet steadily sinking sedimentary basin.

The modes of minor detrital minerals are summarized in Table 11. A decrease of detrital phyllo-silicates and an increase of stable heavy minerals in the Light Member indicate higher maturity than in the Dark Member.

Table 10. Average modal compositions of the Crashsite Quartzite

	Rocks	n	Qz	Kf	Pl	Mus	Bi	Chl	Ep	Cc	Ti	Ap	Gar	Zr	Ru	Op	Orth	Tour	Matrix Seri	Matrix Qz	Lithic fragm. Sch+phy	Lithic fragm. Qzt.+comp.qz	Total
	Shaly subgreyw.	5	27.7	0.6	tr	0.6	tr	5.2	0.6	0.1	1.5	tr	1.3	0.1	tr	4.4	tr	tr	54.2	3.1	0.2	0.4	100.0
Dark	Subgreywacke	8	45.1	1.7	0.1	tr	-	1.8	0.7	4.2	0.2	tr	1.6	tr	tr	1.7	-	-	21.4	11.7	0.2	9.6	100.0
Mbr.	Fsp. subgreyw. +																						
n=21	fsp.qzt.	4	65.3	11.5	-	-	-	1.0	0.2	tr	tr	tr	tr	tr	tr	tr	-	-	10.4	3.5	0.4	7.7	100.0
	Sandy qzt. + qzt.	4	76.7	2.7	-	0.1	-	1.0	tr	0.1	tr	tr	tr	tr	tr	tr	-	-	8.8	6.0	0.1	4.5	100.0
	Shaly subgreyw.	5	22.0	1.9	tr	0.4	tr	6.4	0.5	-	0.7	tr	1.5	0.1	0.2	8.0	-	-	46.0	11.1	-	1.2	100.0
Light	Calc. subgreyw.	2	32.9	1.6	-	-	0.1	0.3	-	56.5	-	-	0.6	-	-	0.1	tr	-	6.3	1.0	-	0.6	100.0
Mbr.	Greyw. + subgreyw.	8	41.3	3.4	0.6	0.6	0.1	2.0	tr	0.1	0.3	tr	0.2	0.2	-	5.7	tr	0.3	32.3	10.5	-	2.3	99.9
n=29	Fsp.-sandy qzt.	2	49.6	12.6	4.0	0.1	0.1	0.6	0.6	3.0	0.1	-	0.3	-	-	0.2	-	-	9.3	9.1	0.5	10.0	100.1
	Sandy qzt. + qzt.	12	73.0	3.7	0.2	0.2	0.5	0.3	0.1	1.1	tr	tr	0.4	0.1	tr	0.3	tr	-	11.6	1.9	0.6	6.0	100.0

The Whiteout Conglomerate

This formation occurs in the Meyer Hills. The lower border was observed both in the eastern and western ridges. A clino-unconformity is suggested at the base as already mentioned (p. 17).

The conglomerate is black, poorly sorted, with a coarse- to medium-grained sandsone matrix and scattered pebbles and cobbles up to 80 cm across. The matrix is composed mainly of calcite, sericite, quartz, and hematite. The quartz grains include rutile needles and some are composite grains. Microcline perthite exceeds albitic plagioclase. Most pebbles and cobbles are well rounded, and limestone and quartzite are dominant. Granites and gneisses occupy a large proportion, mainly as potash-feldspar porphyritic granite and garnet-biotite gneiss. Small amounts of reddish sandstone, basic volcanics, skarn gneiss, and sericite-chlorite schist were also found. Small fragments of chert, mylonitic quartz rock, graphite shale, calcite-quartz schist, muscovite sandstone, dolomite, biotite schist, and greywacke were detected under microscope. This suggests a granite-gneiss source area covered by low-grade metamorphic rocks.

On the western slope of the Holt Peak at the NE corner of the Meyer Hills, a layered and sorted succession about 10 m thick occurs near the base of this formation, with conglomeratic horizons in dominantly dark shaly beds. A marine tillite origin of this formation (Craddock et al. 1964) is acceptable from the lithology.

The basal surface of this formation shows gentle smooth folds, of several hundred meters' wavelength, and a few decimeters' amplitude,while the Crashsite Quartzite just below has stronger folds with a few hundred meters' wavelength and up to a hundred meters' amplitude. This structural contrast may largely depend upon the total difference of competency related to the bedding thick-

Table 11. Relic minerals in the Crashsite Quartzite

Mus	Bi	Ep	Sph	Gar	Zr	Rutile bg Qz		
71	3	67	57	52	57	62	Dark M (n=21)	% of rocks including each min.
27	8	66	69	76	86	72	Light M (n=29)	
0.5	0.1	2.2	4.7	5.9	0.3	-	Dark M (n=21)	Max % (mode)
3.4	6.3	1.3	1.7	6.2	0.5	-	Light M (n=29)	

ness of the rocks, but the possibility of a clino-unconformity is not excluded.

Total observed thickness of this formation is 400 m; the upper limit can not be seen in this area.

Petrology of the igneous rocks

The igneous rocks occur in two areas: along the western limb of the major anticline and in the Wilson Nunataks. The former comprises the volcanic pile of the Heritage Group, called the pre-Middle Cambrian volcanics below. The latter cuts the folded presumptive Edson Hills Formation and is assumed to be of Late Paleozoic age.

PRE-MIDDLE CAMBRIAN VOLCANICS

Petrography:

This volcanic activity is represented by a continuous eugeosynclinal sequence of the Heritage Group (Figs. 2 & 3). In the Middle Horseshoe Formation, the rocks of the pillow lava (Table 3) have olivine (chlorite-serpentine pseudomorph), pyroxene and hornblende phenocrysts, and dusty plagioclase laths occur occasionally in the recrystallized matrix. In the dark polymitic conglomerate, the cobbles comprise hornblende plagioclase rocks of diabasic texture and olivine-pyroxene gabbro with primary hornblende and biotite. Typical rhombporphyry and green phyllite occur below the upper calcareous unit.

The upper part of the volcanic succession belongs to the Edson Hills Formation. The green rocks in the Liberty Hills are mainly hornblende porphyry converted into green phyllite, partly with distinct flowage of the plagioclase laths. The mafic minerals show a corroded outline, with pseudomorphs of chlorite and opaques. Amygdaloidal texture appears as light spots. In the Hyde Glacier area, the dacite sheet (Table 5) has mafic minerals totally decomposed, while the plagioclase has kept its outline. Idiomorphic quartz grains show corroded, hexagonal shapes and the plagioclase has albite to andesine compositions. The matrix is totally devitrified and altered, while the phenocrysts are relatively well preserved. Above this is a thick pile of

varicoloured agglomerates, the matrix being green in the lower 50 m, purple for 100 m, and again green for 50 m. The uppermost unit observed has a black matrix. The most common volcanic blocks are rhombporphyry, andesite, and felsite, commonly showing amygdaloidal texture. More volcanic horizons are expected to be present in the upper part due to the occurrence of moraine blocks of volcanic rocks.

On the ridge north of the Drake Ice Fall, boulders of andesites, dacite, and gabbroic rocks occur on the surface. These rocks are assumed to be derived from ice-covered parts of the Edson Hills Formation in the upper part of the ice fall. The gabbros include a distinct amount of fresh clinopyroxene. Some of these rocks may be from the gabbro of the Soholt Peaks reported by Craddock et al. (1964), but here they are included tentatively in the Edson Hills Formation. Diabasic rocks with poikilitic clinopyroxene and prismatic plagioclase and doleritic rocks with amygdaloidal texture are also found. More than a half of the boulders are dacitic rocks, some with a glassy matrix. Amygdaloidal texture is common in these rocks and large plagioclase and quartz phenocrysts have been preserved. The quartz shows a bipyramidal corroded outline in some rocks. The matrix is totally recrystallized into low-grade metamorphic mineral assemblages. Spherulitic texture of quartz is distinct in one of the glassy rocks which can be called a parlite. Welded angular glass fragments are also observed. These acidic rocks show close petrographic similarities to the volcanic rocks of the Early Cambrian Taylor Formation, Central Trans-Antarctic Mts. (Stump 1974 and 1976).

Chemistry:

Chemical analyses of 24 selected rocks were made by fluorescence (Si, Al, Fe, Mn, Mg, Ca, and P), flame photometry (K, and Na), titration (FeO), and the Penfield tube method (H_2O and others) The stratigraphic positions of the analysed samples are shown in Figs. 2 and 3, and detected primary minerals are listed in Table 12. The chemical data and norm values are given in Tables 13 and 14, respectively.

The analysed rocks make two groups, the basic rocks: $45\% < SiO_2 < 52.5\%$ (nos. 1—11 and 13—20) and the acidic ones: $69\% < SiO_2 < 76.5\%$ (nos. 12 and 21—24). Intermediate rocks have not been found.

The acidic rocks (5 samples) are three quartz keratophyres and two rhyolites after the classification of Rittman (1952); four of these are tholeiites, and one is a Na-alkalic rock with impregnation of Cu. All acidic rocks have excess Ab and Q and lie outside the eutectic valley of the feldspar-quartz system, indicating strong (secondary) alteration in the matrix.

Using the norm classification (Yoder and Tilley 1962), 79% of the analysed basic rocks are silica saturated; 53% are olivine basalts and 26% are quartz basalts, while 21% are undersaturated alkali olivine basalts containing normative Ne (Fig. 6). However, most olivine basalts are classified as alcalic rocks in the alkali-SiO_2 diagram (Fig. 7), and 11% of the analysed basic rocks are subalkalic according to the Hawaiian standard (MacDonald

Table 12. Classification and petrographic summary of the analysed Pre-Middle Cambrian magmatic rocks. Numbers and symbols as in the figures

Form.	No	Relic mins.,rock name	Norm Qz	Ne	Ol	Classification	Macdonald & Katsura, 1964	Middlemost, 1975
Edson Hills Fm	18 ⊕	Cpx,plg: gabbro	-	-	10.76	Oliv.tholeiite	Thol.olivine basalt	Sub-alk.(flood basalt)
	20 ⊕	Plg :amygd.dolerite	4.51	-	-	Thol.basalt	Thol.basalt (Qz)	Sub-alk.(flood basalt)
	19 O	Cpx,plg: porphyrite	-	-	12.06	Oliv.tholeiite	Olivine basalt	Transitional (K)
	13 O	Hbl,plg: porphyrite	-	0.85	11.06	Alk.oliv.basalt	Alkali-olivine basalt	Alk. (hawaiite)
	14 O	Cpx,hbl,plg: porphyr.	3.84	-	-	Thol.basalt	Thol.basalt (Qz)	Transitional (K)
	15 O	Cpx,plg: basalt	-	-	13.21	Oliv.tholeiite	Olivine basalt	Transitional (Na)
	16 O	Plg: amygd.basalt	3.81	-	-	Thol.basalt	Alkali basalt	Alk. (hawaiite)
	17 O	Plg: andesite porph.	-	-	13.71	Alk.oliv.basalt	Alkali-olivine basalt	Transitional (Na)
Middle Horseshoe Fm	1 X	Cpx,hbl,plg: gabbro.	-	-	14.32	Oliv.tholeiite	Thol.oliv/oliv basalt	Alk. (hawaiite)
	2 X	Plg: schistose lava	-	-	1.24	Oliv.tholeiite	Alkali basalt	Alk. (hawaiite)
	3 X	Plg: rhomb-porphyre	1.06	-	-	Thol.basalt	Quartz basalt	Transitional (K)
	4 X	Cpx,hbl,plg: Rh-porph.	-	-	0.71	Oliv.tholeiite	Thol./alkali basalt	Trnasitional (K)
	5 ⊗	Oliv, cpx,plg: gabbro	-	-	16.66	Oliv.tholeiite	Thol.oliv/oliv. basalt	Sub-alk.(flood basalt)
	6 X	Oliv, cpx,plg: Porphyrite	-	-	9.46	Oliv.tholeiite	Olivine basalt	Alk. (trachy basalt)
	7 X	Cpx,plg: amygd.basalt	-	5.79	7.63	Alk.oliv.basalt	Basanite	Alk. (K-basalt)
	8 X	Cpx,hbl,bi,plg: db-por.	1.34	-	-	Thol.basalt	Thol.basalt (Qz)	Transitional (K)
	9 X	Hbl,plg,kf: Porphyrite	-	-	3.30	Oliv.tholeiite	Alkali basalt	Transitional (K)
	10 X	Ol,cpx,bi,plg,qz: por.	-	-	0.73	Oliv.tholeiite	Alkali basalt	Transitional (K)
	11 X	Ol,cpx,plg: porphyrite	-	1.20	12.93	Alk.oliv.basalt	Alkali-olivine basalt	Alk. (trachy basalt)
Edson Hills Fm			Qz	Ol	Ab+An	Classification	Kano (1959)	Miyashiro (1975)
	21 △	Plg: glassy dacite	34.22	9.57	50.47	Dacite	Sub-alkalic	Tholeiite
	22 △	Qz: Dacite	42.57	22.08	23.34	Rhyodacite	Sub-alkalic	Tholeiite
	23 △	Plg,qz: parlite	40.39	16.77	35.80	Dacite	Sub-alkalic	Tholeiite
	24 ⚠	Plg: andesite (Cu-bg)	19.89	4.37	71.18	Andesite	Alkalic	Alkalic (Na)
M.H.Fm	12 ▲	Plg: amygdaloid.lava	30.95	13.42	41.85	Dacite	Sub-alkalic	Tholeiite

Table 13. Chemical analyses of the Pre-Middle Cambrian magmatic rocks from the Heritage Range, Ellsworth Mountains

No.	SiO_2	TiO_2	Al_2O_3	Fe_2O_3	FeO	MnO	MgO	CaO	Na_2O	K_2O	P_2O_5	H_2O	Total	Cr	Ni	Co	Ba	Sr	Rb	Cu	V	Zr
1	52.31	.98	15.81	1.64	6.60	.15	6.44	7.22	4.28	1.90	.27	2.33	99.93	150	160	60	660	1150	80	130	240	98
2	51.08	1.01	17.15	8.83	1.40	.11	1.87	5.24	5.15	2.62	.29	4.68	99.43	44	109	65	625	210	74	114	173	28
3	51.34	1.50	17.13	3.73	4.20	.12	3.40	7.56	3.38	3.22	.57	2.37	98.52	82	142	64	990	815	73	106	240	254
4	51.71	1.46	15.04	2.29	6.60	.15	5.90	6.39	2.95	3.15	.41	2.49	98.54	200	160	65	775	750	85	180	237	56
5	49.25	.77	14.40	1.73	6.50	.14	10.51	9.15	2.55	1.46	.12	3.15	99.73	636	323	77	450	440	45	170	95	30
6	51.13	1.16	16.77	2.57	5.30	.13	6.61	7.24	3.44	2.53	.25	2.74	99.87	45	145	89	880	690	65	167	189	110
7	45.17	1.47	14.60	10.30	2.10	.15	6.43	8.27	3.77	2.20	.56	4.88	99.90	175	185	85	520	370	40	125	255	100
8	49.48	1.17	17.60	4.58	5.20	.16	5.39	8.31	2.76	1.86	.30	2.69	99.50	69	124	64	445	590	45	108	210	107
9	48.59	1.62	15.68	6.89	3.20	-	7.18	4.84	.99	6.49	.63	3.68	99.79	44	105	83	650	330	43	338	247	68
10	50.92	1.15	17.12	3.14	5.90	.16	5.35	6.55	2.76	3.15	.28	2.95	99.43	74	127	50	940	350	80	74	196	56
11	50.41	.62	15.78	5.35	5.40	.14	6.64	6.45	4.04	2.60	.21	3.24	100.88	159	162	44	480	670	60	53	150	86
12	69.30	.63	11.89	1.69	5.30	.14	.92	1.28	3.78	2.16	.09	2.18	99.36	201	196	67	675	670	65	144	100	435
13	48.08	1.27	15.77	1.65	6.00	.11	4.75	7.54	4.02	1.65	.31	8.36	99.51	78	150	96	465	510	65	150	185	120
14	49.45	1.24	16.59	3.61	3.50	.11	3.97	7.22	2.78	2.65	.30	8.59	100.01	96	142	29	700	680	80	117	195	118
15	50.83	1.32	18.14	3.54	5.90	.16	5.92	5.68	5.14	.87	.34	2.94	100.78	40	135	75	530	915	20	125	212	113
16	51.67	.88	14.60	7.54	1.30	.19	1.69	8.66	4.29	2.15	.24	6.33	99.54	73	105	41	600	42	70	128	146	56
17	47.47	1.20	18.51	4.99	5.00	.16	5.37	5.61	5.22	.58	.30	5.01	99.42	51	117	92	175	780	25	133	226	80
18	47.75	1.98	15.42	-	9.70	.14	8.07	8.31	2.85	.43	.37	4.38	99.40	218	198	65	340	460	12	144	305	38
19	49.13	1.52	15.10	3.39	6.30	.15	7.77	7.91	2.93	2.53	.59	2.83	100.15	171	175	67	810	1240	35	71	225	136
20	49.42	1.40	14.11	2.01	5.80	.13	4.91	9.37	2.46	1.59	.60	8.97	100.77	250	210	85	455	715	35	160	218	97
21	75.15	.11	11.03	.15	2.50	.04	.53	.49	5.13	1.56	.01	2.89	99.59	173	100	67	265	133	60	72	20	145
22	74.20	.42	11.61	2.10	3.80	.10	.20	.03	2.47	3.56	.05	1.15	99.69	92	144	46	1270	100	115	145	77	672
23	76.26	.32	10.33	1.06	2.80	.05	.54	.89	3.37	2.73	.05	1.14	99.54	113	104	48	530	95	45	82	237	280
24	70.60	.33	14.40	1.96	1.90	.04	.32	1.34	7.54	.74	.10	1.35	100.62	61	110	61	190	205	65	750	50	80
a	50.14	1.85	18.84	3.27	7.03	.15	2.22	8.51	5.04	1.39	.67	1.02	100.13	88	110	61	590	730	17	127	277	136
b	49.40	1.91	17.97	2.17	8.30	.17	4.42	7.41	3.54	1.57	.24	1.77	98.87	78	157	95	675	718	40	84	300	47
c	46.74	2.80	14.76	2.69	11.30	.23	4.53	7.68	3.35	1.48	.39	3.56	99.51	49	135	76	640	380	15	143	420	75
d	57.36	1.63	15.33	2.14	7.50	.16	3.54	6.82	3.66	.50	.36	1.10	100.10	105	27	73	240	500	20	68	220	123
e	46.09	2.12	15.46	1.92	8.21	.25	3.24	7.91	4.95	.28	.62	8.45	99.50	46	102	51	140	375	17	66	134	112
f	47.11	3.66	11.70	2.25	14.56	.26	5.18	9.61	3.09	.50	.51	.82	99.25	92	127	100	360	430	-	138	590	56

1—24: refer to Table 3. a—f: Late Paleozoic magmatic rocks, a: gabbro pegmatite, b: plagioclase porphyritic gabbro, c: medium-grained gabbro, d: quartz gabbro, e: coarse-grained gabbro, f:porphyrite dyke.

Table 14. Norm values of the Pre-Middle Cambrian magmatic rocks and the Late Paleozoic igneous rocks

No.	Qz	Or	Ab	An	Ne	Wo	Hy	Di	Ol	Mt	He	Il	Ap	Sal.	Fem.	Mol % An in Pl
1	-	11.36	38.87	18.49	-	-	0.55	12.73	14.32	1.73	-	1.37	0.58	68.72	31.28	32
2	-	16.40	48.95	16.91	-	-	0.57	6.88	1.24	1.23	5.70	1.49	0.65	82.25	17.75	26
3	1.06	19.87	31.73	23.03	-	-	7.02	9.79	-	4.07	-	2.18	1.24	75.69	24.31	42
4	-	19.39	27.56	19.29	-	-	18.78	8.73	0.71	2.49	-	2.12	0.90	66.27	33.73	41
5	-	8.77	23.32	23.99	-	-	6.92	17.16	16.66	1.84	-	1.10	0.25	56.07	43.93	51
6	-	15.27	31.21	23.44	-	-	6.53	9.18	9.46	2.74	-	1.64	0.54	69.91	30.09	43
7	-	13.76	26.14	17.35	5.79	-	-	17.70	7.63	1.90	6.31	2.17	1.24	63.05	36.95	40
8	1.34	11.41	25.73	31.33	-	-	15.32	7.55	-	4.97	-	1.70	0.65	69.82	30.18	55
9	-	40.25	9.34	20.18	-	-	16.16	0.52	3.30	4.25	2.21	2.38	1.41	69.77	30.23	68
10	-	19.34	25.72	25.99	-	-	17.86	4.68	0.73	3.41	-	1.66	0.61	71.05	28.95	50
11	-	15.59	34.87	17.53	1.20	-	-	10.86	12.93	5.68	-	0.88	0.46	69.19	30.81	34
12	30.95	13.42	35.75	6.10	-	-	9.38	-	-	1.86	-	0.93	0.19	87.63	12.37	(C=1.40)15
13	-	10.60	37.84	21.88	0.85	-	-	13.27	11.06	1.88	-	1.92	0.70	71.17	28.83	37
14	3.84	17.19	27.39	27.43	-	-	9.61	7.79	-	4.14	-	1.90	0.69	75.86	24.14	50
15	-	5.18	46.45	24.05	-	-	3.12	1.68	13.21	3.73	-	1.85	0.72	75.69	24.31	34
16	3.81	13.80	41.78	15.45	-	6.41	-	10.75	-	1.30	4.83	1.32	0.55	74.84	25.16	27
17	-	3.55	46.53	26.52	1.45	-	-	0.38	13.71	5.45	-	1.74	0.66	78.06	21.94	36
18	-	2.65	26.84	29.40	-	-	17.60	9.05	10.76	-	-	2.89	0.81	58.89	41.11	52
19	-	15.28	26.93	21.09	-	-	5.45	12.12	12.06	3.63	-	2.17	1.26	63.30	36.70	44
20	4.51	10.31	24.28	25.04	-	-	12.60	17.43	-	2.31	-	2.15	1.37	64.14	35.86	51
21	34.22	9.57	47.99	2.48	-	-	5.36	-	-	0.17	-	0.15	0.02	94.29	5.71	(C=0.03) 5
22	42.57	22.08	23.34	-	-	-	4.77	-	-	2.31	-	0.62	0.05	92.23	7.75	(C=4.24) 0
23	40.39	16.77	31.56	4.24	-	-	4.92	-	-	1.16	-	0.47	0.11	93.35	6.65	(C=0.39)12
24	19.89	4.37	67.89	3.29	-	0.13	1.92	-	-	1.41	0.44	0.47	0.21	95.44	4.56	5
a	-	8.29	39.29	24.96	3.92	-	-	10.64	5.41	3.46	-	2.61	1.43	76.46	23.54	39
b	-	9.62	32.93	29.49	-	-	9.92	5.52	6.88	2.35	-	2.76	0.53	72.04	27.96	47
c	-	9.28	31.96	22.19	-	-	4.71	12.44	11.41	2.98	-	4.15	0.87	63.43	36.57	41
d	-	3.11	29.14	17.42	-	-	10.90	23.30	7.18	2.47	-	5.36	1.12	49.68	50.32	37
e	11.85	3.06	33.72	24.53	-	-	15.23	6.22	-	2.29	-	2.33	0.76	73.15	26.85	42
f	-	1.83	43.59	21.03	3.18	-	-	14.14	9.36	2.21	-	3.25	1.42	69.63	30.37	33

C:corundum

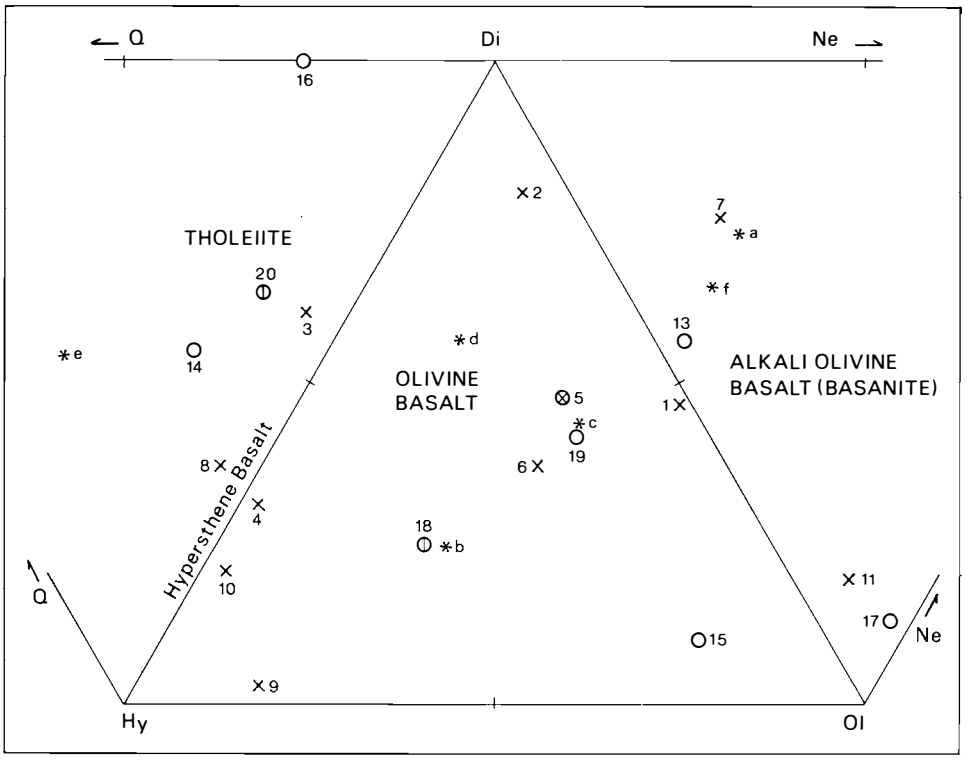

Fig. 6. *Norm classification of the basic rocks (after Yoder and Tilley 1962). Symbols and Nos. refer to Table 12. Stars: the late Paleozoic igneous rocks of Wilson Nunataks.*

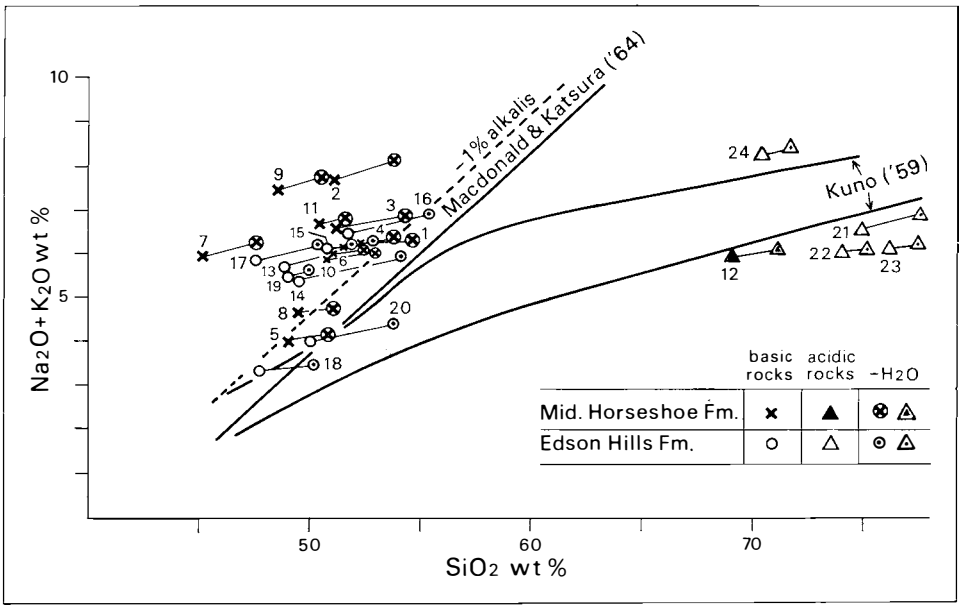

Fig. 7. *Alkali-SiO_2 diagram of the pre-Middle Cambrian volcanic rocks. Symbols and Nos. refer to Table 12. — H_2O: anhydrous base.*

and Katsura 1964). If 1% of alkalis was subtracted to adjust for a presumable addition during secondary processes, 37% becomes sub-alkalic. The Edson Hills Formation has a higher proportion of sub-alkalic rocks (Table 15). The alkalic rocks were classified after Middlemost (1975), with unhydrous base and without subtraction of 1% alkalis, as shown in Table 16. All transitional rocks of the Middle Horseshoe Formation are K-alkalic (see Table 12), then, the K-alkalic rocks occupy 67% (91% of the basic rocks) of the analysed rocks from this formation. In the Edson Hills Formation, the Na-alkalic rocks (hawaiite) comprise more than twice the amount of the K-alkalic rocks, including the transitional rocks. From Table 12, a shift of chemical characteristics of the basic rocks from K-alkalic, via Na-alkalic >> K-alkalic, to tholeiites >> calc-alkalic+K-alkalic in ascending stratigraphic order is evident, associating with a distinct increase of acidic rocks in the later phase.

Stable minor elements were examined to estimate the tectonic setting of the volcanism. The TiO_2 and P_2O_5 are plotted in Fig. 8A (Bass et al. 1973). Most present basic rocks have higher P_2O_5 and lower TiO_2 than the oceanic rocks, being projected in and around edges of the field of continental alkalic rocks. Sample No. 5, the gabbro boulder from the conglomerate, is the only sub-alkalic rock in the Middle Horseshoe Formation.

The Sr-Zr diagram, Fig. 8B, showing high contents of Sr, also supports the conclusion that the present basic rocks are of a non-oceanic type.

Most of the heavy metallic elements, i.e. Ni, Co, V, Cr, and Cu, show small variations in the large range of differentiation represented by the FeO^*/MgO value. One example is shown in Fig. 9A. The almost horizontal trend of the Ni contents is clearly different from that of the abyssal and the continental margin rocks (Miyashiro 1975). The Ni contents of the present acidic rocks is distinctly higher than that of the oceanic rocks and the continental tholeiites as shown in Figs. 9A and 9B, while that of the basic rocks overlaps the fields of the latter.

It can be concluded that the present rocks are of non-oceanic types, and the association of shallow sea sediments on the continental crust as oolitic limestone and coarse-grained clastics support this conclusion.

The K-alkalic volcanic rocks are distributed in limited tectonic settings on the present earth's surface: the back-arc areas and the rift tectonic zones. Therefore, the differentiation trends of the major elements of the present rocks were compared with those of various alkalic rocks from other regions in Figs. 10A, -B, -C, and -D, as Miyashiro (1974 and 1975) did for the ophiolites of the orogenic zones. Since the FeO^*/MgO values of the present basic rocks are mostly lower than 2.0, no conclusive idea is obtained from the SiO_2 and FeO^* diagrams. However, rapid increases of the TiO_2 and K_2O in the basaltic composition range suggest a trend similar to that of the continental and back-arc type alkalic rocks. A small amount of intermediate rocks (the proportion among the analysed rocks may be representative for the actual abundance) in the present case reduces the possibility of a back-arc

Table 15. Percentages of the sub-alkalic rocks with different bases of classification

		anhydrous base						anhydrous -1% alk					
		TH		CA		total sub-alk		TH		CA		total sub-alk	
Edson Hills Formation (n=12	basic (n=8)	13	34	13	8	26	42	25	42	25	17	50	59
	acidic (n=4)	75		0		75		75		0		75	
Middle Horseshoe Formation (n=12)	basic (n=11)	0	8	9	8	9	16	9	17	18	17	27	34
	acidic (n=1)	100		-		100		100		-		100	

Table 16. Percentages of the alkalic rocks

	K-alk	Na-alk	Trans.		Total alk		
Edson Hills Fm. (n=12)	0	25	33	K: 16.5 Na:16.5	basic (n=8)	75	58
					acidic (n=4)	8	
Middle Horseshoe Fm. (n=12)	25	17	42	K: 42 Na: 0	basic (n=11)	91	84
					acidic (n=1)	0	

Table 17. Abundance of various rock series comparing with the continental alkalic rock provinces (in % of the analysed rocks)

	Ellsworth Mts		Ethiopia		Circum Japan Sea (n=92)
	Mid HS Fm (n=12)	Edson Hills Fm (n=12)	Trap Series (n=73)	Aden Series (n=65)	
CA	8	8	1	3	7
TH	8	42	30	42	41
Na-alk	17	34	32	29	23
K-alk	67	16	37	26	26
Intermediate rocks ($55 < SiO_2 70$)	0	33	18	22	34
Acidic rocks ($SiO_2 > 70$)	8	0	29	30	30

Table 18. Partial analyses of alkali-elements of the Late Paleozoic igneous rocks

No	K ppm	Rb ppm	Sr ppm	K/Rb
HJ 59C	116	.58	523.84	200.0
YO/60E	3387	5.35	343.67	633.1
74-YO 160	7488	24.99	326.44	299.6
WS 32.1	8053	28.46	261.95	283.0
WS 32.2	10419	34.49	288.97	302.1
HJ 59B	21112	84.83	284.59	248.9
HJ 59A	37300	127.77	171.24	291.9

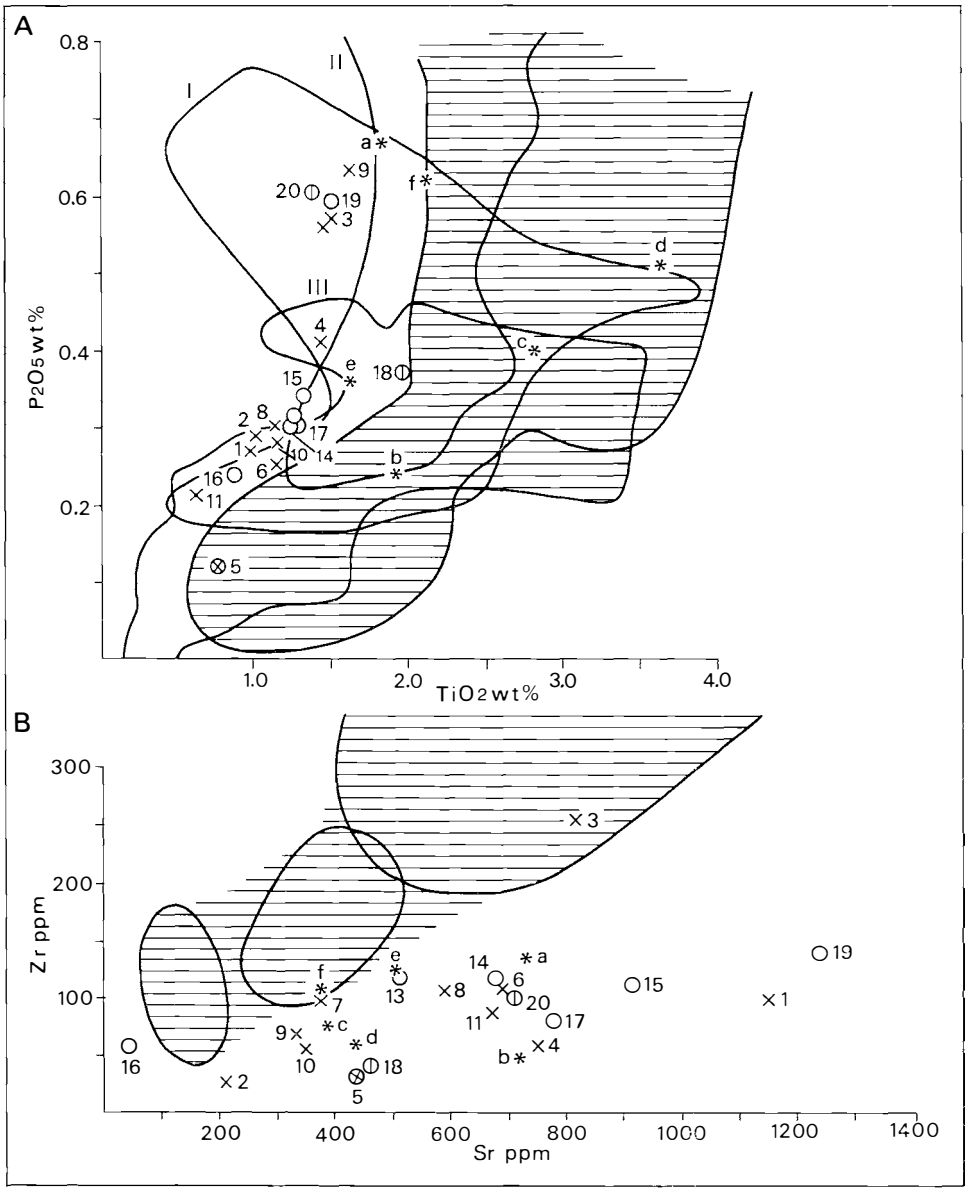

Fig. 8. *Minor element ratios.*

Symbols and Nos. refer to Table 12. Stars: the late Paleozoic igneous rocks.

8-A: *P_2O_5-TiO_2 ratios. Lined area: oceanic basalts (Pacific: Bass et al. 1973, Hawaiian alkalic rocks: Macdonald and Katsura 1964, Galapagos alkalic rocks: McBirney and Williams 1969). Curves: I — Ethiopian Trap series (Mohr 1960), II — Circum Japan Sea alkalic rocks (Ono 1962), III — Mesozoic dolerites of Gondwanian continent (Karroo and Ferrar dolerites).*

8-B: *Zr-Sr ratios. Lined area: oceanic basalts (after Bass et al. 1973).*

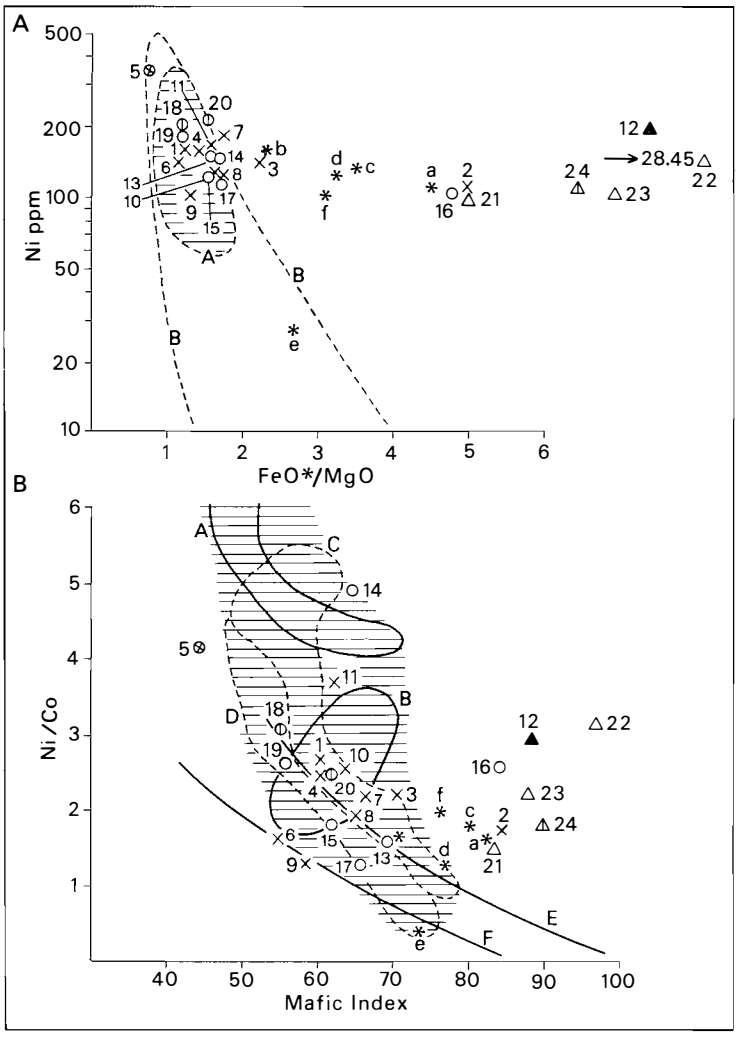

Fig. 9. *Differentiation of minor elements.*
Symbols and Nos. refer to Table 12. Stars: late Paleozoic igneous rocks.
9-A: *Ni differentiation. Lined area: A — abyssal basalts. Broken curve: basalts of island-arcs and active continental margins (both A and B after Miyashiro 1974).*
9-B: *Ni/Co ratios to the mafic index. Lined area: oceanic basalts, including curves A and B of Ford (1970) and C and D of Fleischer (1968). Solid lines: Continental dolerites, E — Skaergaard rocks and F — Tasmanian dolerites, both after Fleischer (1968).*

origin. In the African Rift zone, the earlier volcanism tends to have more K-alkalic rocks and less intermediate+acidic rocks (Table 17). Referring to this tendency, the volcanic rocks of the Middle Horseshoe Formation can be considered as the products of an early stage of rift tectonics on a continental crust.

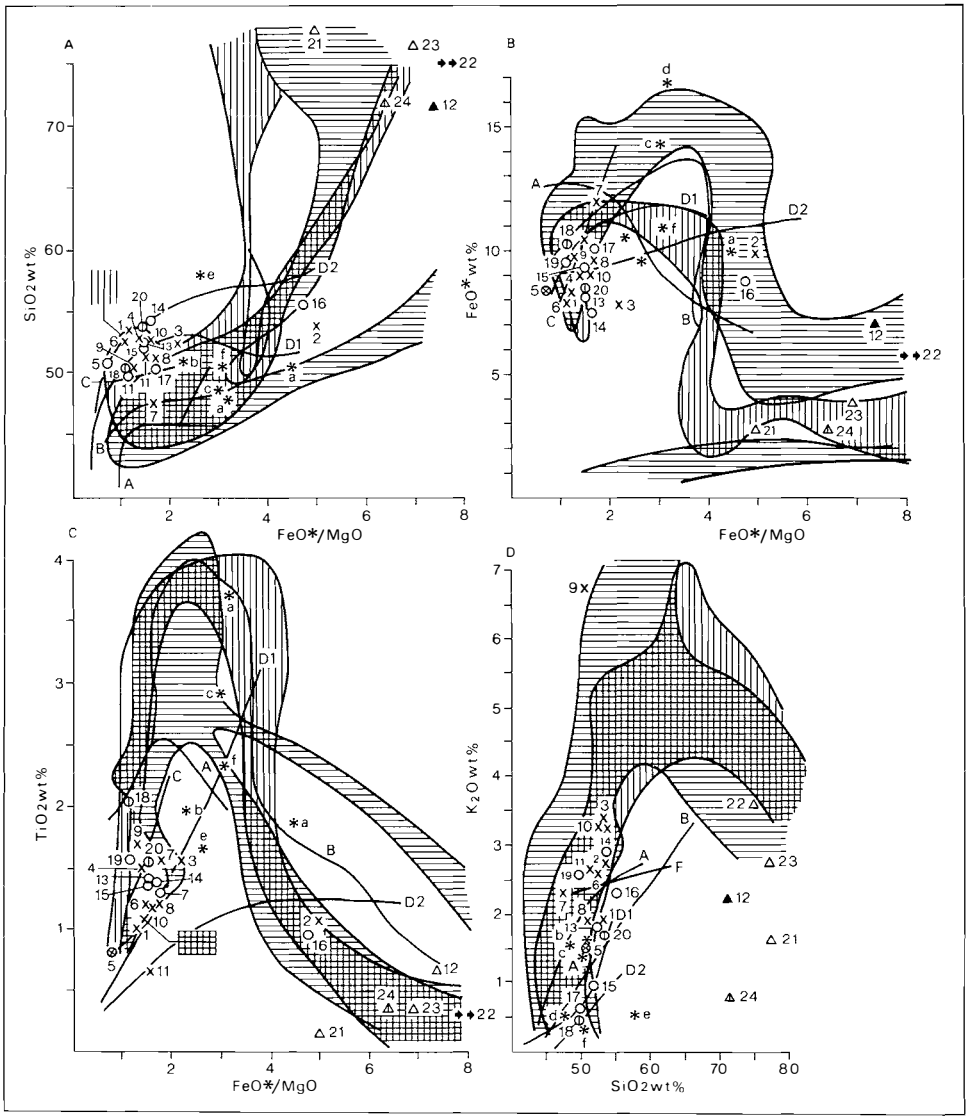

Fig. 10. *Oxide differentiation trends in terms of FeO*/MgO and SiO_2 wt. %. Symbols and Nos. refer to Table 12. Stars are the late Paleozoic igneous rocks.*

10-A: *SiO_2 differentiation.*

Horizontally lined area: alkalic rocks from African Rift Valley. Vertically lined area: Circum Japan Sea alkalic rocks. Curves: A — Hawaiian alkalic rocks, B — Galapagos alkalic rocks, C — abyssal basalts, D — Mesozoic dolerites of Gondwanian continent, D-1 Karroo dolerites, D-2 Ferrar dolerites. These are the same in 10-B, -C and -D.

10-B: *FeO* differentiation ($FeO^* = FeO + 0.9Fe_2O_3$).*

10-C: *TiO_2 differentiation.*

10-D: *K_2O-SiO_2 diagram.*

LATE PALEOZOIC IGNEOUS ROCKS

Petrography:

These rocks were observed in the Wilson Nunataks. The gabbro occurs as a small sheet-like stock 80 m thick, and porphyrite dykes a few metres wide cut both the gabbro and the country rocks. The contact of the gabbro to the country rocks is sharp and has a narrow zone of thermal metamorphism; shale was hardened by silicification and spots of chlorite were formed. The gabbro sent out some echelon dykes from the main body 300 m to the north. These gabbro dykes have a large variation of lithology among and within the dykes: medium-grained homogeneous facies, pegmatoids, feldspar porphyritic facies and diabasic rocks, and associated silicified and layered inclusions of shale.

The hornblende porphyrite dykes shows weak flowage structures and many cavities. No deformation has been observed, but all constituent minerals were strongly altered. Hornblende phenocrysts are represented by the pseudomorph of secondary minerals and some relic clinopyroxene grains occur in the hornblende.

The gabbro shows distinct ophitic texture, but the primary minerals are totally decomposed. Clinopyroxene and plagioclase are rarely included in the hornblende. A large amount of opaque minerals, showing a peculiar grid-pattern, is characteristic. Some parts of dense rocks have interstitial quartz and biotite due to contamination from the surrounding rocks. Seams of plagioclase porphyroblasts, with sub-idiomorphic grains up to 1—2 cm size, occur locally concordant to the walls of the gabbro dyke. The main facies of gabbro is a medium-grained ophitic hornblende gabbro, partly grading into coarse- and fine-grained facies.

Chemistry:

Five litholigic varieties of the gabbro and a hornblende porphyrite were analysed by the same methods as the pre-Middle Cambrian volcanics, and the results are shown in Tables 13 and 14. Most rocks, excluding the contaminated one (sample e), have less than 50% SiO_2, no normative quartz and high TiO_2 and FeO (i.e. normative ilmenite). The pegmatitic gabbro and the porphyrite have normative nepheline and are alkalic basalt in composition (Fig. 6).

The main facies of the gabbro is Fe-rich, Na-alkalic rock, and the plagioclase pophyroblastic and coarse-grained ophitic ones are transitional rocks of a Na-alkalic type after Middlemost (1975). The contaminated rock is projected in the tholeiite field of the norm classification (Fig. 6). On the alkali-SiO_2 diagram (Fig. 11A), all uncontaminated rocks are alkalic, even if 1% of the alkalis is substracted as secondary modification, and are hawaiite and Na-basalt (Fig. 11B). On the cation triangular diagram (Fig. 12), low total Fe, especially low Fe^{+3} indicating low oxidation conditions, and high Na are characteristic. The differentiation trends do not fit in with any Mesozoic basic rocks of the Transantarctic Mts. (Gunn 1966; Ford 1970) or

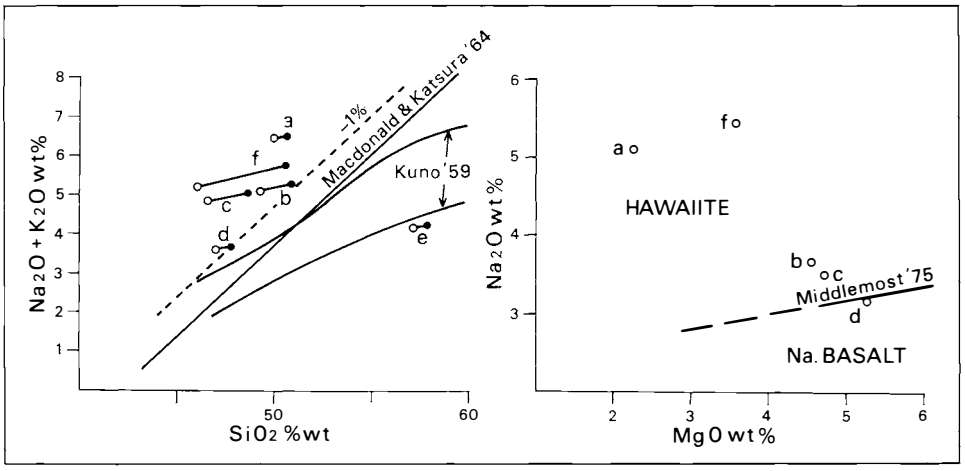

Fig. 11. *Classification of the late Paleozoic igneous rocks of Wilson Nunataks.*
a—f: see Table 12.
11-A: *Alkali-SiO_2 diagram. Open circles: on hydrous base. Dots: on anhydrous base.*
11-B: *Classification of the alkalic rocks (after Middlemost 1975).*

Dronning Maud Land (Neethling 1972). A rhyolite-andesite series of Jurassic volcanics and K-rich affinity of keratophyre of the Carboniferous period in the Antarctic Peninsula (Adie 1972) show little similarity with the present rocks.

No oceanic characters are seen in Figs. 8B, 9A and 9B. However, in the TiO_2-P_2O_5 diagram (Fig. 8A), the present rocks are projected mostly in the field of oceanic rocks. But their occurrence, cutting through several thousands of metres of shallow sea sediments, does not support their oceanic floor origin.

The solitary nature is also shown by the Sr/Rb ratios and by the high Sr contents (Fig. 13A) of seven additional partial analyses of K, Sr, and Rb (Table 18). The $Sr^{87/86}$ ratios of the Mesozoic dolerites in Gondwanaland show two groups: the Karroo - Serra Geral type having low $Sr^{87/86}$ ratios, and the Ferrar - Tasmanian one with high ratios (Compston et al. 1968). These two groups are well separated by the K/Rb ratios, having the border line around K/Rb = 300 (Erlank and Hofmeyr 1966, 1968; Gunn 1965; and Faure et al. 1974). The K/Rb ratios of the present rocks have a frequency mode lower than 300 (Fig. 13B) and this suggests a high $Sr^{87/86}$ ratio as in rocks which have been assumed to be formed by the mixing of crustal materials in magma. This is an additional indirect support of a non-oceanic origin of the present rocks. Some high K/Rb ratios of the present rocks may be caused by high modal contents of hornblende as Jakes and White (1970) have shown.

In Figs. 10A, -B, -C, and -D, the SiO_2, TiO_2 and K_2O differentiations are well comparable with the trends of the continental alkalic rocks.

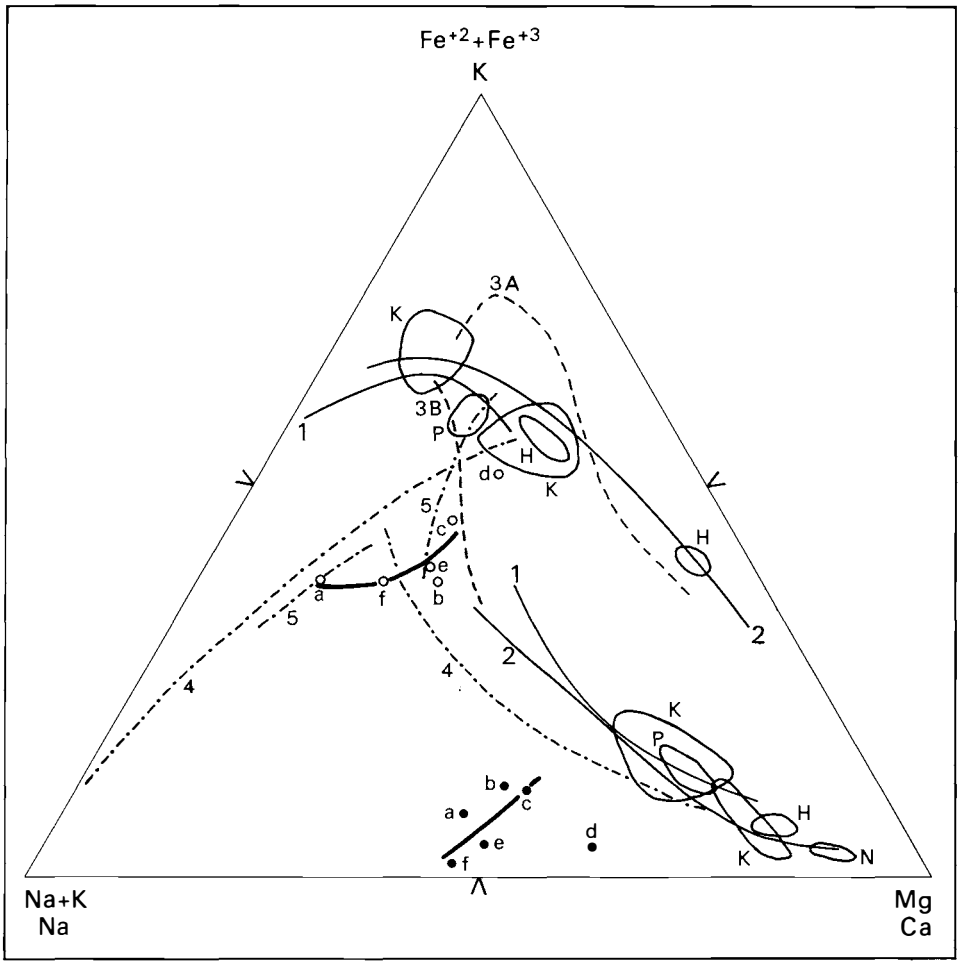

Fig. 12. *Cation ratios of the late Paleozoic igneous rocks. a—f: refer to Table 12. Solid curves: Ferrar dolerites from various localities. K — Kirkpatrick basalts (Elliot 1972). N — Lake Vanda Sill, H — hypersthenic tholeiites, P — pigeonitic tholeiites (N,H, and P after Gunn 1966), 1 — New Mt. Sill (Gunn 1966), 2 — Paleozoic(?) - Mesozoic Borg intrusion, Dronning Maud Land (Neethling 1972), Broken curves: Dufek intrusion, Pensacola Mts. (Ford 1970). 3-A: mafic trend, 3-B: felsic trend. Chained curves: volcanic rocks of Antarctic Peninsula (Adie 1972). 4 — Jurassic rhyolite-andesite suit, 5 — Carboniferous keratophyres. Thick solid curves: present rocks.*

Structure

The main structures which are shown in Figs. 1 and 14, are relatively simple. The dips and strikes in the Crashsite Quartzite areas are those of the average trend of a lithologic unit.

REGIONAL FOLD STRUCTURES

The major anticline, actually an anticlinorium, runs almost linear in the NW-SE strike along the western part of the mapped area. The axial plunge is

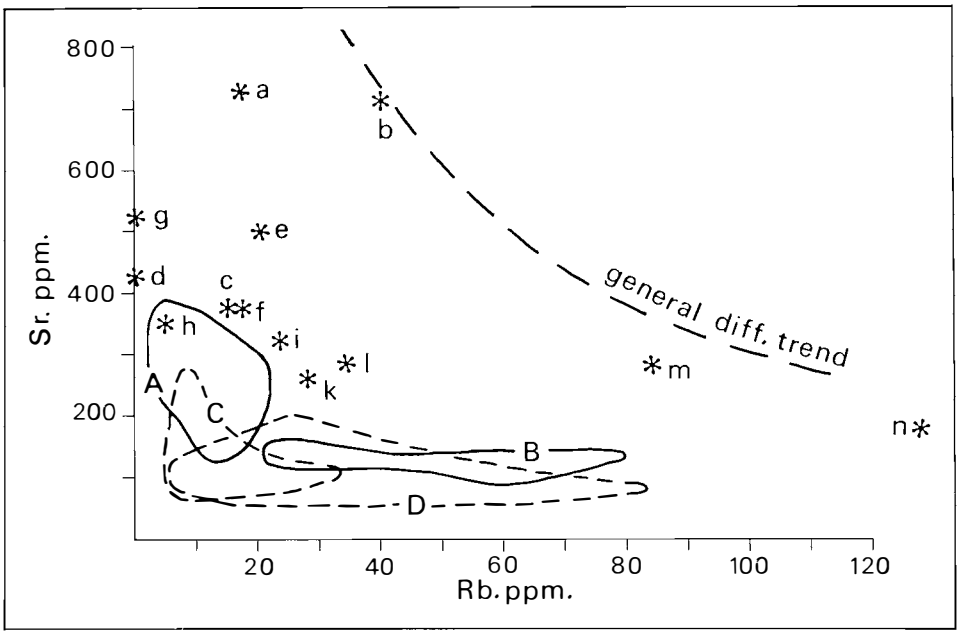

Fig. 13. *Minor element ratios of the late Paleozoic igneous rocks. a—f refer to Table 12, for g—n, see Table 18.*
13-A: *Sr-Rb ratios. Mesozoic dolerites (Faure and Elliot 1971): A — Dronning Maud Land, B — Transantarctic Mts., C — post-Borg tholeiites of Mesozoic(?) age. Precambrian Borg tholeiites: D — Dronning Maud Land (C and D after Neethling 1972).*

very gentle or horizontal in the south, and to the NW in the north of the Union Glacier. The fold style is cylindrical and asymmetric with a steep eastern limb. The western limb shows a homoclinal structure with moderate SW dips as far as observed. This structure indicates tectonic translation from the SW.

Another regional anticline occurs in the SE around the Wilson Nunataks, having a cylindrical and symmetric style, with the axis striking NW-SE and a gentle NW plunge. This structure is presumptive and based on the interpretation that the rocks in this area are of the Heritage Group.

Between these two anticlines, a synclinorium of the Crashsite Quartztite about 30 km wide occurs. The structure drawn after the calculated fold envelopes is very gentle, the axis is located asymmetrically in the eastern part, and the local fold axes have gentle plunges both to the N and S. The style of the local folds is asymmetric, cylindrical, having steep eastern limbs, some are overturned to the east (Fig. 14).

The Whiteout Conglomerate in the Meyer Hills shows a local shallow syncline with the limbs dipping less than 50g.

All these regional structures were, no doubt, formed in a single deformation system by tectonic pressure from the SW. The age of deformation is un-

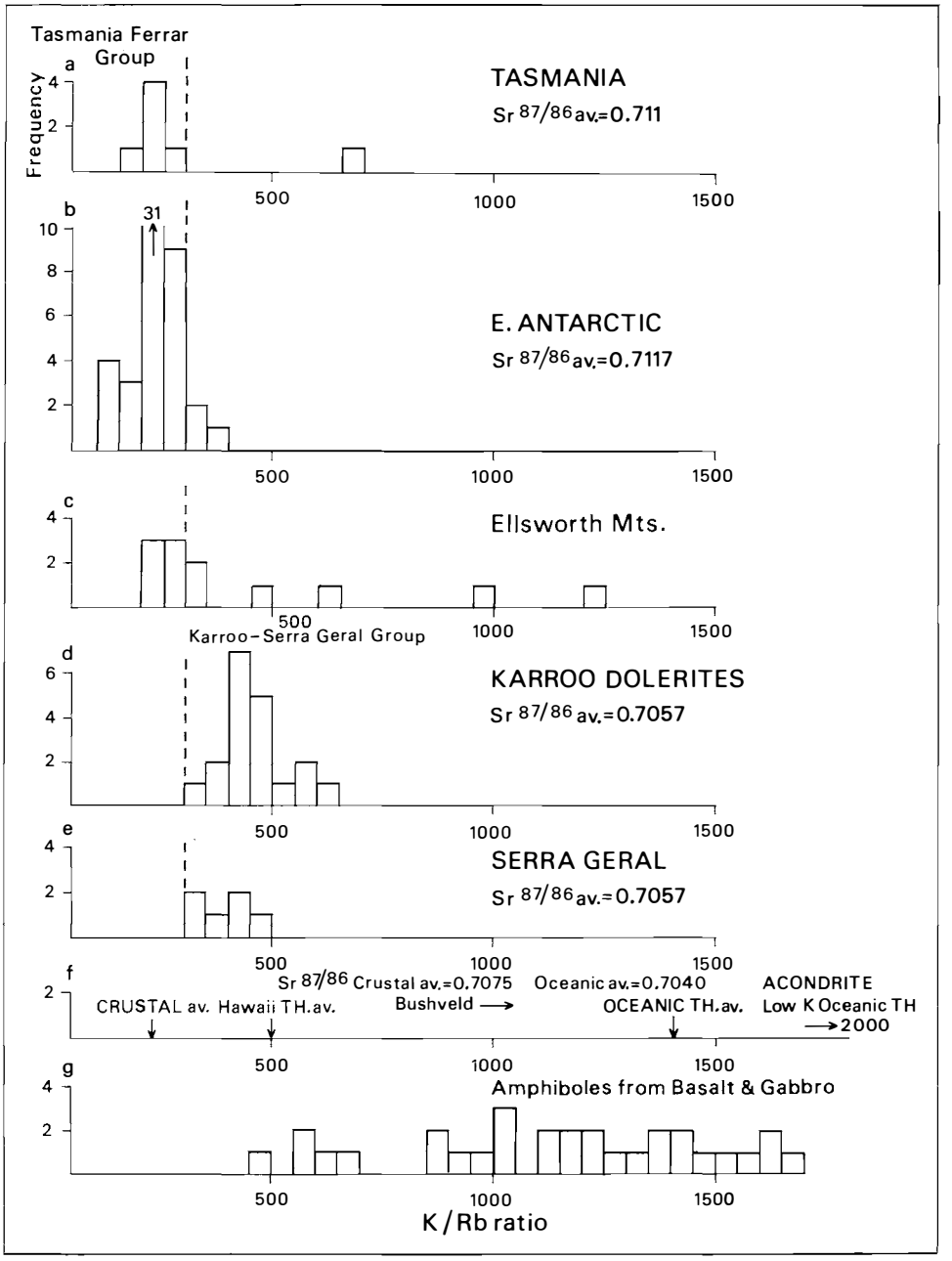

13-B: *K-Rb ratios in relation to the other Gondwanian Mesozoic dolerites. a: after Compston et al. 1967 and Erlank and Hofmeyr 1966, b: after Compston et al. 1968, Gunn 1966, and Faure et al. 1974, c: present area, d: MacDougall 1963 and Erlank and Hofmeyr 1966, e: Erlank and Hofmeyr 1966, f: Taylor 1967, g: Jakes and White 1970.*

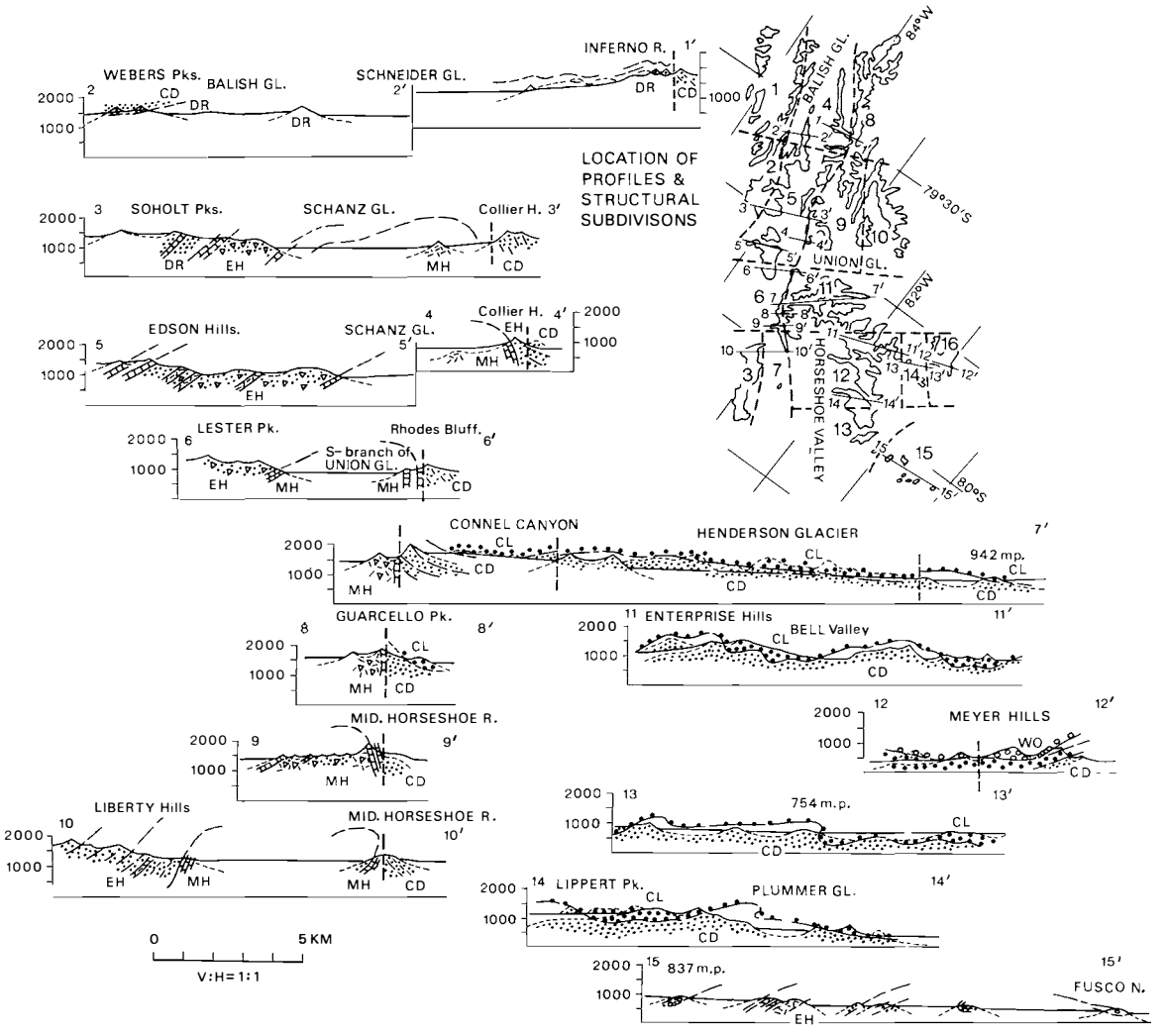

Fig. 14. *Geologic profiles of the southern Heritage Range. MH: Middle Horseshoe Formation, EH: Edson Hills Formation, DR: Dunbar Ridge Formation, CD: dark member of the Crashsite Quartzite, CL: light member of the Crashsite Quartzite, WO: Whiteout Conglomerate.*

known. The youngest Whiteout Conglomerate was included in the deformation, and accordingly the main deformation phase is later than the Permo-Carboniferous tilloid period. However, the possible clino-unconformity at the base of the Whiteout Conglomerate suggests that deformation may have started before the Late Paleozoic glaciation in this area.

THE FAULTS

Two systems of faults, the strike faults and the transverse faults, occur in this area and both are of a dip-slip nature along steep or vertically dipping fault planes.

The largest one cuts the eastern limb of the major anticline in the total length of the mapped area. The fault plane is almost vertical with downthrow of the eastern block, and locally a reverse fault develop with steep western dips. The throw is calculated to several km in the south and several hundreds of metres in the north; thus, this is a hinge fault. This fault sends a sub-parallel branch into the Collier Hills, having the same sense of displacement.

A small strike fault occurs in the NW part of the Enterprise Hills, being a hinge fault with an opposite sense of rotation from the largest one. This fault disappears in the middle of the Enterprise Hills. A small oblique fault in the southern part of the Enterprise Hills, estimated on airphotos, may be a continuation of this fault.

The strike fault in the middle of the Meyer Hills has a vertical fault plane with few hundred metres' downthrow of the eastern block. The fault zone is about 100 m wide in the southern part.

Two transverse faults occur along the Union Glacier and were detected by the displacements of the oolitic limestone bed at Rhodes Bluff. The fault planes are vertical, and the throw is vertical, the northern blocks were down-thrown less than 100 m. The trend of these faults is parallel to the direction of the cross-joint system (Fig. 16).

THE LOCAL FOLD STRUCTURES

All regional structures include numerous parasitic folds, especially in the Crashsite Quartzite. The folds are of tight chevron and isoclinal styles and have less than a hundred metres wave length with large amplitudes. The mesoscopic structural elements were summarized for 16 subareas as shown in Fig. 15.

All girdles of the bedding planes show cylindrical folds of the NW-SE striking axes with moderate to gentle plunges. The major anticline has an axial culmination in the No. 6 subarea, the northern edge of which is cut by the transverse faults. The southern subarea No. 7 is actually composed of scattered nunataks and the girdle pattern suggests a fault block structure.

Very gentle and horizontal axes are common in the synclinorium area. Subarea No. 15 may consist of fault blocks. The Meyer Hills, subarea No. 16, shows almost horizontal fold axes.

The poles of these bedding girdles coincide well with the observed fold axes and lineations represented by the intersection of the cleavages and bedding. Almost all bedding patterns show the maxima on the eastern limb with steep dips, indicating the tectonic transport from the SW.

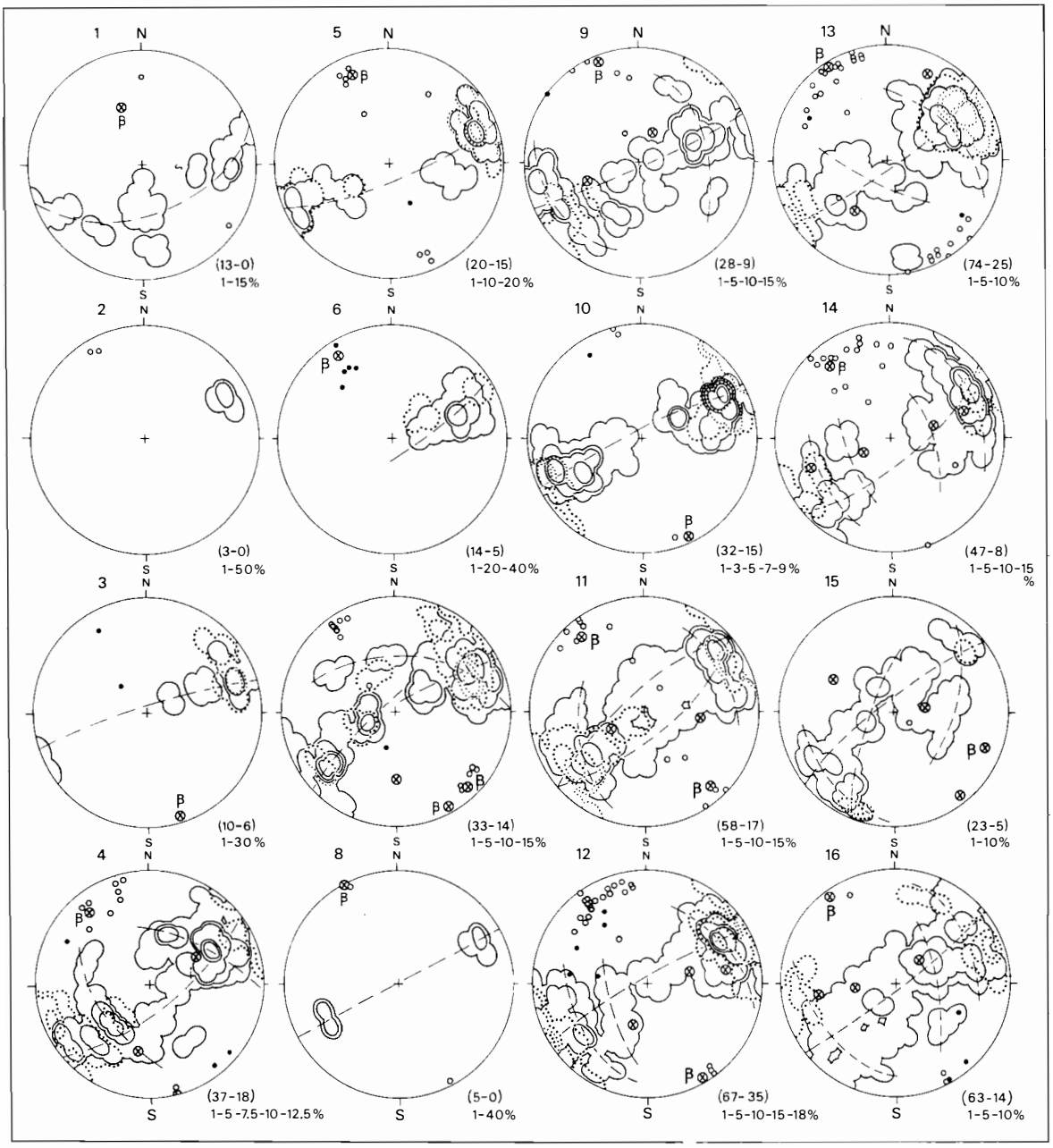

Fig. 15. *Fabric diagrams of the subareas (subdivision is shown in Fig. 14).*
Full-line contours: beddings, the percentages are shown at the right bottom of each figure. Dotted contours: cleavages. Circle with cross and β: calculated main fold axis. Circle with cross: subordinate fold axes. Open circle: observed small fold axes. Dots: observed other lineations. Nos. in brackets to the right at the bottom of each figure: No. of observed bedding and No. of observed cleavage, respectively.

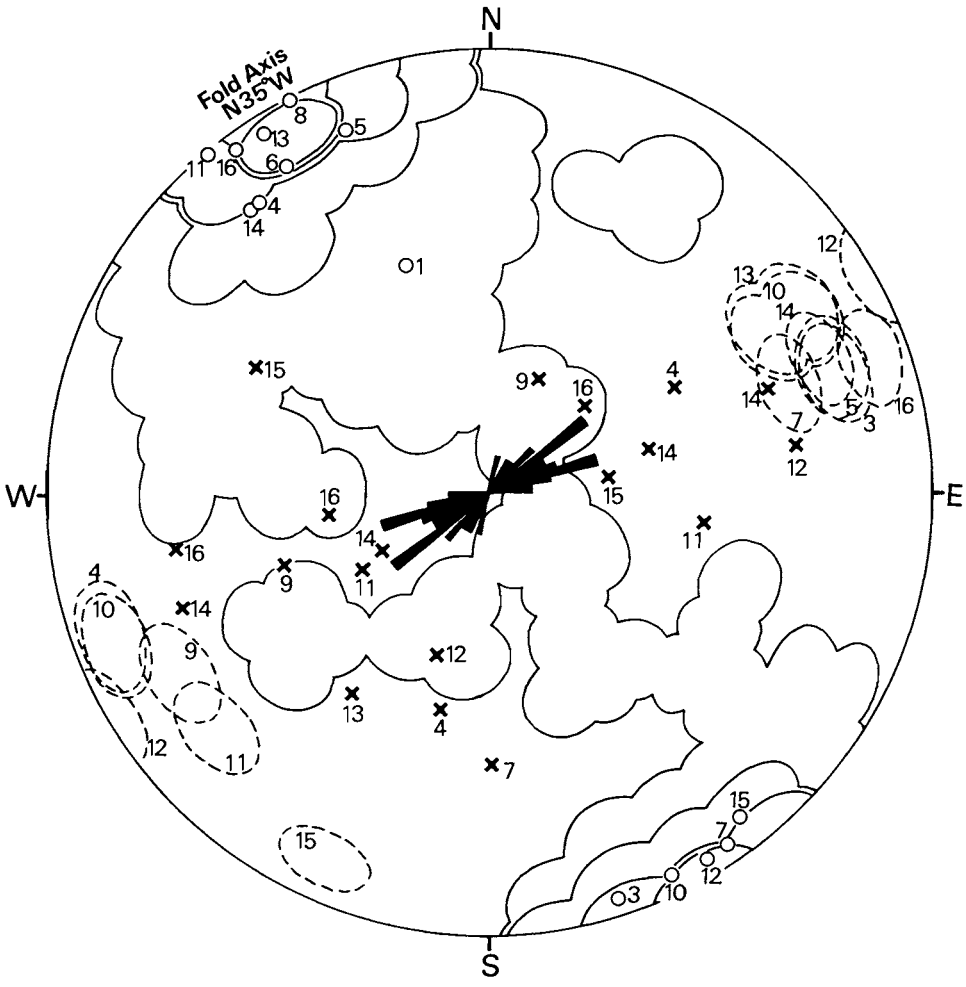

Fig. 16. *Composite fabric diagram summarizing the relationships among different structural elements. Nos.: subareas, refer to Fig. 14. Full-lined contours: all observed small fold axes and lineations. Broken contours: cleavage maxima from the subareas. Rosette: strikes of the joints. Open circle with Nos.: calculated main fold axis from each subarea. Cross with Nos.: calculated subordinate fold axes from the numbered subareas.*

The strikes of bedding and axial plane cleavages are mostly parallel, the latter having steeper dips. The cleavages in the middle part of the synclinorium (subareas Nos. 10, 11, and 12) have roughly vertical dips and a few subareas (Nos. 4 and 9) have east-dipping maxima, while most of the remaining (Nos. 3, 5, 6, 7, 13, 14, and 16) show westerly dips.

Some subordinate girdles of bedding are distinguished in subareas Nos. 4, 9, 11, 12, 13, 14, 15, and 16. In general, the axial trends of these subordinate girdles are conformable with the strike of the transverse faults and the cross-joints (Fig. 16). Accordingly, these deformations can be explained as secondary disturbance caused by block movements.

Metamorphism

Cleavages are developed strongly in the argillaceous and volcanigenic rocks, in the rocks of the Middle Horseshoe Formation, especially along the large strike fault.

In all siliceous sedimentary rocks, quartz, chlorite, sericite, and carbonates are well recrystallized in the matrix, while large detrital flakes of muscovite and biotite are commonly preserved. Plagioclase and garnet show weak alteration with partial clouding/albitization and chloritization, respectively. Medium- to coarse-grained detrital quartz grains have kept their general clastic shape, but the margins are recrystallized, and authigenic overgrowth occurs in a few rocks of examined quartzites.

The constituent minerals of all the volcanic rocks were strongly decomposed under almost static conditions retaining original outlines of phenocrysts and ophitic texture, although cleavages developed to some extent. The plagioclase converted into albite + sericite + carbonates + epidote, and the hornblende into actinolite + epidote + chlorite + sphene + opaques. The matrix of the rocks changed into a dense mixture of sericite + chlorite + carbonates + quartz + albite + opaques. A little amount of potash-feldspar and pale brown biotite occurs interstitially in the matrix of the K-rich rocks. Minor amounts of calcite and dolomite occur in the strongly crushed matrix along the cleavages. All observed hornblende and pyroxene are relics from the original magmatic associations. Dark brown biotite occurs as interstitial constituent in the gabbros of the Middle Horseshoe Formation. This suggests a progressive increase of metamorphism in the lower part of the sedimentary succession.

This metamorphic grade is common from the Edson Hills Formation to the Whiteout Conglomerate for more than 7,000 m in thickness. However, the Polarstar Formation of the Sentinel Range, stratigraphically higher than the Whiteout Conglomerate, shows the metamorphic grade of the laumontite facies with dominant illite and carbonates in the matrix (Castle and Craddock 1975). The P/T gradient of this metamorphism is calculated to be about 200° C/Kb, i.e. the high-T type of metamorphic facies series.

lower side: Preh + Cc + Qz → Ep + Act + V . . . . .about 330—350°C
upper side: decomposition of Fe-chlorite . . . about 550—600°C
both in the pressure range of 1—5 Kb.

Most analysed volcanic rocks are projected in the field of epidote-actinolite-chlorite in the ACF diagram (Fig. 17). The metamorphic grade is the actinolite-greenschist facies, correlatable to the zone III and IV of New Zealand and the chlorite- and the biotite-zone of Scotland. The temperature range can be limited by the reactions:

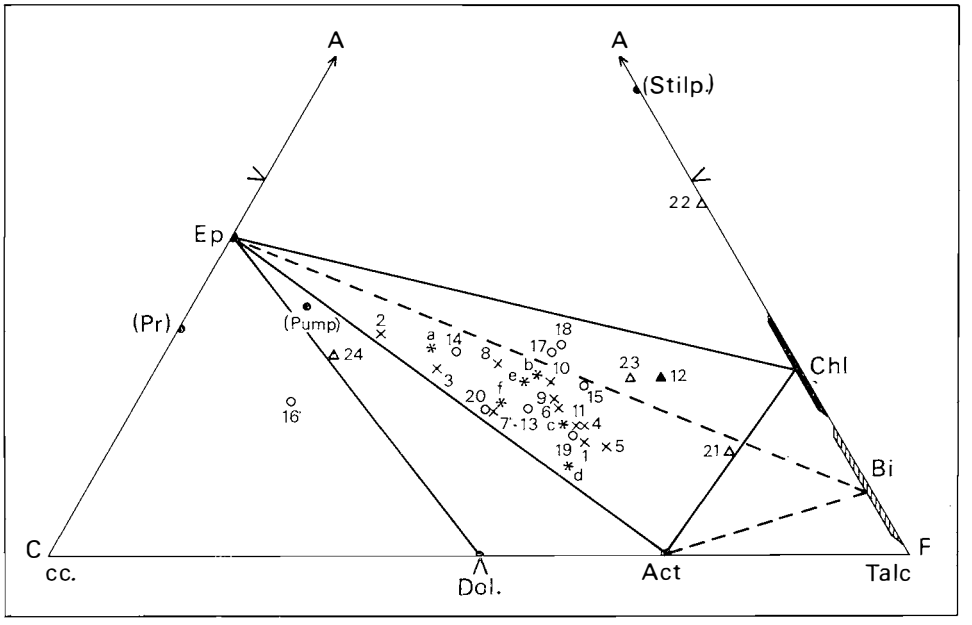

Fig. 17. *ACF diagram of the analysed ingenous rocks. Symbols and Nos. refer to Table 12, stars are of the late Paleozoic igneous rocks.*

Acknowledgements

The research described in this paper was made possible through generous logistic support from the National Science Foundation, Office of Antarctic Programs. We thank all NSF, USARP, and US Navy personnel for kind and effective assistance.

The authors are also grateful to Dr. C. Craddock for valuable guidance and for critically reviewing the manuscript.

References

ADIE, R. J., 1972: Evolution of volcanism in the Antarctic Peninsula. In: ADIE, R. J. (ed.) *Antarctic geology and geophysics:* 137—141. Oslo. Universitetsforlaget.

BASS, M. N., R. M. MOBERLY, J. M. RHODES, SHIH CHI-YU, and S. E. CHURCH, 1973: Volcanic rocks cored in the central Pacific, Leg 17 Deep Sea Drilling Project. In: WINTERER, E. L. and J. I. EVING (eds.) *Initial Report D.S.D.P. 17*. Washington.

CASTLE, J. W. and C. CRADDOCK, 1975: Deposition and metamorphism of the Polarstar Formation (Permian). Ellsworth Mountains. *Antarct. Jnl. U.S.*, 10 (5): 239—241.

CATHCART, J.B. and D.L. SCHMIDT, 1977: Middle Paleozoic sedimentary phosphate in the Pensacola Mountains, Antarctica. *U.S.G.S. Professional Paper* 456-E: 1—18.

CLARKSON, P. D., 1972: Geology of the Shackleton Range: a preliminary report. *Br. Antarct. Surv. Bull.* No. 31: 1—15.

COMPSTON, W., I. McDOUGALL, and K. S. HEIER, 1968: Geochemical comparison of the Mesozoic basaltic rocks of Antarctica, South Africa, South America and Tasmania. *Geochim. Cosmochim. Acta.* 32 (2): 129—149.

CRADDOCK, C., 1969. Geology of the Ellsworth Mountains. In: BUSHNELL, V. C. and C. CRADDOCK (eds.) Geologic maps of Antarctica. *Antarct. Map Folio Ser.* Folio 12, Pl. IV.

CRADDOCK, C., J. J. ANDERSON, and G. F. WEBERS, 1964: Geological outline of the Ellsworth Mountains. In: ADIE, R. J. (ed.) *Antarctic geology:* 155—170. Amsterdam, North-Holland Publishing Company.

DOTT, R. H. Jr., 1964: Wacke, greywacke and matrix — what approach to immature sandstone classification? *Jnl. Sedim. Petrol.* 34: 625—632.

ELLIOT, D. H., 1972: Major oxide chemistry of the Kirkpatrick Basalt, central Transantarctic Mountains. In: ADIE, R. J. (ed) *Antarctic geology and geophysics:* 413—418. Oslo. Universitetsforlaget.

ERLANK, A. J. and P. K. HOFMEYR, 1966: K/Rb and K/Cs ratios in Karroo dolerites from South Africa. *Jnl. Geophys. Res.* 71: 5439—5445.

ERLANK, A. J. and P. K. HOFMEYR, 1968: K/Rb ratios in Mesozoic tholeiites from Antarctica, Brazil and India. *Earth & Planet. Sci. Lett.* 4: 33—38.

FAURE, G. and D. H. ELLIOT, 1971: Isotope composition of strontium in Mesozoic basalt and dolerite from Dronning Maud Land. *Br. Antarct. Surv. Bull.,* No. 25: 23—27.

FAURE, G., J. R. BAUMANN, D. H. ELLIOT, and L. M. JONES, 1974: Strontium isotope composition and petrogenesis of the Kirkpatrick Basalt, Queen Alexandra Range, Antarctica. *Contr. Min. Petrol.* 48: 153—169.

FLEISCHER, M., 1968: Variation of the ratio Ni/Co in igneous rock series. *Jnl. Wash. Acad. Sci.* 58: 108.

FORD, A. B., 1970: Development of the layered series and capping granophyre of the Dufek intrusion of Antarctica. In: VISSER, D. J. L. and von GRUENWALDT (eds.) Symposium on the Bushveld Igneous Complex and other layered intrusions. *Geol. Soc. S. Afr. spec. publ.* 1: 492—510.

— 1972: Weddell Orogeny — Latest Permian to Early Mesozoic deformation at the Weddell sea margin of the Transantarctic Mountains. In: ADIE, R. J. (ed.) *Antarctic geology and geophysics:* 419—425. Oslo. Universitetsforlaget.

GUNN, B. M., 1965: K/Rb and K/Ba ratios in Antarctic and New Zealand tholeiites and alkali basalts. *Jnl. Geophys. Res.* 70 (24): 6241—6247.

— 1966: Modal and element variation in Antarctic tholeiites. *Geochim. Cosmochim. Acta.* 30 (9): 881—920.

JAKES, P. and J. R. WHITE, 1970: K/Rb ratios of rocks from island arcs. *Geochim. Cosmochim. Acta.* 34: 849—856.

JAKES, P. and J. R. WHITE, 1972: Major and trace elements abundances in volcanic rocks of orogenic areas. *Geol. Soc. Am. Bull.* 83: 29—40.

KUNO, H. 1959: Origin of Cenozoic petrographic provinces of Japan and surrounding areas. *Bull. Volcan.,* Ser. 2, 20: 37—76.

LAUDON, T. S., L. L. LACKEY, P. G. QUILTY, and P. M. OTWAY, 1969: Geology of eastern Ellsworth Land. In: BUSHNELL, V. C. and C. CRADDOCK (eds.), Geologic maps of Antarctica. *Antarct. Map Folio Ser.* Folio 12, Pl. III.

MACDONALD, G. A. and T. KATSURA, 1964: Chemical composition of Hawaiian lavas. *Jnl. Petrol.,* 5: 82—133.

McBIRNEY, A. R., and H. WILLIAMS, 1969: Geology and petrology of the Galapagos Islands. *U.S.G.S. Mem.* 118: 1—197.

MIDDLEMOST, E. A. K., 1975: The basalt clan. *Earth Sci. Rev.,* 11: 337—364.

MIYASHIRO, A., 1975: Classification, characteristics and origin of ophiolites. *Jnl. Geol.,* 83: 249—281.

— 1974: Volcanic rock series in island arcs and active continental margins. *Am. Jnl. Sci.* 247: 321—355.

MOHR, P. A., 1960: *The geology of Ethiopia.* 268 pp. Adis Abeba.

NEETHLING, D. C., 1972: Comparative geochemistry of Proterozoic and Paleo-Mesozoic tholeiites of western Dronning Maud Land. In ADIE, R. J. (ed.) *Antarctic geology and geophysics:* 603—616. Oslo, Universitetsforlaget.

ONO, K., 1962: *Chemical composition of volcanic rocks in Japan.* Geol. Surv. Japan, 441 pp., Tokyo.

PETTIJOHN, F. J., 1949: *Sedimentary rocks.* Harper & Brothers. 526 pp., New York.

RITTMANN, A., 1952: Nomenclature of volcanic rocks. *Bull. Volcan.* 12.

SCHOPF, J., 1969: Ellsworth Mountains: Position in West Antarctica due to sea-floor spreading. *Science.* 164 (3875): 63—66.

STUMP, E., 1974: Volcanic rocks of the Early Cambrian Taylor Formation, central Transantarctic Mountains. *Antarct. Jnl.* 9 (5): 228—229.

— 1976: Accretionary lapilli and lithophysal spherulites from the Taylor Formation, Queen Maud Mountains. *Antarct. Jnl.* 11 (5): 247—248.

TURNOCK, A. C., 1960: The stability of iron chlorites. *Carnegie Inst. Year Book* 59: 98—103.

WALKER, F. and A. POLDERVAART, 1949: Karroo dolerites of the Union of South Africa. *Bull. Geol. Soc. Am.* 60 (4): 591—705.

WEBERS, G. F., 1972. Unusual Upper Cambrian fauna from West Antarctica. In: ADIE, R. J. (ed.) *Antarctic geology and geophysics: 235—237.* Oslo, Universitetsforlaget.

WILLIAMS, P. L., 1969: Petrology of Upper Precambrian and Paleozoic sandstones in the Pensacola Mountains, Antarctica. *Jnl. Sedim. Petrol.* 39 (4): 1455—1465.

YODER, H. S. and C. S. TILLEY, 1962: Origin of basalt magma: an experimental study of natural and synthetic rock systems. *Jnl. Petrol.* 3: 342—353.

Age relationships of Mesozoic basalt lava and dykes in Vestfjella, Dronning Maud Land, Antarctica*

BY HARALD FURNES[1] AND JOHN G. MITCHELL[2]

Abstract

The thick pile of tholeiitic basalt in Vestfjella, Dronning Maud Land, consists of a large number of subaerial compound flows, strongly altered by synvolcanic hydrothermal activity. Four of the lavas yielded Triassic K-Ar ages (200 ± 6 to 231 ± 10 m.a.). The lava sequence is cut by a large number of fresh basalt dykes of both tholeiitic and alkaline affinities. Twelve of the dykes yielded Middle to Upper Jurassic K-Ar ages (156 ± 4 to 172 ± 2 m.a.), coinciding with intense magmatic activity elsewhere in Dronning Maud Land and the Transantarctic Mountains. The age obtained for the Vestfjella lavas shows that magmatic activity started earlier in Dronning Maud Land than had been previously supposed. The time span of magmatic activity in Dronning Maud Land, prior to the break-up of Antarctica and Africa in Upper Jurassic time, can now be demonstrated to be of about the same duration as the early Mesozoic «Karroo» magmatic activity in S.E. Africa, i.e. about 50 m.y. The Vestfjella magmatic activity was apparently not continuous, and the Triassic volcanic activity may possibly represent an abortive rifting event.

Introduction

A characteristic feature of the Transantarctic Mountains which define the western margin of the continental shield of East Antarctica (Adie 1977), is the widespread occurrence of Jurassic basalt lavas and dykes (e.g. Rex 1972; Elliot 1972). One of the best-known basalt sequences, the Kirkpatrick basalt (179—163 m.a.), covers an area of about 110 km² in the Central Transantarctic Mountains, and may represent a remnant of a formerly extensive flood-basalt field (Elliot 1970, 1972). The Middle to Upper Jurassic basalt lavas and compositionally similar intrusives which may collectively be referred to as the Ferrar Group, overlie or intrude the Beacon Supergroup of late Palaeozoic to early Mesozoic age (Barret et al. 1972).

* Publication No. 13 of the Norwegian Antarctic Research Expeditions. (1976/77).

[1] Geologisk institutt, avdeling A, Allégaten 41, 5014 Bergen, Norway.

[2] School of Physics, University of Newcastle upon Tyne, Newcastle upon Tyne, NE 1 7 RU, England.

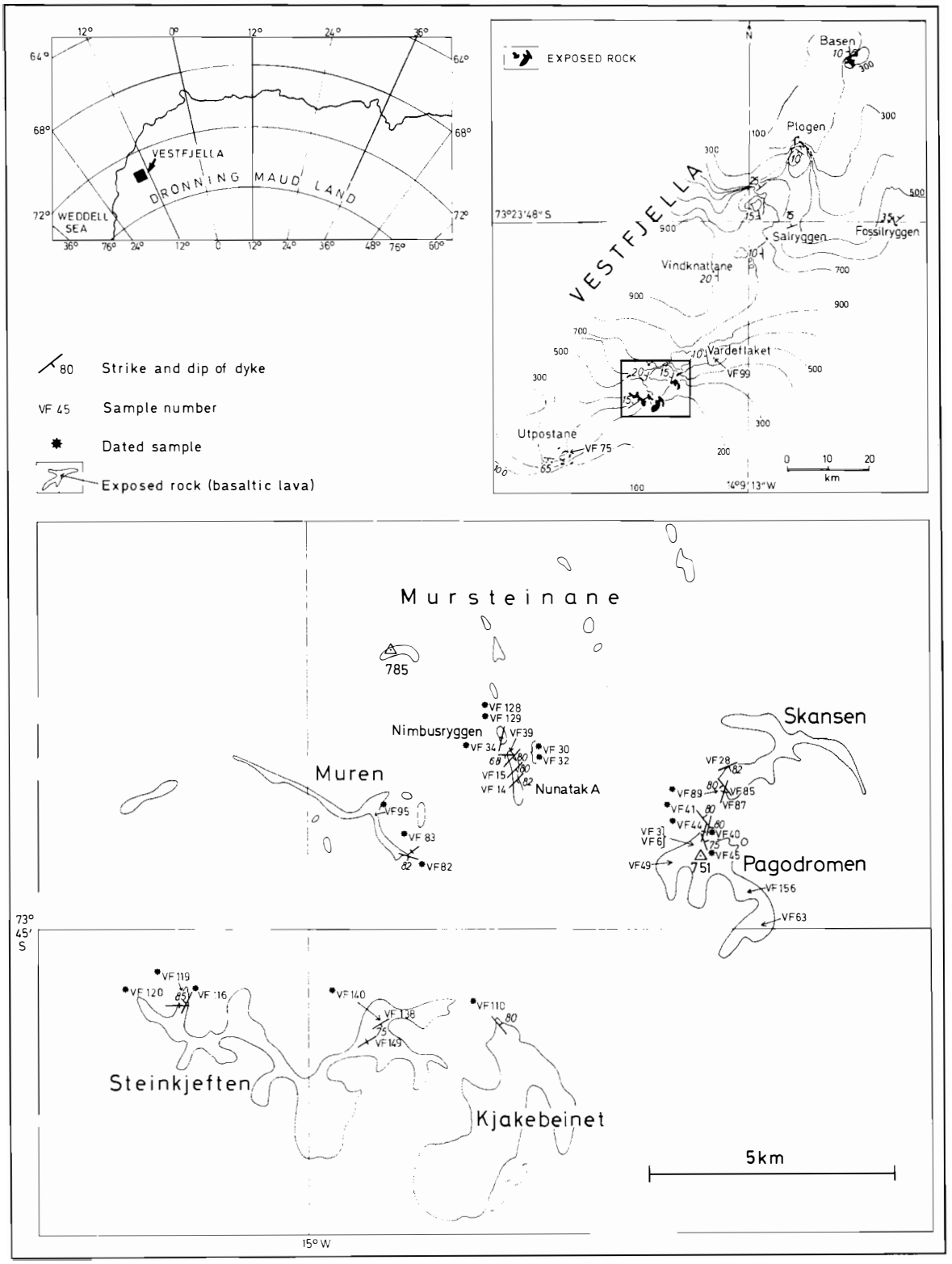

Fig. 1. *Map showing exposures (of basalt lava mainly), and sample location.*

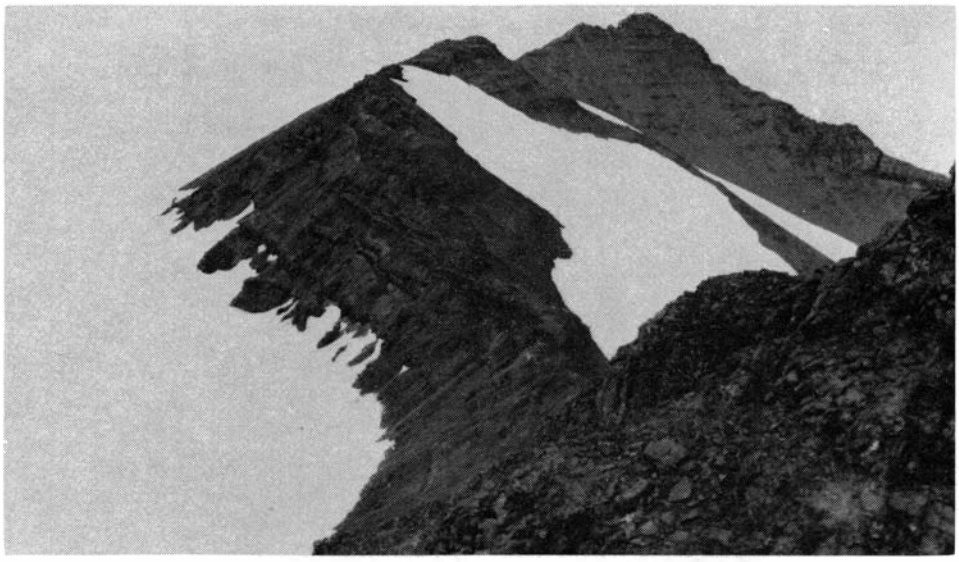

Fig. 2. *The lava pile on the southeastern part of Pagodromen, showing a number of flows.*

In the reconstruction of Gondwanaland the Jurassic basaltic magmatism of the Ferrar Group in Antarctia is an important feature, since stratigraphic correlation can be made with the basaltic lavas and intrusives of the Karro System in South Africa (Walker and Poldervaart 1949). It has been proposed that the tholeiitic Kirkpatrick flood basalts are related to the break-up of Gondwanaland (Barret and Elliot 1972).

The present paper deals with the thick basalt lava sequence of possibly Upper Triassic age, and the later dyke swarms of middle to late Jurassic age in Vestfjella, Dronning Maud Land (Fig. 1).

Geological description

The Vestfjella mountains consist of a number of nunataks arranged in a NNE—SSW direction over a distance of about 130 km (Fig. 1). By far the most dominant rock type is basalt lava, with insignificant amounts of intercalated volcaniclastic rocks. Hjelle and Winsnes (1972) estimated the lava sequence to be about 2000 m thick, but more recent investigations would indicate that a thickness of 2500 m is more realistic (Hjelle, pers. comm.).

The easternmost nunatak in Vestfjella, Fossilryggen (Fig. 1), consists of quartz sandstones with intercalated fossiliferous shales which contain Permian plant fossils (Hjelle and Winsnes 1972). The base of the volcanic succession in Vestfjella is nowhere exposed, so it is impossible to tell what substrate the lava pile rests upon, or its exact relations to the Permian sandstone of the region.

The lava sequence is built up of a large number of subaerial flows ranging in thickness from about 1 to 25 m (Fig. 2). Flows are usually of compound

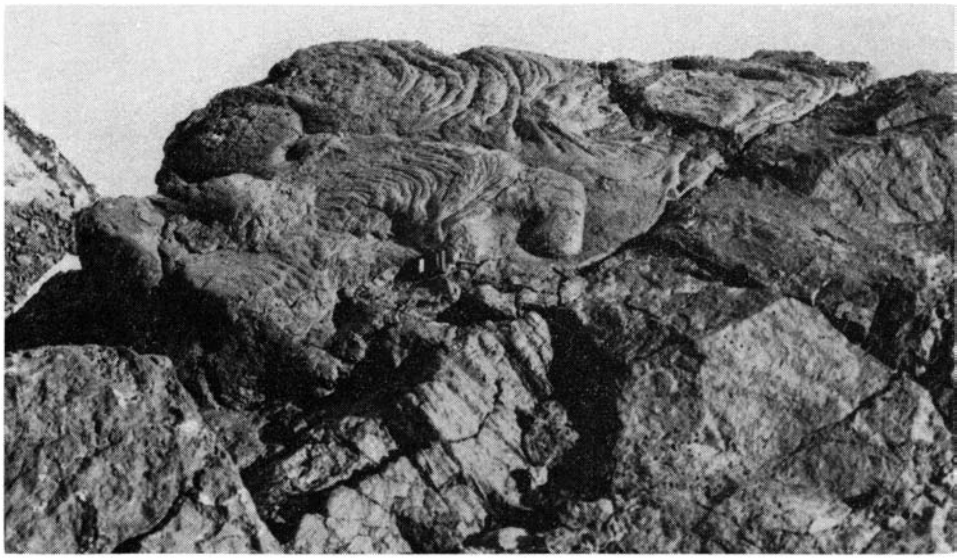

Fig. 3. *Ropy pahoehoe flow units. Northern part of Nunatak A.*

nature, and can often be subdivided into a number of pahoehoe flow units (Fig. 3) or massive flow units with undulating surfaces. The top surface of massive flow units may occasionally consist of aa type lava (Fig. 4). The lavas vary considerably, from strongly vesicular to non-vesicular.

Bent pipe vesicles at the bottom of flow units, as well as ropy structures on the surface of pahoehoe bodies (Figs. 3,5), give some indication of the flow direction of the lava (Waters 1960). Ropy pahoehoe indicates, in general, a flow direction from V/NV to E/SE (Fig. 6a), and the pipe vesicles from SE to NW and NW to SE, giving an average (which is also a maximum) flow direction from WSW to ENE (Fig. 6b). Most of the measurements are from bent pipe vesicles of a number of flows on the SE side of Pagodromen (Fig. 1). Within one flow all pipe vesicles show the same flow direction, whereas adjacent separate flows may show nearly 180° deviations in flow direction.

The lava flows are in general strongly altered, though relatively fresh lavas (usually those which are non-vesicular) can be found. Zones of strongly altered material occasionally cut relatively fresh lava flows. This indicates that the alteration is due to syn- or post-volcanic hydrothermal activity.

The lava pile is cut by a large number of basalt dykes, and by an olivine gabbro body at Utpostane (Fig. 1). The dykes are, in contrast to the lava pile they intrude, very fresh. The thickness varies from about 0.5 m to 10 m, averaging 3.6 m (38 dykes). The approximate strike of the dykes are: E-W, NE-SW, N-S, NW-SE, and the dip is invariably steep to vertical (Fig. 7, 8).

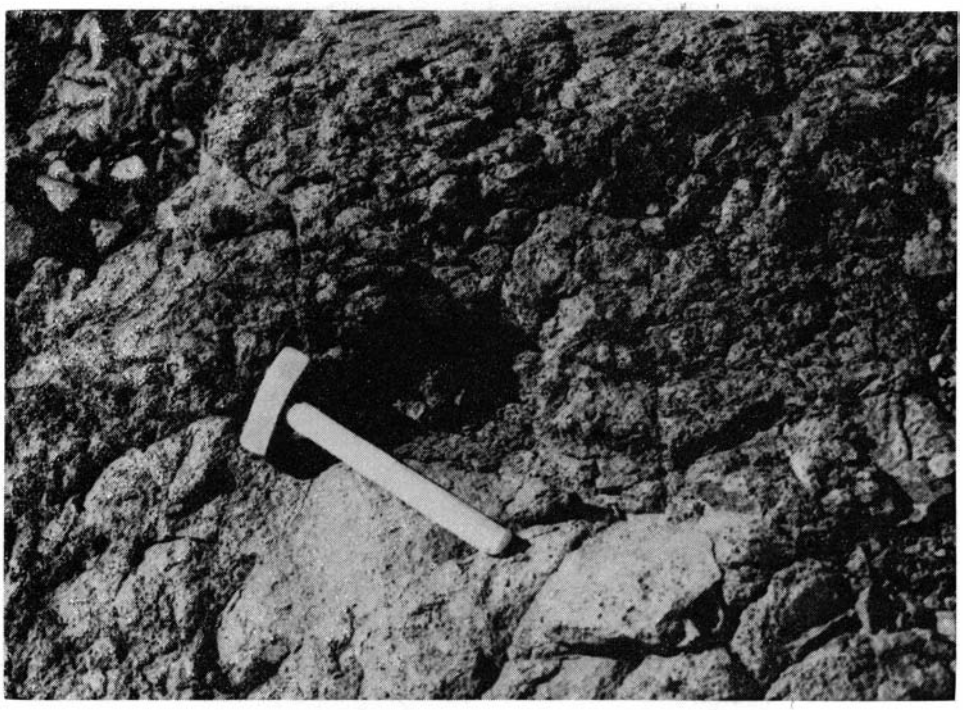

Fig. 4. *Rubbly aa type lava surface on a flow. Northwestern part of Steinkjeften.*

Fig. 5. *Bent pipe vesicles at the base of a flow, showing flow direction from right to left. Southeastern part of Pagodromen.*

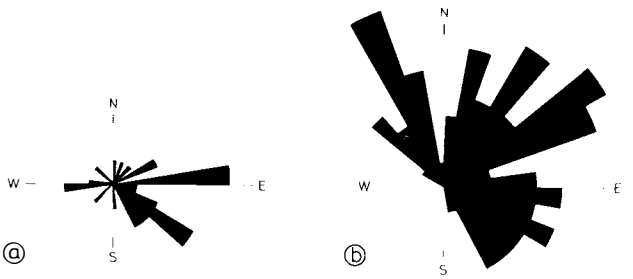

Fig. 6. *Rose diagram showing flow direction of lava.*
a) 28 measurements of ropy structures on pahoehoe flow units.
b) 95 measurements of bent pipe vesicles at the base of flows.

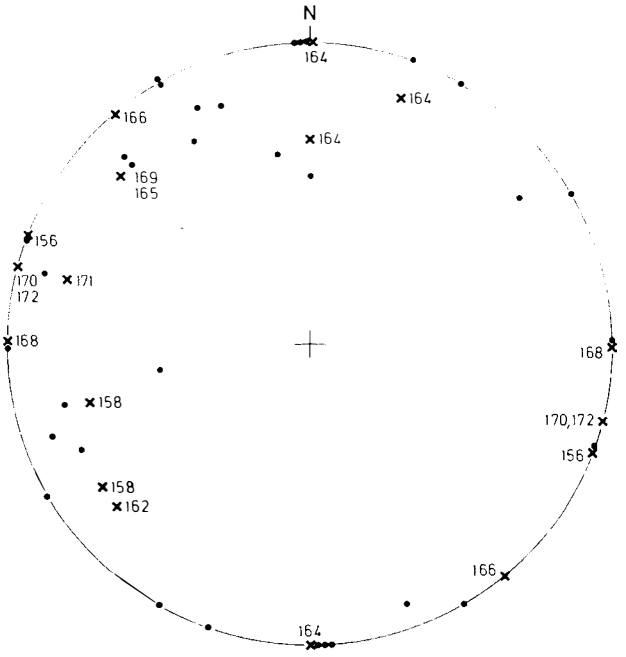

Fig. 7. *Poles to strike and dip of dykes. Crosses show dated dykes, and their ages are indicated in m.y.*

Petrography

Lava

The lavas range from strongly porphyritic to aphyric. Two specimens (VF 140 and VF 95, see Table 1) are distinctly different from the others in containing up to 40% olivine-(altered), together with clinopyroxene-, and plagioclase phenocrysts. Olivine (mostly replaced by iron oxide, serpentine minerals and chlorite) is the main phenocryst phase, and mineralogically these lavas may be classified as picritic basalts. The clinopyroxene phenocrysts are optically positive, have moderate 2V, and are pale brown, features consistent

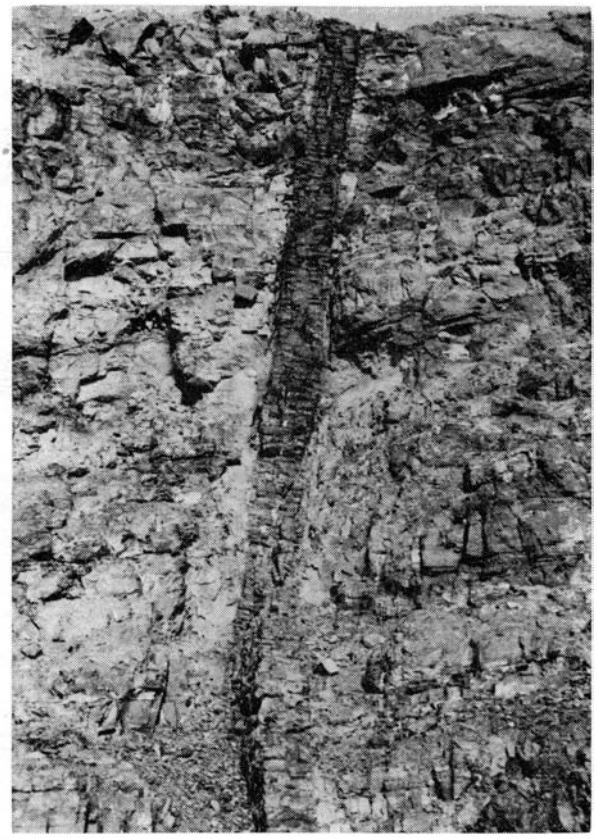

Fig. 8. *Steeply dipping dyke cutting altered, subhorizontal lava flows. The dyke is about 2 m thick. Southwestern Skansen.*

with augite. Plagioclase is optically determined as labradorite. It may be strongly replaced by calcite. Textural relationships between the phenocryst phases, show the following order of crystallization: olivine, clinopyroxene, plagioclase.

The phenocryst phases in the other lava specimens are clinopyroxene and plagioclase, of which the former was the first phase to crystallize. Plagioclase is, however, volumetically the dominant of the two.

Groundmasses consist of basic plagioclase, clinopyroxene (probably augite), opaques, and some chlorite.

The specimens, for which analyses are presented, are nearly free of amygdales. The amygdales occurring consist of quartz, calcite, and chlorite. However, other authigenic minerals found in vesicles and cavities in the lavas are zeolite, prehnite and epidote. Textural relationships show that zeolite was the first secondary mineral to crystallize. It is replaced or overgrown by prehnite, which again is overgrown by epidote.

Dykes

Apart from sample VF 149 (Table 2) which contains about 20 percent phenocrysts (basic plagioclase and clinopyroxene), the remaining samples

Table 1.
Chemical analyses of lava from Vestfjella.

	VF 140	VF 95	VF 156	VF 119	VF 63	VF 70	VF 39		VF 6	VF 89	VF 49
SiO_2	46.21	46.11	49.64	50.41	50.13	49.23	50.47	49.62	49.24	49.20	50.13
Al_2O_3	10.67	11.98	14.71	14.26	14.32	14.22	14.28	13.59	15.15	15.52	12.76
TiO_2	1.19	1.21	1.47	1.55	1.39	1.85	1.62	1.69	1.56	1.60	2.32
Fe_2O_3	4.77	1.39	2.40	4.01	1.51	1.73	3.45	0.73	2.58	1.15	4.41
FeO	7.37	10.10	9.09	8.23	9.91	9.80	8.42	10.58	8.42	9.95	10.10
MgO	14.39	13.63	7.28	7.13	7.11	6.70	6.55	6.38	5.79	5.53	4.67
CaO	8.37	10.17	10.49	12.02	9.95	10.77	9.40	9.18	10.93	10.93	8.06
Na_2O	1.32	1.10	2.75	0.94	1.90	2.15	2.66	2.63	2.06	2.08	2.53
K_2O	0.11	0.15	0.46	0.21	0.78	0.17	1.27	0.46	0.51	0.09	0.67
MnO	0.17	0.18	0.16	0.18	0.17	0.17	0.17	0.16	0.18	0.16	0.20
P_2O_5	0.17	0.19	0.27	0.24	0.23	0.27	0.29	0.24	0.25	0.31	0.44
H_2O	2.84	3.69	2.12	1.65	3.32	1.12	2.15	2.67	1.79	1.81	2.25
V	196	188	229	246	204	281	237	258	236	219	334
Cr	880	692	230	161	136	250	183	210	175	72	39
Co	55	51	42	42	46	43	42	45	40	38	49
Ni	483	384	76	73	89	76	67	55	63	49	24
Zn	42	50	51	51	55	59	61	56	55	49	73
Rb	7	6	8	2	19	3	19	10	6	3	10
Sr	222	191	273	224	339	332	290	359	319	305	234
Y	10	9	13	12	14	13	13	15	14	14	21
Zr	56	57	68	75	69	80	68	65	62	69	123
Nb	9	11	11	9	9	9	10	10	10	11	12
La	5	2	3	6	3	5	5	2	4	5	10
Ce	31	29	30	33	30	28	33	24	21	34	45
Nd	17	18	18	22	19	19	23	15	14	21	29
Cu	11	45	50	58	42	60	68	40	76	43	81

Table 2.
Chemical analyses of dykes from Vestfjella.

	VF 75	VF 34	VF 110	VF 28	VF 66	VF 85	VF 82	VF 99	VF 30	VF 15	VF 32	VF 138
SiO_2	46.23	45.78	49.81	49.48	48.49	45.80	47.14	48.52	48.70	48.47	48.44	47.44
Al_2O_3	13.84	14.02	14.21	14.88	14.59	15.57	14.65	15.28	13.66	14.87	13.59	13.92
TiO_2	1.52	2.09	1.33	0.87	1.85	1.94	1.84	1.60	1.90	1.77	1.90	2.03
Fe_2O_3	3.02	5.52	4.40	1.08	3.23	1.86	4.27	2.38	2.30	3.34	1.44	3 78
FeO	9.39	8.98	7.70	8.98	9.46	10.40	8.34	8.71	10.51	8.90	11.07	9.20
MgO	8.72	8.69	8.69	8.29	7.53	7.34	6.96	6.70	6.67	6.52	6.50	6.09
CaO	13.87	10.73	10.76	9.99	11.59	11.52	11.64	10.61	10.53	11.51	10.18	9.79
Na_2O	1.88	2.47	0.86	3.14	2.11	0.78	2.00	2.13	2.41	2.14	2.48	2.22
K_2O	0.04	0.63	0.56	0.18	0.24	0.40	0.48	0.62	0.51	0.41	0.68	0.59
MnO	0.19	0.20	0.19	0.14	0.19	0.17	0.18	0.17	0.18	0.18	0.19	0.20
P_2O_5	0.08	0.41	0.27	0.15	0.27	0.27	0.27	0.30	0.30	0.32	0.29	0.24
H_2O	0.13	2.78	1.73	2.11	0.64	2.58	1.57	1.47	1.57	1.70	1.32	2.13
V	326	267	220	198	310	252	242	205	284	261	266	297
Cr	276	207	391	310	219	121	123	236	115	249	113	67
Co	38	50	46	43	43	47	46	41	45	43	44	45
Ni	69	113	198	67	59	73	71	82	55	65	54	58
Zn	42	65	51	59	64	65	65	60	67	70	67	60
Rb	3	13	7	4	3	5	9	13	6	6	12	12
Sr	217	369	290	282	243	230	230	283	278	300	279	311
Y	6	13	12	9	13	14	14	13	12	12	13	14
Zr	17	108	82	58	83	95	89	70	101	71	103	101
Nb	7	12	10	8	11	13	12	10	11	10	11	10
La	n.d.	18	9	1	4	5	7	2	12	8	12	9
Ce	14	47	34	24	31	37	34	29	42	31	40	37
Nd	8	33	22	16	21	26	25	24	29	23	29	27
Cu	13	96	65	37	66	101	89	61	86	68	90	92

Table 2. cont.

	VF 128	VF 129	VF 120	VF 44	VF 87	VF 40	VF 149	VF 116	VF 83	VF 41	FV 45	VF 14
SiO_2	49.71	51.32	45.35	51.38	48.31	47.55	52.72	48.17	50.33	48.52	48.12	48.00
Al_2O_3	14.30	14.28	13.31	13.78	13.34	12.52	14.91	12.23	12.54	13.10	11.99	12.69
TiO_2	1.93	2.19	3.09	2.19	3.14	3.22	1.59	4.21	2.88	2.74	3.63	3.83
Fe_2O_3	1.99	1.44	5.82	1.44	3.86	3.16	2.53	2.79	2.83	4.44	1.81	4.76
FeO	10.70	11.80	10.29	13.16	12.15	12.90	8.42	13.91	12.49	10.36	14.03	11.63
MgO	5.99	5.28	5.21	5.17	4.98	4.94	4.91	4.87	4.80	4.78	4.66	4.45
CaO	10.27	9.26	10.36	9.42	9.93	9.54	8.33	8.90	8.67	9.16	8.98	8.81
Na_2O	2.24	2.49	2.43	2.68	1.11	2.90	2.43	1.22	2.60	2.74	2.65	2.75
K_2O	0.56	1.00	0.62	0.81	0.80	0.83	1.43	0.89	1.02	1.17	0.86	1.23
MnO	0.18	0.17	0.21	0.21	0.22	0.22	0.15	0.23	0.20	0.19	0.22	0.20
P_2O_5	0.30	0.35	0.49	0.29	0.45	0.45	0.30	0.61	0.41	0.50	0.51	0.57
H_2O	1.26	1.09	1.90	0.88	1.73	0.86	1.61	1.18	1.21	1.16	1.11	1.27
V	273	257	402	319	340	344	229	391	336	299	326	435
Cr	80	60	36	34	53	53	26	56	60	62	59	44
Co	45	42	52	48	49	50	39	51	47	45	48	48
Ni	52	42	40	35	34	31	44	33	30	29	26	29
Zn	58	58	69	66	68	70	59	77	77	69	80	85
Rb	12	20	14	15	12	19	25	23	20	25	19	23
Sr	273	310	415	289	293	259	373	275	272	370	280	355
Y	15	19	15	16	20	20	17	27	19	18	26	21
Zr	123	161	145	118	145	145	165	209	157	149	178	203
Nb	11	13	14	11	17	17	14	19	12	16	18	16
La	14	21	17	16	19	23	26	28	21	25	25	29
Ce	49	55	58	49	60	52	62	64	60	68	58	73
Nd	32	39	41	31	43	41	40	56	41	44	45	56
Cu	76	73	93	131	143	147	26	205	79	32	171	164

are either aphyric or contain at the most about 5 percent phenocrysts. The phenocryst assemblages are as follows:

1) Olivine + clinopyroxene + plagioclase
2) Clinopyroxene + plagioclase + (?) basaltic hornblende
3) Clinopyroxene + plagioclase
4) Plagioclase
5) Olivine

The olivine phenocrysts are, in contrast to those in the lavas, rather fresh and only partly replaced by iron oxide along cracks and edges. They are optically negative, $2V \approx 90°$, indicating a Mg-rich olivine (forsterite or Mg-rich chrysolite). Optical properties of the clinopyroxenes indicate augite (opt. pos., moderate 2V), and the plagioclase is labradorite. Zoning in the plagioclase, both normal and oscillatory, is common. The (?) basaltic hornblende is characterised by its straight extinction and yellow to dark reddish brown pleocroism. The crystal margins, and sometimes large parts of the grains, are charged with iron oxide. It is variably altered to dark green chlorite.

Groundmasses consist of basic plagioclase, clinopyroxene, opaques and some minor amounts of chlorite.

Geochemistry

Methods

The analyses have been made by the XRF method (Padfield and Gray 1971; Flanagan 1973) with glass beads for the major elements and pressed pellets for the trace elements. Ferrous iron was determined by titration.

Lavas

The compositions of the analysed lava samples are shown in Tables 1 and 3. In an alkali-silica diagram all the analyses plot well within the tholeiitic field as defined by MacDonald and Katsura (1964), and apart from one sample (VF119) there is a slight positive relationship between $Na_2O + K_2O$ and SiO_2 (Fig. 9a). Such a relationship could be the result of differentia-

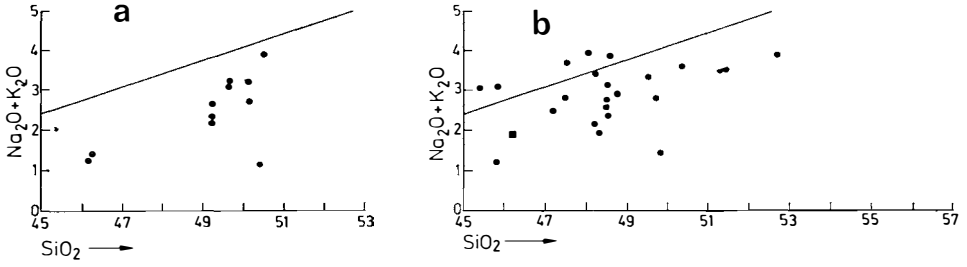

Fig. 9. *Alkali-silica relationships, showing a) lava, and b) dykes and chilled margin of gabbro (filled square). Tholeiitic-alkalic boundary: After* MACDONALD *and* KATSURA *(1964).*

tion. The samples VF 95 and VF 140 are both picritic basalts, whilst sample VF 49 may be classified as a basaltic andesite on the basis of its high TiO_2, total Fe, and low MgO (Table 1). However, if such a trend was the result of crystal fractionation, a well-defined trend towards iron enrichment should also be expected on an AFM diagram. Although selected samples may define such a trend, the total sample population shows some scatter (Fig. 10a).

Dykes

Table 2 and 3 show the chemical compositions of the dyke rocks. It is indicated by the alkali-silica relationships (Fig. 9b) that tholeiitic as well as alkaline basalts may be represented. The presence of two types of basalt may possibly account for the scatter of points in the AFM diagram (Fig. 10b), since tholeiitic basalts probably will show a stronger iron enrichment during fractionation than an alkaline basalt.

Table 3.
Ranges, averages and standard deviation of the lava and dyke analyses from Vestfjella.

	Lava (n = 11)			Dykes (n = 24)		
	Range	×	s	Range	×	s
SiO_2	46.11—50.47	49.13	1.54	45.35—52.72	48.49	1.81
Al_2O_3	10.67—15.52	13.77	1.44	11.99—15.57	13.84	0.98
TiO_2	1.19— 2.32	1.59	0.31	0.87— 4.21	2.30	0.85
Fe_2O_3	0.73— 4.77	2.56	1.40	1.08— 5.82	3.06	1.33
FeO	7.37—10.58	9.27	1.02	7.70—14.03	10.54	1.83
MgO	4.67—14.39	7.74	3.20	4.45— 8.72	6.20	1.42
CaO	8.06—12.02	10.02	1.19	8.33—13.87	10.18	1.25
Na_2O	1.10— 2.66	2.10	0.64	0.78— 3.14	2.20	0.63
K_2O	0.09— 1.27	0.44	0.36	0.04— 1.43	0.69	0.33
MnO	0.16— 0.20	0.17	0.01	0.14— 0.23	0.19	0.02
P_2O_5	0.17— 0.44	0.26	0.07	0.08— 0.61	0.35	0.13
H_2O	1.12— 3.69	2.31	0.76	0.13— 2.78	1.46	0.59
V	188—334	239	42	193—435	295	62
Cr	39—880	275	264	26—391	127	102
Co	38— 55	45	5	38— 52	46	4
Ni	24—483	131	152	26—198	58	36
Zn	42— 73	55	8	42— 85	65	9
Rb	2— 19	8	6	3— 25	13	7
Sr	191—359	381	56	217—373	295	50
Y	9— 21	13	3	6— 27	16	5
Zr	56—123	72	18	17—209	120	47
Nb	9— 12	10	1	7— 19	13	3
La	2— 10	5	2	n.d.—29	15	9
Ce	21— 45	31	6	14— 73	46	15
Nd	14— 29	20	4	8— 56	33	12
Cu	11— 81	52	20	13—205	92	48

Table 3 shows the average composition of the dyke rocks and lavas. In general the dykes are slightly richer in TiO_2, K_2O, P_2O_5, Rb, Zr, La, Ce and Nd than the lavas. Such features are to be expected, since alkaline basalts are richer in the above mentioned oxides and elements (and other incompatible elements) than tholeiitic basalts (Table 4).

Table 4.

Average composition of Vestfjella tholeiitic and alkaline basalt dykes, compared with other continental-, ocean rise-, and alkaline basalts.

	1A	1B	2	3	4	5	6	7	8
SiO_2	48.9	47.0	50.4	49.9	51.8	52.1	50.3	49.8	47.7
Al_2O_3	14.0	13.1	15.5	13.5	15.3	14.2	14.3	16.0	15.6
TiO_2	2.1	3.0	0.4	1.3	0.9	1.1	2.2	1.5	2.3
Fe_2O_3	2.6	4.7	1.0	5.5	1.1	11.7	3.5	2.0	2.6
FeO	10.5	10.8	7.8	6.3	10.6		9.3	7.5	7.9
MgO	5.9	5.6	10.6	6.0	6.4	7.4	5.9	7.5	8.0
CaO	10.3	9.7	10.9	9.2	9.9	10.7	9.7	11.2	8.9
Na_2O	2.1	2.7	1.4	2.4	2.5	2.1	2.5	2.8	3.8
K_2O	0.6	0.9	0.4	0.8	0.7	0.7	0.8	0.1	1.6
MnO	0.2	0.2	0.2	0.2	0.2	0.2			0.2
P_2O_5	0.3	0.5	0.1	0.1	0.1				0.5
V	281	349	126	250	270				190
Cr	139	80	352	170	270	217	100	300	207
Co	45	49	62	30	30	49	40	32	
Ni	60	48	249	45	70	81	100	100	175
Rb	12	19	12	37	20	21	30	1	26
Sr	279	354	100	180	400	186	350	135	524
Y	15	17					30	30	25
Zr	112	150	53	85		92	200	100	222
Nb	12	15					20	5	32
La	13	22					27	4	29
Ce	43	60					40	12	59
Nd	30	43							31

Index to Table 4.

1A. Average of tholeiitic basalt dykes (n = 15) from Vestfjella (this account).

1B. Average of alkaline basalt dykes (n = 5) from Vestfjella (this account).

2. Basaltic sill (Painted cliff sill), Jurassic Ferrar dolerite, Antarctica (GUNN 1966).

3. Basalt lava, Lesotho, SE Africa (COX and HORNUNG 1966).

4. Diabase, Karroo, SE Africa (WALKER and POLDEVAART 1949).

5. Average composition of basalt (high TiO_2, Q-normative type) dykes of eastern North America (WEIGAND and RAGLAND 1970).

6. Average composition of continental tholeiites (CONDIE 1976) Nb value: average of continental basalts (PEARCE and CANN 1973).

7. Average composition of ocean rise tholeiite (CONDIE 1976). Nb value (PEARCE and CANN 1973).

8. Average composition of alkaline basalts (MARSH 1976). Rb, La, Ce, Nd values (KAY and GAST 1973). Nb value: average of ocean island basalts (PEARCE and CANN 1973).

Petrogeneses of the Vestfjella basalt (lava and dykes)

Table 4 shows the average composition of the Vestfjella basalt (lava and dykes), compared with various continental-, ocean rise tholeiitic-, and alkaline basalts. With respect to elements that during partial melting preferentially enter the melt (incomparatible elements), it is apparent from this compilation of data that the Vestfjella basalts and continental basalts in general, possess an intermediate position between typical tholeiitic ocean rise-, and alkaline basalts. This is particularly reflected in oxides such as TiO_2 K_2O and the trace elements, Rb, Sr, Nb, La, and Ce.

In general tholeiitic basalts (i.e. ocean rise tholeiites) are generated by a much higher degree of partial melting of mantle material than alkaline basalts. Theoretical calculations based on REE concentrations indicate that tholeiitic melts can be produced by 5—30 percent partial melting of ultramafic mantle material (e.g. Schilling 1971; O'Nions and Grønvold 1973), whereas alkaline basalts form by 0,5—2 percent melting (e.g. Kay and Gast 1973). These figures agree well with the experimental results of Mysen and Holloway (1976).

A characteristic feature of the Vestfjella basalt dykes and lava is the low Y content (Tables 1—4). This could be a consequence of the melts having been generated from a garnet-bearing mantle source that still had garnet in the residue, since garnet is the only major mantle mineral into which Y (and HREE) is strongly partitioned. Model calculation on the basis of Ni and REE show that both the Vestfjella basalt lavas and dykes could have been produced by small to moderate (about 2—10 percent) degrees of partial melting of garnet lherzolite (Furnes and Neumann in prep.). Such magnitudes of partial melting are in accordance with the figures suggested above for the generation of both alkaline- and tholeiitic basalts. Batches of magma were subsequently modified by some 10—40 percent olivine fractionation.

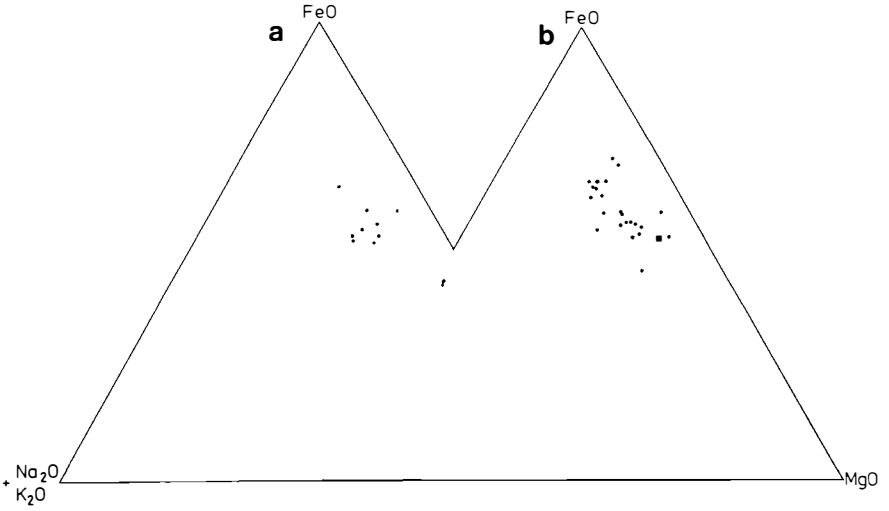

Fig. 10. *AFM diagram, showing plots of a) lava, and b) dykes and chilled margin of gabbro (filled square).*

Tectonic setting

The late Carboniferous to early Permian sandstones, upon which the early Mesozoic lava piles of Dronning Maud Land (in Vestfjella, Heimefrontfjella, and Kirwanryggen, see Fig. 12) rest, or are in association with (in Vestfjella), are considered to be of continental type (Hjelle and Winsnes 1972).

The present geochemical work suggests the same geotectonic environment for the basalts. On the empirically based Ti-Zr-Y discriminant diagram for basaltic rocks (Pearce and Cann 1973, the Vestfjella basalt lava and dykes invariably plot in the «within-plate» field (Fig. 11), despite large variations in these element abundances (Tables 1—3). This geochemical feature for both lava and dykes, the latter representing both tholeiitic and alkaline basalts, can more easily be understood from the rare earth element abundances in the rocks which suggest that the partial material would have to be a garnet-bearing herzolite (Furnes and Neumann in prep.). Thus, as long as garnet is a residual mantle phase after melting has taken place, only small amounts of Y will enter the melt since the distribution coefficient $Ky^{Gar/liq}$ is large. This will consequently bring the Ti-Zr-Y plots into the «within-plate» field of Pearce and Cann (1973) as shown in Fig. 11.

Age relationships

Four lava and twelve dyke specimens have been dated using the Potassium-Argon method. Whole-rock analyses were performed by crushing the samples to about 1 mm chips in order to homogenise the material prior to argon analysis. Part of this material was then reduced to about 200 mesh size for potassium analysis. Determination of potassium content was by flame photometry on an EEL 450 instrument with Lithium internal standard. Argon iso-

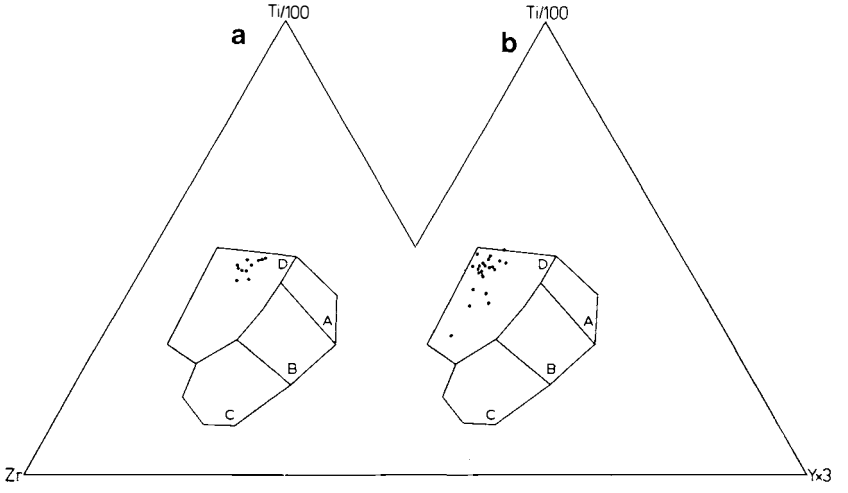

Fig. 11. *Ti-Zr-Y discriminant diagram (after* PEARCE *and* CANN *1973), showing fields of «within-plate» basalts (D), low potassium tholeiites of island arcs (A+B), ocean floor type basalts (B), and calc-alkaline basalts (C). a) Lava, and b) dykes and chilled margin of gabbro (filled square).*

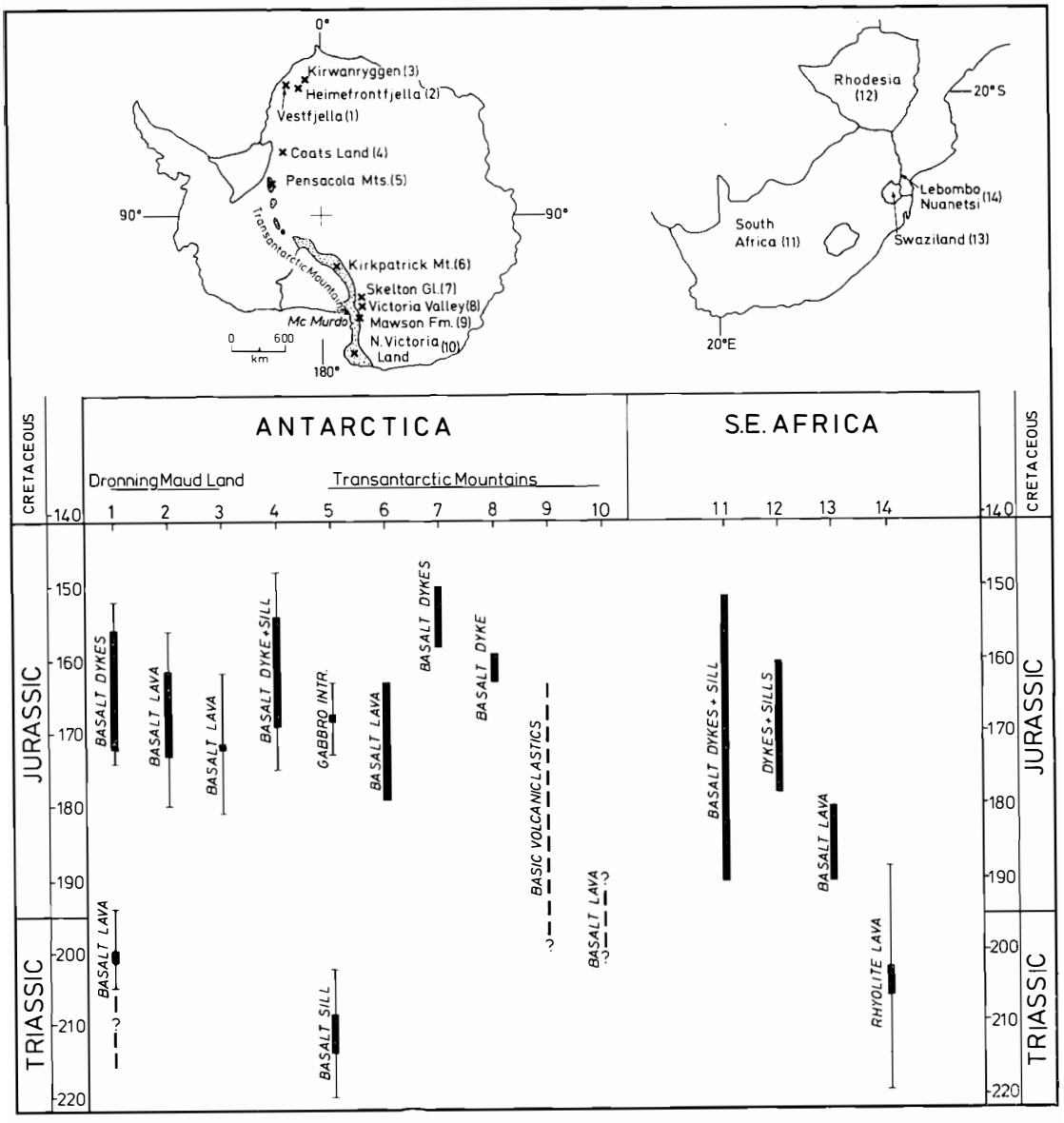

Fig. 12. *Periods of magmatic activity in Antarctica and Africa prior to the late Jurassic break-up of the continents. Thin lines with bar: standard deviation; thick dashed lines: age uncertain.*

Data sources from: 1. This account; 2. REX (1972); 3. AUCAMP *et al. (1972); 4. REX (1972); 5.* FORD *(1972); 6.* ELLIOT *(1972); 7.* MCDOUGALL *(1963); 8.* MCDOUGALL *(1963); 9.* BORNS *and* HALL *(1969),* BORNS *(pers. comm.): 10.* GAIR *(1967); 11.* MCDOUGALL *(1963); 12.* SNELLING *(1966); 13.* SNELLING *and* REX *(1967),* MANTON *(1968).*

topic analyses were performed by isotope dilution on an MS10 spectrometer, the gas extraction system being coupled directly to the instrument. Sample weights for argon analysis were about 2 gm.

The mean potassium and argon contents are given in Tables 5 and 6 with the mean age and one standard deviation error determined from the reproducibility of the analyses.

In an attempt to avoid uncertainties in the interpretation of the K-Ar data arising from the possible occlusion of «initial» argon in the dykes, we have analysed materials from both the chilled margins, as well as from the centres of the dykes. No correlation between the measured K-Ar age, and the distance from contact was observed, and in fact, in the two dykes where both margin and centre were analysed (VF30 and VF32; VF128 and VF129) the K-Ar ages within a single dyke were indistinguishable, and the mean ages of the two dykes were coincident. We conclude, therefore, that the possible effects of initial argon in these dykes can be ignored.

The dyke ages range from 156 ± 4 m.a. to 172 ± 2 m.a. (middle to late Jurassic) and are significantly younger than the ages obtained for the lavas, 200 ± 6 m.a. to 231 ± 10 m.a. which they cut, by some thirty million years, at least. The relationship between the strike of the dykes and their ages is shown in Fig. 7. The dykes with the oldest apparent ages strike approximately N-S. This is, however, the strike of some of the youngest dykes, suggesting that repeated intrusions of magma occurred in relation to an already established tectonic pattern.

The interpretation of the lava ages is complicated by the degree of alteration they exhibit and by the range of ages which were obtained. Two of the samples (VF95 and VF140) collected from Muren and Steinkjeften respectively (Fig. 1) are from a distinctive olivine/pyroxene/plagioclase-phyric lava which is a readily identifiable marker horizon in the lava pile. This horizon is generally fresh (apart from some alteration of the olivine) and the concordant age of 200 ± 3 m.a. obtained we believe to be the best estimate of the «age» of the succession. Lava VF89 lies below the preceding two samples which is consistent with its older age (231 ± 10 m.a.). However, in neither the nearly continuous E-W section from Kjakebeinet to Steinkjeften, nor anywhere else in the studied sequence, is there any evidence of major breaks in the volcanic activity such as would be necessary in order to invoke a 30 m.a. time span for the extrusion of the succession. Sample VF119 is from stratigraphically the highest level, and its measured age, 219 ± 7 m.a., is inconsistent with its position in the pile. We are unable to account, on the basis of these limited data, for the observed discrepancies but suggest that the age of the lava pile is at least 200 ± 3 m.a., though it may possibly be older by an indeterminate amount, at least 30 m.a.

Since the lava pile has been subject to a subsequent thermal event, as is evident from the generally strong alteration of the vesicular lava and deposition of authigenic minerals in vesicles, the possibility should be considered that the K-Ar ages have been reset. The mineral paragenesis places some constraints on the minimum and maximum temperatures attained in the lava pile during alteration. The widespread occurrence of epidote indicates that the temperature was at least 250°C (Tomasson and Kristmannsdottir 1977). The pres-

ence of zeolite(s) overgrown by prehnite suggests an upper temperature limit of about 320°C (Coombs et al. 1959).

It seems clear that this secondary mineral formation is not related to regional metamorphism, but to a local hydrothermal event. This implies that temperature gradients were extremely high, and furthermore that the warm water percolating through the sequence would generally follow permeable layers. The temperature may have been lower in nonpermeable layers, for instance the non-vesicular lava, than the 250—320°C suggested above.

Since the alteration of the lava pile has to be related to a source of heat, it may be due to:

1) Hydrothermal activity contemporaneous with, or slightly after the outpouring of the lava.
2) Hydrothermal activity related to shallow magma chamber(s) from which the later dykes were derived.

It appears unlikely that heat released from shallow magma reservoirs can possibly account for the alteration and secondary mineralization, since the dykes themselves are all rather fresh. Since the intrusion of dyke magma occupied a time span of at least some 16 m.a., one might expect the oldest dykes to have suffered the same degree of alteration as the lava.

It is thus considered most plausible that the lava pile suffered hydrothermal alteration prior to dyke intrusion, and that the alteration was related to the magmatic event that resulted in the outpouring of the lava. This may lend some support to the lava pile as representing a remnant of a central volcano.

Typical features for central volcanic activity, as for example richly exampli fied in Iceland, and the African rift valleys, can be summarized as follows according to Grønvold (1972); King and Chapman (1972); Fridleifsson (1973); and Saemundsson and Noll (1974):

1. Hydrothermal activity mainly contemporaneous with the life span of the volcano.
2. Lavas or pyroclastics ranging in composition from basalt to rhyolite.
3. Intrusive activity.
4. Short life span of the volcanic activity (from less than 1 m.a. to a few m.a.).

Apart from the hydrothermal activity mentioned, the other three characteristic features are not well demonstrated in the Vestfjella lava pile. However, from the chemistry of the lavas (Table 1), it is evident that the lava pile does not represent a chemically monotonous sequence (sample VF 49 for example is considerably differentiated). There is also some intrusive activity represented by altered gabbro and a dyke (at the southwestern side of Skansen, see Fig. 1) which apparently are syngenetic with the lava. It should be realized, however, that the investigated rocks are situated at a high level in the sequence, where intrusive phases are unlikely to be abundantly represented.

The K-Ar ages of the lava samples can not be used to indicate a rapid deposition of the lava sequence (Table 6). It is stressed, however, that there is no geological evidence in the investigated sequence for any clear breaks in the volcanic activity.

Thus, if the lava pile represents the remnant of a central volcano, it would mean that the hydrothermal event took place within the short life span of the magmatic activity. Thus, the ages obtained for the lavas (200 m.a. is considered as the most plausible) would give the age of lava extension, even if the K-Ar clock had been reset by the hydrothermal event.

Comparison with other areas

It has been demonstrated, on the basis of K-Ar ages, that the basalt lavas in Vestfjella represent an older (minimum 30 m.a.) magmatic event than that represented by the associated dykes. The dykes, ranging in age from mid- to late Jurassic (172—156 m.a.) can readily be correlated with the regional magmatic activity represented by the lavas and intrusives of the Ferrar Group in the Transantarctic Mountains (Fig. 12).

The age of the lavas, however, appears unusual when compared with other post-Palaeozoic basalt lava sequences in Dronning Maud Land and in the Transantarctic Mountains in general. Apart from some basalt sills in the Pensacola Mountains which are thought to be of mid-Triassic age (Ford 1972), and some basic volcaniclastics and lavas in Victoria Land which contain interbedded fossiliferous sediments that may be of Upper Triassic or Lower Jurassic age (Borns and Hall 1969; Gair 1967), the Vestfjella lavas are considerably older than any other occurrences (Fig. 12).

It has been demonstrated that prior to late Jurassic times, Antarctica and SE Africa still formed a continuous land-mass (e.g. Dietz et al. 1972; Elliot 1972; Smith and Briden 1977; Bergh 1977).

It is clear from the radiometric ages of SE African basic and acid lavas and intrusives (McDougall 1963; Snelling 1966; Snelling and Rex 1967; Manton 1968), that magmatic activity there commenced in the late Triassic times and continued during the Jurassic period until approximately 150 m.a. ago (Fig. 12). It would thus appear that the lava pile in Vestfjella is stratigraphically more closely related to the SE African lavas than to the Lower Mesozoic lavas of Dronning Maud Land and the Transantarctic Mountains.

It seems quite clear that the dated dykes from Vestfjella represent a distinct episode of intense magmatic activity in mid-Jurassic time in Dronning Maud Land and the Transantarctic Mountains (Fig. 12), and that continuous magmatic activity lasted for about 30 m.a. prior to the rifting between Africa and Antarctica in late Jurassic time.

On the basis of the present analyses (Tables 5, 6), it is evident that a pronounced time gap exists between two distinct magmatic events in the Vestfjella region.

The relationship between igneous activity and continental break-up in general, has been summarized by Scrutton (1973). From his compilation of

data, it seems that intense igneous activity spanned a period of 30—40 m.a. on an average before break-up took place, «but minor activity may take place over several more tens of millennia» (op. cit.). Vine and Hess (1971) proposed a period of 25 m.a. as being normal. According to the radiometric dates from SE Africa, as summarized in Fig. 12, igneous activity spanned a period of 50 m.a. prior to the upper Jurassic separation of Africa from Antarctica.

Table 5.
Whole rock potassium-argon analyses of basalt dykes from Vestfjella.

Sample	K_2O*	Radiogenic** Argon $MM^3GM^{-1}x10^3$	Atmospheric*** Contamination	Age (Ma) ≠
VF 44	0.959	5.15	18.6	156 ± 4
VF 41	1.30	7.08	22.9	158 ± 3
VF 45	0.984	5.37	21.6	158 ± 2
VF 110	0.570	3.19	27.9	162 ± 2
VF 34	0.670	3.80	29.3	164 ± 2
VF 82	0.512	2.90	28.3	164 ± 3
VF 120	0.680	3.84	30.2	164 ± 2
VF 83	1.110	6.37	17.3	166 ± 2
VF 30	0.512	3.00	27.7	169 ± 5
VF 32	0.705	4.03	22.7	165 ± 2
VF 116	0.970	5.63	18.3	168 ± 2
VF 40	0.965	5.70	19.7	171 ± 3
VF 128	0.629	3.71	27.4	170 ± 2
VF 129	1.12	6.65	13.2	172 ± 2

$\lambda_e = 0.584 \times 10^{-10} yr^{-1}$

$\lambda\beta = 4.72 \times 10^{-10}\ yr^{-1}$

$\frac{^{40}K}{K} = 1.19 \times 10^{-2}$ atom percent

*Potassium determination: mean of four analyses.
**Argon determination: mean of two analyses.
***Atmospheric Contamination figure is the higher of two values from duplicate argou analyses.
≠ Mean age and one standard deviation estimate of error.

Table 6.
Whole rock potassium-argon analyses of basalt lava from Vestfjella.

Sample	K_2O*	Radiogenic** Argon $MM^3\,GM^{-1} \times 10^{-3}$	Atmospheric*** Contamination	Age (Ma) ≠
VF 89	0.102	0.829	56.2	231 ± 10
VF 95	0.186	1.30	47.6	200 ± 6
VF 119	0.211	1.62	39.3	219 ± 7
VF 140	0.138	0.968	64.3	201 ± 4

Decay constants and footnotes as for Table 5.

The new dates for the Vestfjella lavas presented in this account, would suggest that igneous activity in Dronning Maud Land covers the same time interval as that in SE Africa, and not merely 17. m.a. as indicated by previous radiometric dates of basalt lavas from this region of Antarctica, and by the dykes reported here. Apparently this magmatic event was not so continuous as in SE Africa (Fig. 12).

It is well known that continental igneous activity and rifting may take place over a long period without the formation of a new ocean, as exemplified by the rift system of East Africa. This rift system has been active since the Upper Triassic, with intermittent breaks in activity in upper Triassic —, and Upper Cretaceous to Miocene times (Scrutton 1973). Sowerbutts (1972) related this activity to the break-up of Gondwanaland, and not necessarily as a precursor of separation in East Africa.

Our tentative proposal for the apparent short-lived Upper Triassic continental type basaltic volcanism in Vestfjella, is that they may reflect an abortive rifting event. The duration of this volcanic activity is not known, but if the volcanic succession represents the remnant of a central volcano, as suggested above, the activity is likely to have taken place over only a short time (in the order of one or a few million years).

The later magmatic event in Vestfjella and Dronning Maud Land, lasting for some 30 m.a. (Middle to Upper Jurassic time) resulted in the separation of Africa from Antarctica, giving birth to the SW Indian Ocean.

Summary

The thick basaltic pile in Vestfjella consists of hydrothermally altered subaerial compound (pahoehoe to rubbly aa type) flows. Four K-Ar age determinations yielded Triassic dates ranging from 200 ± 6 to 231 ± 10 m.a., of which the youngest seems most plausible on geological grounds.

Preliminary chemical analyses of the lava show that they range from picritic basalt to basaltic andesite of tholeiitic affinity. There are also some altered intrusives which apparently are genetically related to the lavas. These features may indicate that the lava pile in Vestfjella represents the remnant of a central volcano.

A large number of basalt dykes of both tholeiitic and alkaline affinity, and a large gabbro body cut the lava pile. The ages of twelve dykes were determined, yielding middle to upper Jurassic ages (156 ± 4 to 172 ± 2 m.a.). Since the dykes are all fresh, the 172 ± 2 m.a. age post-dates the alteration event of the lava pile.

The time of dyke intrusion in Vestfjella coincides with a widespread magmatic activity in western Dronning Maud Land (Heimefront-fjella and Kirwanryggen) and in the Transantarctic Mountains, and span a time interval of some 30 m.a.

The timing of the effusive activity gives some new constraints of the time

span of magmatic activity in Dronning Maud Land prior to the break-up of Antarctica and Africa. Radiometric dating of lavas and intrusives in SE Africa (MacDougall 1963; Snelling 1966; Snelling and Rex 1967; Manton 1968) indicates some 50 m.a. of magmatic activity prior to break-up of the two continents. A similar time interval of magmatism, though not necessarily continuous, can now also be demonstrated for western Dronning Maud Land. The intense, but probably short magmatic activity represented by the lava pile in Vestfjella may possibly represent an abortive rifting event.

Acknowledgements

We would like to thank the following persons for discussion and critical comments on the manuscript: B. A. Sturt, B. Robins, A. Hjelle, and R. Løvlie. One of us (H.F.) would also like to thank R. Løvlie, A. Hjelle, and L. Sømme for the good companionship during fieldwork in Vestfjella. J. E. Lien and E. Irgens kindly prepared the illustrations.

References

ADIE, R. J., 1977: The geology of Antarctica: a review. *Phil. Trans. Roy. Soc. Lond.* 279: 123—130.

AUCAMP, A. P. H., L. G. WOLMARANS, and D. C. NEETHLING, 1972: The Urfjell Group, a deformed (?)early Palaeozoic sedimentary sequence, Kirwanveggen, Western Dronning Maud Land. In: *Antarctic Geology and Geophysics. (*ADIE, R. J. ed.) 557—562.

BARRET, P. J., and D. H. ELLIOT, 1972: The early Mesozoic volcaniclastic Prebble Formation, Beadmore Glacier Area. In: *Antarctic Geology and Geophysics (ADIE*, R. J. ed.): 403—409.

BARRET, P. J., G. W. GRINDLEY, and P. N. WEBB, 1972: The Beacon Supergroup of east Antarctica. In; (ADIE, R. J. ed.). *Antarctic Geology and Geophysics:* 319—332.

BERGH, H. W., 1977: Mesozoic sea floor off Dronning Maud Land, Antarctica. *Nature* 269: 686—687.

BORNS, H. W. and B. A. HALL, 1969: A re-investigation of the Mawson Tillite, Victoria Land, East Antarctica. *Science* 166: 870—872.

COOMBS, D. S., A. D. ELLIS, W. S. FYFE, and A. M. TAYLOR, 1959: The zeolite facies, with comments on the interpretation of hydrothermal syntheses. *Geochim. Cosmochim. Acta* 17: 53.

CONDIE, K. C., 1976: Trace-element geochemistry of Archean greenstone belts. *Earth Sci. Rev.* 12: 393—417.

COX, K. G., and G. HORNUNG, 1966: The petrology of the Karroo basalts of Basutoland. *Am. Mineral.* 51: 1414—1432.

DIETZ, R. S., J. C. HOLDEN, and W. P. SPROLL, 1972: Antarctica and continental drift. In: (ADIE, R. J. ed.) *Antarctic geology and geophysics:* 837—842.

ELLIOT, D. H., 1972: Aspects of Antarctic geology and drift reconstructions. In: (ADIE, R. J. ed.). *Antarctic geology and geophysics:* 849—858.

ELLIOT, D. H., 1972: Major oxide chemistry of the Kirkpatrich basalt, Central Transantarctic Mountains. In: (ADIE, R. J. ed.) *Antarctic Geology and Geophysics:* 413—425.

FAURE, G., and D. H. ELLIOT, 1971: Isotope composition of strontium in Mesozoic basalt and dolerite from Dronning Maud Land. *Br. Antarct. Surv. Bull.* 25: 23—27.

FLANAGAN, F. J., 1973: 1972-values for international geochemical reference standards. *Geochim. Cosmochim. Acta* 37: 1189—1200.

FORD, A. B., 1972: Weddel orogeny — latest Permian to early Mesozoic deformation at the Weddell Sea margin of the Transantarctic Mountains. In: (ADIE, R. J. ed.). *Antarctic Geology and Geophysics:* 419—425.

FRIDLEIFSSON, I. B., 1973: *Petrology and structure of the Esja Quaternary volcanic region, southwest Iceland.* D. Phil.thesis, Oxford University. 208 pp.

GAIR, H. S., 1967: The geology from the upper Rennick glacier to the coast, northern Victoria Land, Antarctica. N.Z.J. *Geol. Geophys.* 10: 309—344.

GRØNVOLD, K., 1972: *Structural and petrochemical studies in the Kerlingarfjøll regi central Iceland.* D. Phil. thesis, Oxford University, 237 pp.

GUNN, B. M., 1966: Model and element variation in Antarctic tholeiites. *Geochim. Cosmochim. Acta* 30: 881—920.

HJELLE, A., and T. WINSNES, 1972: The sedimentary and volcanic sequence of Vesfjella, Dronning Maud Land. In: (ADIE, R. J. ed.) *Antarctic Geology and Geophysics* 539—547.

KAY, R. W., and P. W. GAST, 1973: The rare earth content and origin of alkali-rich basalts. *Jour. Geol.* 81: 653—682.

KING, B. C., and G. R. CHAPMAN, 1972: Volcanism in the Kenya rift valley. *Phil. Trans. R. Soc. Lond. A.* 271: 185—208.

MACDONALD, G. A., and T. KATSURA, 1964: Chemical composition of Hawaiian lavas. *J. Petrol.* 5: 82—133.

MANTON, W. I., 1968: The origin of associated basis and acid rocks in the Lebombo-Nuanetsi igneous province, southern Africa, as implied by strontium isotopes. *J. Petrology* 9; 23—39.

MARSH, B. D., 1976: Some Aleutian andesites: their nature and source. *Jour. Geol.* 84: 27—45.

MCDOUGALL, I., 1963: Potassium-argon age measurements on dolerites from Antarctica and South Africa. *J. Geophys. Res.* 68: 1535—1545.

MYSEN, B. O., and J. R. HOLLOWAY, 1976: Rare earth fractionation with controlled partial melting of peridotite. *Carnegie Inst. Washington Year Book* 1975: 675—678.

O'NIONS, R. K., and K. GRØNVOLD, 1973: Petrogenetic relationships of acid and basic rocks in Iceland: Sr-isotopes and rare-earth elements in late and postglacial volcanics. Earth Planet. *Sci. Lett.* 19: 397—409.

PADFIELD, T., and A. GRAY, 1971: *Major element rock analyses by X-ray fluorescence — a simple fusion method.* N. V. PHILLIPS, analytical equipment FS 35, Eindhoven.

PEARCE, J. A., and J. R. CANN, 1973: Tectonic setting of basic volcanic rocks determined using trace element analyses. *Earth Planet Sci. Lett.* 19: 290—300.

REX, D. C., 1972: K-Ar age determinations on volcanic and associated rocks from the Antarctic Peninsula and Dronning Maud Land. In: (ADIE, R. J. ed.) *Antarctic Geology and Geophysics:* 133—136.

SAEMUNDSSON, K., and H. NOLL, 1974: K/Ar ages of rocks from Husafjell, western Iceland, and the development of the Husafell central volcano. *Jøkull* 24: 40—58.

SCHILLING, J.-G., 1971: Sea-floor evolution: rare-earth evidence. *Phil. Trans. Roy. Soc. Lond. A.* 268: 663—706.

SCRUTTON, R. A., 1973: The age relationship of igneous activity and continental break-up. *Geol. Mag.* 110: 227—234.

SMITH, A. G., and J. C. BRIDEN, 1977: *Mesozoic and Cenozoic paleocontinental maps.* Cambridge University Press, 66 pp.

SNELLING, J. N., 1966: *Ann. Rep. for 1965, Overseas Geol. Surv.*

SNELLING, J. N., and D. C. REX, 1967: African geochronology 1966. *Progr. Rep. 67/1, Inst. Geol. Sci.*

SOWERBUTTS, W. T. C., 1972: Rifting in Eastern Africa and the fragmentation of Gondwanaland. *Nature Phys. Sci.* 235: 435—437.

TOMASSON, J., and H. KRISTMANNSDOTTIR, 1972: High temperature alteration minerals and thermal brines, Reykjanes, Iceland. *Contrib. Mineral. Petrol.* 36: 123—134.

VINE, F. J., and H. H. HESS, 1971: Sea-floor spreading. In: (MAXWELL, A. E. ed.) *The Sea* 4. Interscience, New York and London.

WALKER, F., and A. POLDERVAART, 1949: Karroo dolerites of the Union of South Africa. *Bull. Geol. Soc. Am* 60: 591—706.

WATERS, A., 1960: Determining direction of flow in basalts. *Am. J. Sci.* 258: 350—360.

WEIGAND, P. W., and P. C. RAGLAND, 1970: Geochemistry of Mesozoic dolerite dikes from eastern North America. *Contrib. Mineral. Petrol.* 29: 154—214.

Glaciological studies by Landsat imagery of perimeter of Dronning Maud Land, Antarctica

BY OLAV ORHEIM

Introduction

The investigation has utilized Landsat imagery to analyze changes in the Dronning Maud Land coastline between 10° W and 29° E and to obtain statistical data on ocean dynamics, and sea ice and iceberg distribution in this region of the Antarctic.

The imagery for the investigation were provided by National Aeronautics and Space Administration (NASA), USA, for project 28550 for which the author was principal investigator. Altogether 67 images were received, mostly from the 1975/76 austral summer.

Band MSS 7 has been found most useful for the ice studies. The other bands were also used to attempt differentiation between ice floes and icebergs, but with inconclusive results.

The best method to distinguish between the ice shelf edge and the fast ice, and to bring out ice rises on the ice shelf, has been to copy the MSS 7 negatives at 5—10 times «normal» exposure.

Rate of iceberg calving

Fig. 1 reproduces the Dronning Maud Land coastline from 10° W to 29° E, as determined from Landsat imagery, and a comparison with former mapping. The map has been made at scale of 1:1 mill. and the Landsat imagery have in part been positioned by use of rock outcrops of known positions. The former mapping is mostly based on aerial photography with limited ground control, and exists partly as unpublished maps at Norsk Polarinstitutt.

The uncertainty in absolute positions in Fig. 1 is generally a few kilometres, and arises from an estimated uncertainty in the older mappings

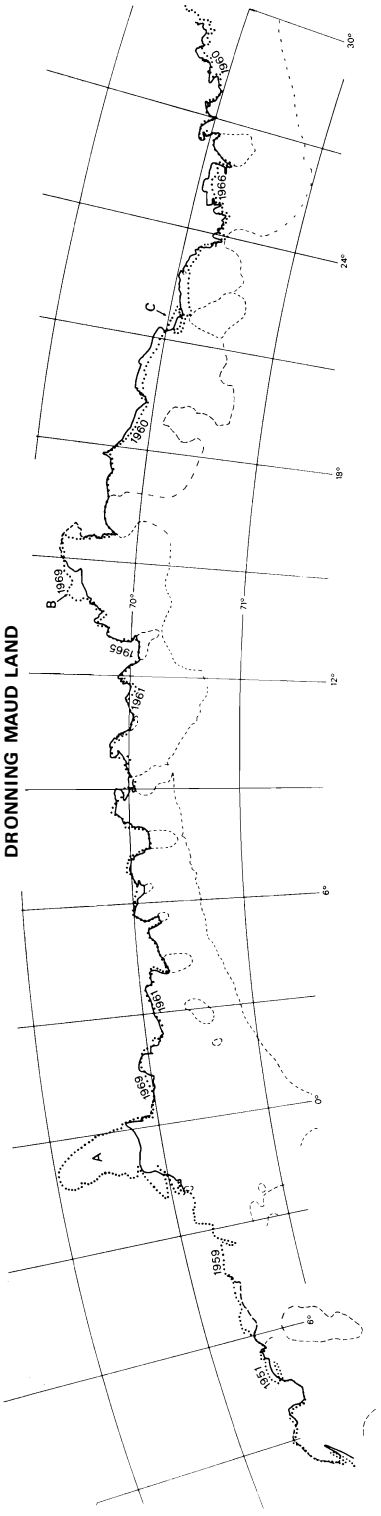

Fig. *Dronning Maud Land coast from 10°W to 29°E. Solid line = coast line determined from Landsat imagery with dashed portions = uncertain data. Dotted line = coast line determined from Norsk Polarinstituti's and other surveys with year as indicated. Thin dashed line = outline of ice rises and inland boundary of ice shelf; double spacing = uncertain areas. Heavy cloud cover on the Landsat imagery between 2° and 10°W prevents complete determination of coastline, ice rises, and inland boundary of ice shelf.*

(Helle, pers. comm.) and in the Landsat imagery (Nye and Thomas 1974). The relative positioning of the two sets of mapping is more precise, with a probably error mostly between 0.5 and 1 km. The reason for this smaller uncertainty is that the two sets of mapping have been made to match at those areas along the coast where ice rises form the coastline. Examination of various mappings and images show that here the coastline retains its shape, and that the change in ice rise positions is below the detectable limit of 1 km in those cases where we have fairly accurate absolute positioning of different mappings. Thus it is a reasonable assumption that there is no significant outward motion of the coast where ice rises form the coastline. The reason is that the absolute ice movement here is relatively small, and perhaps also that calving here is more frequent and in smaller fragments, because of heavy crevassing. Elsewhere the coastline will constantly change positions as a combination of the regular ice outflow, which may be as high as 2 km/yr^{-1}, and the intermittent ice shelf calvings, which at intervals of years or decades remove many-kilometre wide segments of the ice shelf (Orheim 1978; in prep.).

The major changes between the earlier photography and the Landsat imagery are therefore real. Fig. 1 shows three areas where the differences in coastline shapes are caused by calving of large parts of the ice shelf. Area A, Trolltunga, broke off in 1967 (Vinje 1977; Swithinbank, McClain, and Little 1977). The calving of areas B and C and many of the smaller areas (Fig. 1) may not have been described before. Fig. 1 shows also many examples of coastline displacement caused by outward ice flow. The areas of calving where the Landsat coastline is inland of the earlier mappings, cover over 6 000 km^2, which assuming an average thickness of 200 m, equals a calving volume of 1200 km^3. This corresponds to an averagne calving rate from this part of Antarctica of around 60 km^3/year. This clearly is an underestimate as no account is taken of the changes in coastline caused by the outward movement of the ice shelf. The magnitude of this movement and a more detailed description of the coastline changes are presented in Orheim (in prep.).

Drift of icebergs and ice floes

Fig. 2 shows imagery from successive dates (18 and 19 December 1975), from which drift speed determinations were made of the cluster of (probably) icebergs around 7° E. The ice moved westward at between 12 and 20 km/day, with most determinations in the lower range. The only other instance of Landsat imagery sufficiently close in time and space to allow drift determinations, covered a three day period from 27 to 30 October 1975, when ice velocities varied between 9 and 13 km/day, with an average of 10 km/day. In this case the ice moved westwards from 5 to 3° E and there was a convergence in the field amounting to 1.0 x 10^{-7}/sec. These velocities are close to the determinations by Tchernia (1974) and Swithinbank, McClain, and Little (1977), and the feasibility of the method is clearly demonstrated. But

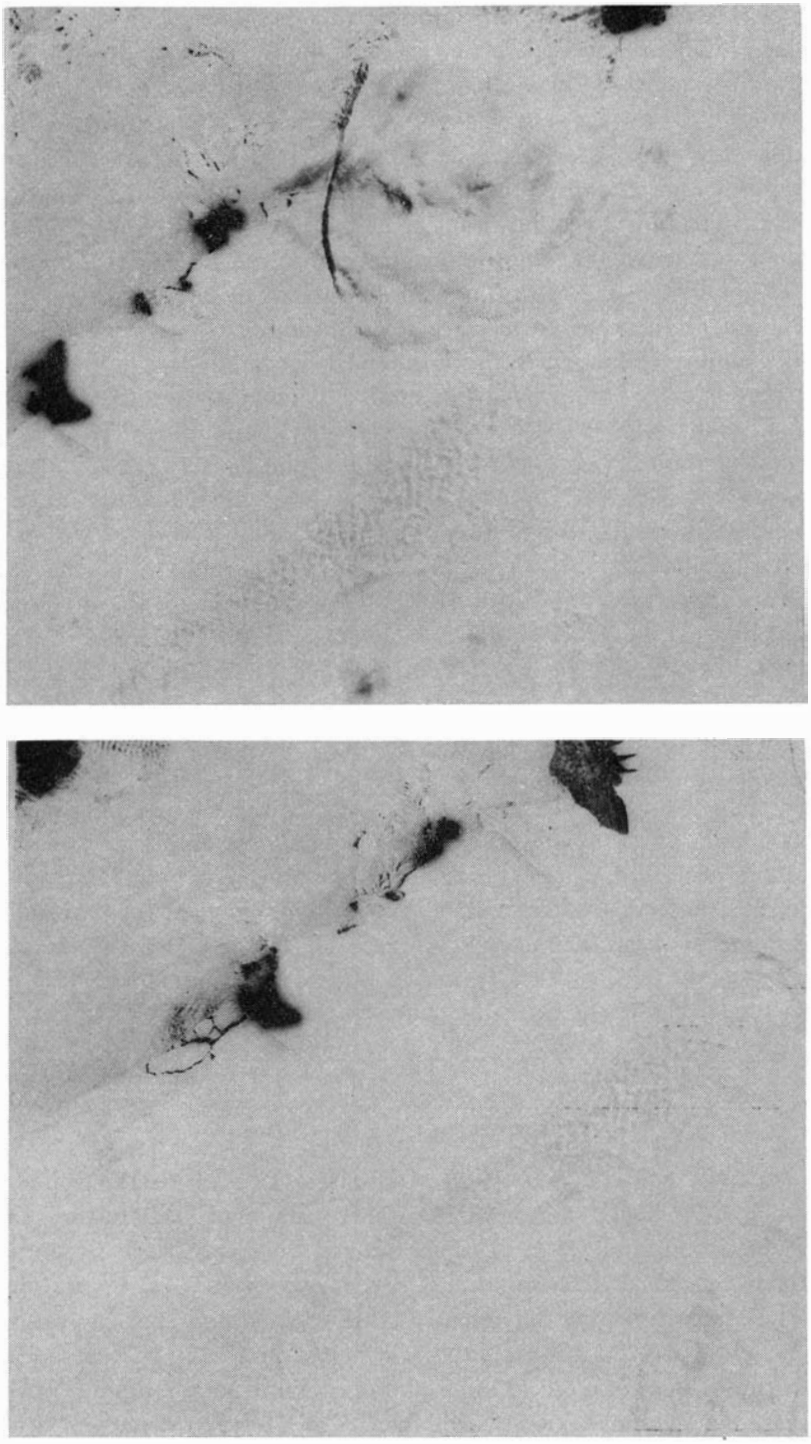

Fig. 2. *Successive Landsat imagery used for ice drift determinations. Above: imagery 2330—07130, obtained on 18 December 1975. Below: imagery 2331—07184, obtained one day later. Both MSS 7.*

the data set is too small to make firm conclusions about the marine currents in the area.

It is not always easy to recognize icebergs within the pack ice. We had hoped to do this at low sun angles by the shadow of the icebergs, which are approximately 20 m above sea level. However, there is commonly open water on one side of icebergs, making it difficult to distinguish the shadow of the berg. And it obviously cannot be assumed that open water within the pack ice indicates presence of icebergs.

We had also hoped to distinguish between floes and bergs by using images at different MSS bands. We expected that the sea ice, which at times is wet with sea water, should be distinguishable from the icebergs. But many images were from early in the season (October and November) when both the sea ice and the bergs are covered by dry snow, and at these times it was not easy to distinguish icebergs from floes. Later in the season the floes have lower albedo than the icebergs, and exhibit marked melt phenomena, and could be distinguished. Thus it is likely that Fig. 2 shows some icebergs surrounded by a darker sea ice, but without ground truth we cannot prove this. The shapes are of course also important, if the shape is rectangular then the chances increase that the object is an iceberg. Furthermore, the sea ice commonly exhibits characteristic deformation features such as shown in Fig. 2.

A combination of several remote sensing techniques would better resolve this question, and there is no doubt that repetitive imagery of an area with recognized floes and bergs would be an inexpensive and very useful technique for charting the marine currents. Because the floes are essentially surface wind/current driven, while the bergs show the combined effect of the surface winds and the integrated ocean currents down to about 200 m, the tracking of both together would give much oceanographic and meteorological information.

Distribution of sea ice and icebergs

Table 1 shows the frequency distribution of the size of the floes, as determined from images at 1:500,000 scale by a semi-automatic planimeter. Six images from October and November 1975, covering altogether an area of over 72,000 km^2, have been considered. Because of high cloudiness it was not possible to find suitable imagery for the rest of the investigation period. Only floes with an area greater than 10 km^2 have been considered, as the determination of the area of smaller floes becomes unreliable.

Around Svalbard in the Arctic there is an indication of a bimodal distribution in the floe sizes (Vinje 1977). This is not established in the more limited material from Antarctica. Instead there is an irregular decrease of the percentage coverage as the sizes of the floes increase from 10 to 100 km^2. The mean area of the 636 floes considered is 30 km^2.

Table 1
Frequency distribution of floe sizes north of Dronning Maud Land

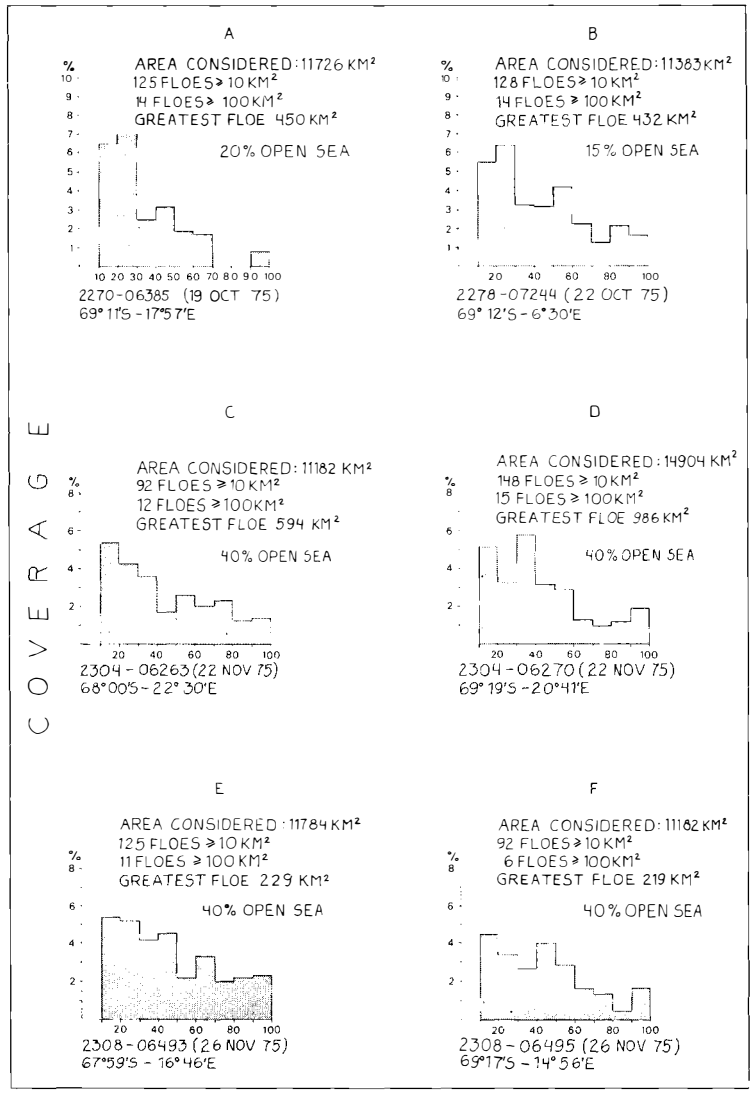

Table 2.
Percentage contribution to the total ice covered area of floes of various sizes.

Imagery Table 1	Ice covered area, km²	Floe-size intervals, km² 0—10	10—100	above 100
A	9380	37	29	34
B	9680	34	35	31
C	6710	26	49	25
D	8940	23	44	33
E	7070	22	47	31
F	6710	48	38	14
Mean	8080	32	40	28

Table 2 shows the percentage of ice covered area represented by the different classes of floe sizes.

The table shows fairly constant percentage coverage from class to class. This indicates that the number of floes roughly changes with a factor of 10 from class to class, i.e. an exponential relationship between number and area of floes.

Ice shelf features

The map, Fig. 1, and Fig. 3, shows several ice rises that could be important sites for future ice drillings for paleoclimatic studies. Half of these are not registered on earlier maps, and we found that they were best recognized by making overexposed copies of the MSS 7 imagery. Table 3 gives the dimensions of the ice rises, as measured from images at 1:1 million scale.

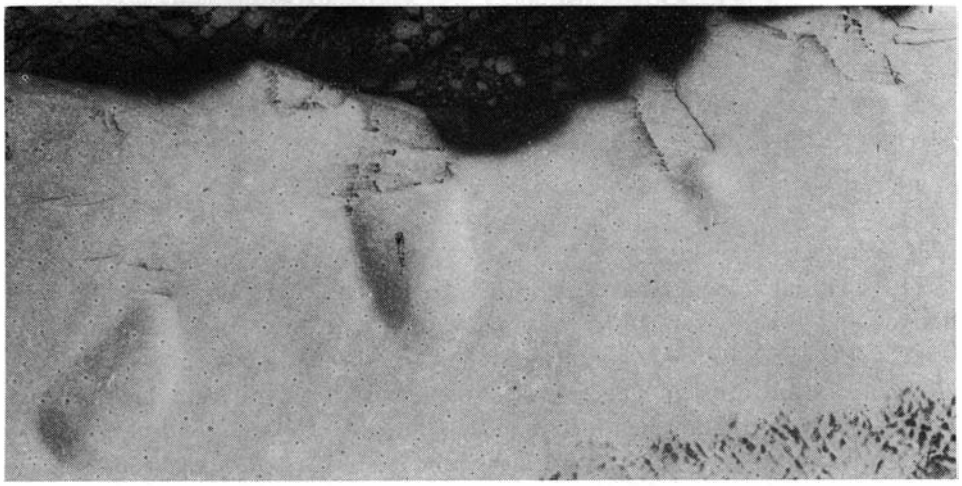

Fig. 3. *Part of Landsat imagery 2278—07250, MSS 7, showing four ice rises at the Dronning Maud Land coast between 3° and 7°E at scale of 1:1.1 mill. These ice rises are only slightly above the general surface of the iceshelf, and can be difficult to see from ground level.*

Table 3
Ice rises recognized from Landsat imagery

No	Ice rise position	Length, km	Width, km	Length / width
1	71°00'S, 6°00'W	80	30	0.38
2	70°50'S, 2°00'W	9	7	0.78
3	70°10'S, 1°45'W	9	5	0.56
4	70°40'S, 2°00'E	10	6	0.60
5	70°30'S, 3°00'E	32	19	0.59
6	70°20'S, 4°30'E	29	19	0.66
7	70°20'S, 5°30'E	11	9	0.82
8	70°10'S, 6°30'E	12	8	0.67
9	70°20'S, 7°30'E	31	19	0.61
10	70°20'S, 9°00'E	40	22	0.55
11	70°00'S, 10°30'E	15	6	0.40
12	70°00'S, 13°00'E	35	10	0.29
13 (?)	70°00'S, 16°00'E	41	35	0.85
14 (?)	70°20'S, 19°00'E	48	34	0.71
15	70°30'S, 22°00'E	55	35	0.64
16	70°10'S, 26°00'E	40	31	0.78

Table 3 probably includes all ice rises observable by Landsat from Dronning Maud Land between 2°W and 20°E. Half of those given in Table 3 are not shown on existing maps. Ice rises can also be seen in the imagery between 2° and 10°W (Fig. 1), but the cloud cover is too high to allow complete determinations. Nos. 13 and 14 are questionable; in the Landsat imagery their southern boundaries appear to join the grounded inland ice sheet at narrow necks. If so, they do not conform to the definition of an ice rise as an isolated elevated feature. Note that the ice rises generally are ellipsoidal, with the short axis about ²/₃ of the long axis. Ice rises of near-circular shapes are unusual. The orientations of the long axes show no systematic variations (Fig. 1).

The Landsat imagery have also provided much other information on land phenomena. The major ice streams are shown with their flowlines, and blue ice fields and snow drift patterns are clearly brought out (Figs. 4 and 5). One interesting and unexpected discovery was the significant melt phenomena shown in Fig. 7, obtained on 10 January and 14 February, 1976. Presumably because of lower albedo the blue ice fields experience considerable melting, with the melt phenomena extending many kms downslope. Some of the darker areas could at first glance be mistaken for solid rock, but examinations of all MSS bands show that the phenomena become very indistinct in

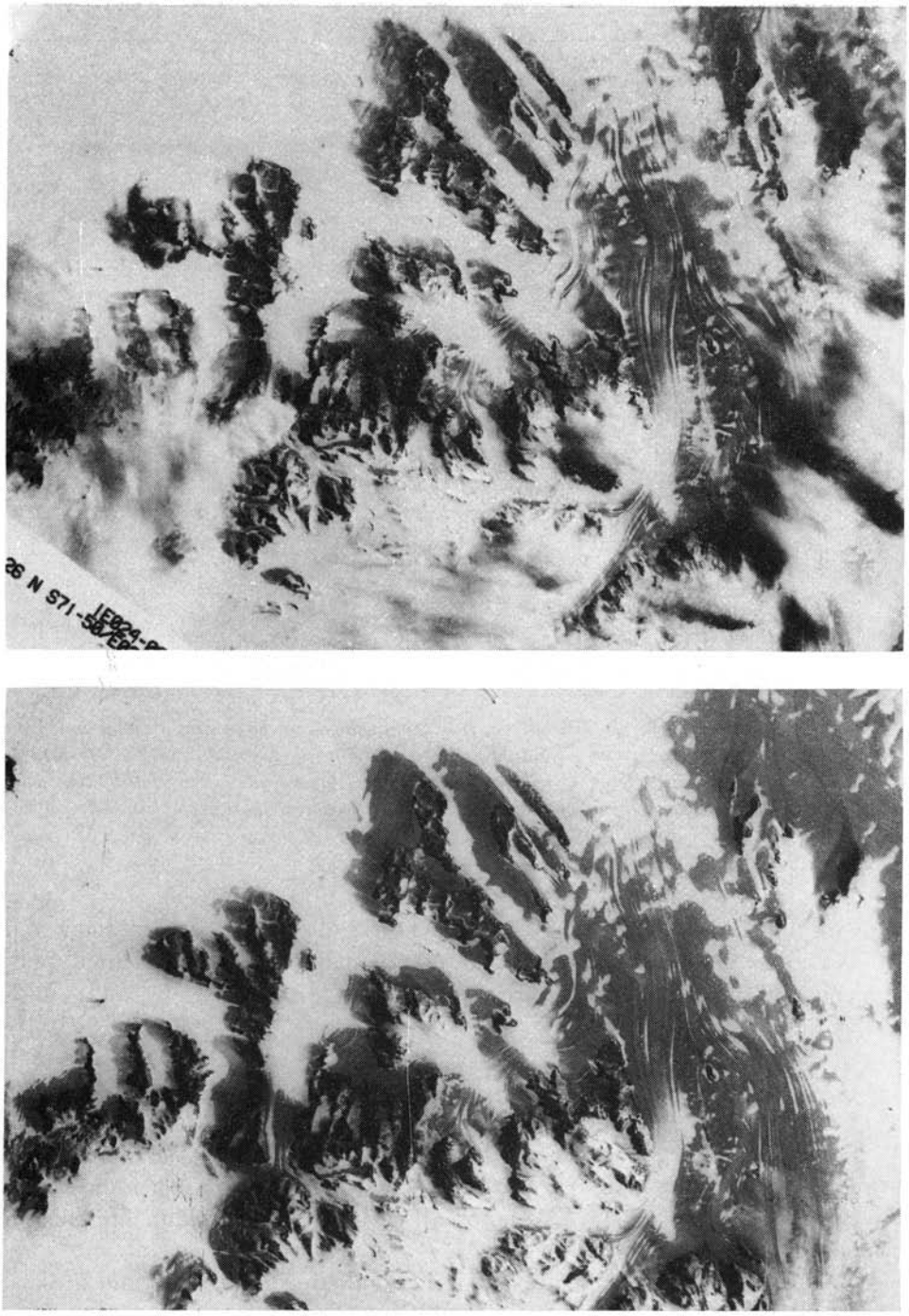

Fig. 4. *Eastern part of Sør-Rondane mountains, with Byrdbreen as the major ice stream on the right hand side of the images. Both pictures have centre at 71°50'S and 25°E, are oriented with N upwards parallel the short sides of the imagery, and are at a scale of 1:1 mill. Above: Part of Landsat image 2279—05480, MSS 7, obtained on 28 October 1975. Below: Part of Landsat image 2388—05522, MSS 7, obtained on 14 February 1976. Note persistent flow patterns, which can be seen to change in appearance during the summer season. The areas of high albedo are reduced, and these must be snow patches with a distribution that follows the glacier surface topography, and which perhaps also reveals the wind patterns. There are also features of low albedo which follow the glacier flow patterns and which probably are moraines. Such linear features which reveal glacier flow can be seen in the Landsat imagery of practically all the mountain ranges of Dronning Maud Land.*

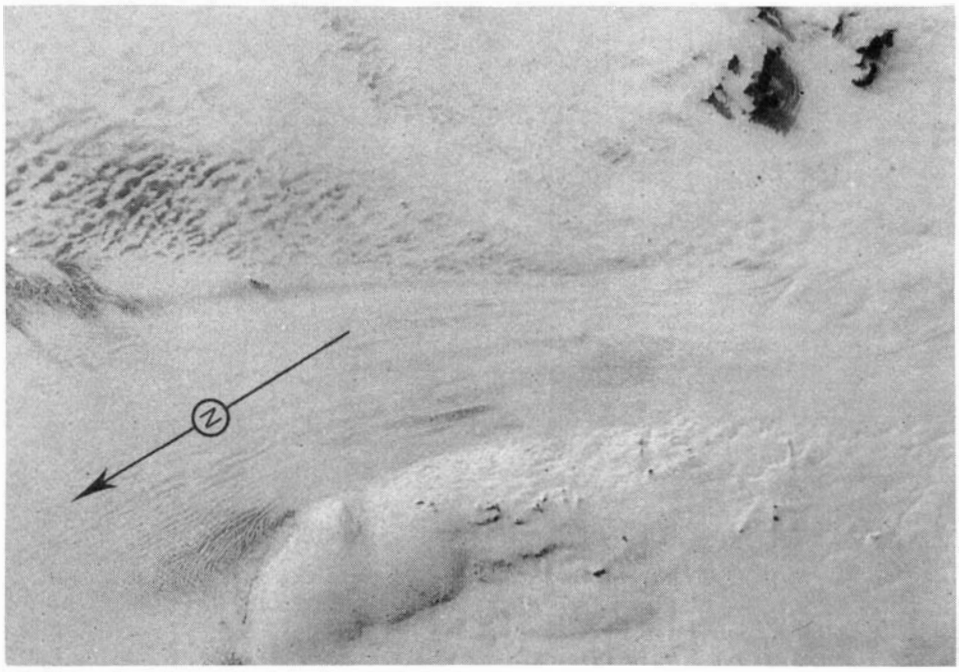

Fig. 5. *South central part of Jutulstraumen, the largest glacier in Dronning Maud Land, with mass outflow exceeding $10^{10} m^3 yr^{-1}$. The figure shows part of Landsat image 2279—07311, MSS 7, obtained on 28 October 1975 with centre of figure at 71°40'S, 0°30'W, scale 1:1 mill., and north given by arrow. Note how the glacier decouples from the bed and becomes afloat in the southern part of the image.*

bands 4 and 5, and it is clear that the imagery shows only water, snow and ice. Note also the persistence of the snow drift patterns south of the melt phenomena, and the crater-like feature visible in both images.

Conclusions

The area of this investigation is remote and not easily accessible, thus study of the Landsat imagery gave much original information. The imagery allowed the production of a nearly complete map of the Dronning Land coastline from 10° W to 29° E. This map will serve as an important reference to compare with future studies.

Comparisons of images show that icebergs drifted between 9 and 20 km/day, and that the number of ice floes of given size decreases exponentially with size, so that each size class covers approximately the same area.

A number of ice rises, which could be important localities for future paleoclimatic studies, have been located, and flow line patterns, melt phenomena and other glacier features have been observed.

The Landsat imagery have a potential for investigation of many problems in inaccessible areas, with which costly expeditions cannot hope to compete.

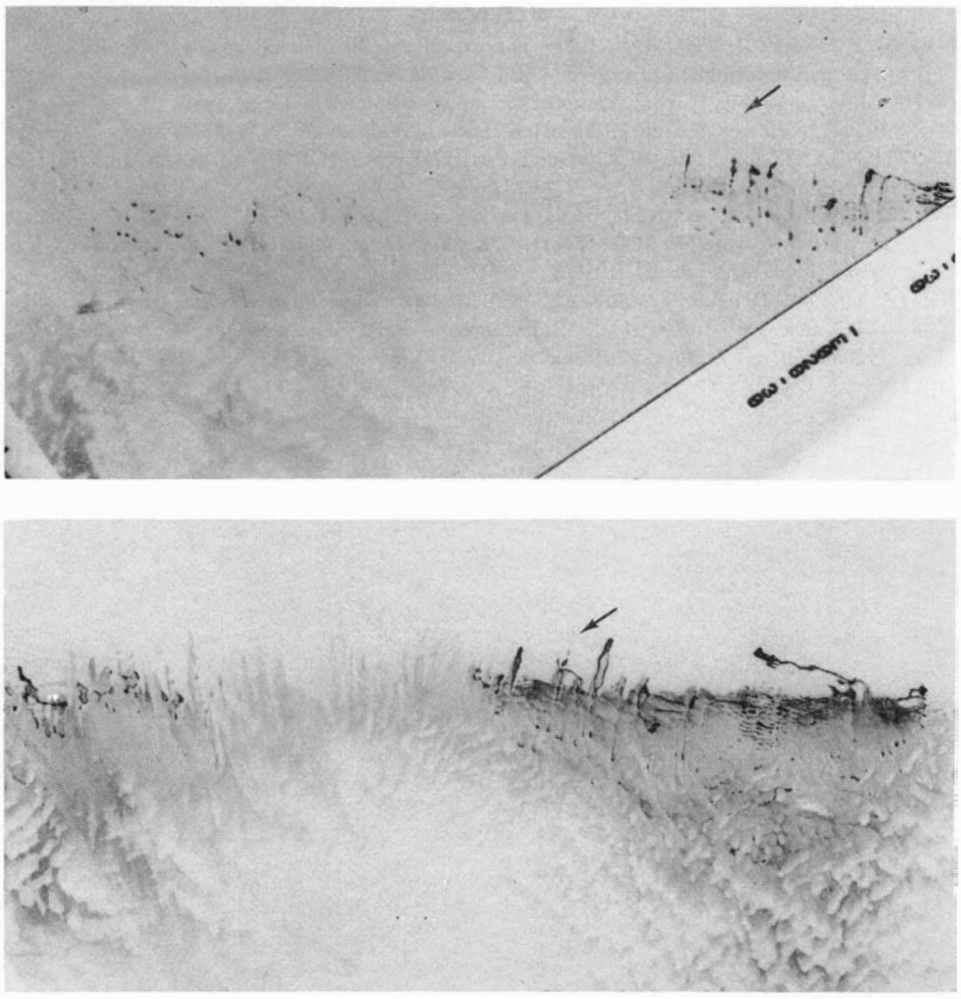

Fig. 7. *Above: Part of Landsat imagery 2353—05581, MMS 7, taken on 10 January 1976, at scale 1:1 mill., with centre of picture at 70°45'S, 27°E, oriented with N, and downslope, upwards parallel the short sides.*

Below: Part of Landsat imagery 2388—05515, MSS 7, taken on 14 February 1976, with scale and orientation as for the upper image and covering approximately the same area. Note the various melt phenomena extending downslope from blue ice fields, and the unchanging pattern of the snowdrifts south of the melt features.

The arrows point to a 2 km long, 1.5 km wide «crater-like» feature, which is clearly visible on the original imagery but may not survive reproduction processes.

Acknowledgements

I gratefully acknowledge helpful discussions with T. Vinje and S. Helle about various aspects of this work. Ø. Finnekåsa helped with the data analysis. We are especially grateful to NASA for supplying the Landsat images.

References

NYE, J. F., and D. R. THOMAS, 1974: The use of satellite photographs to give the movement and deformation of sea ice. *AIDJEX Bulletin* No. 27. Seattle.

ORHEIM, O. (in prep.): Flow of Antarctic ice shelves between 29°E and 44°.

— 1978: Hvorfor er de antarktiske isfjell så store? *Naturen* (6) 1978: 277—280.

SWITHINBANK, C., P. MCCLAIN, and P. LITTLE, 1977: Drift tracks of Antarctic icebergs. *Polar Record* 18 (116): 495—501.

TCHERNIA, M. P., 1974: Étude de la dérive antarctique Est-Ouest au moyen d'icebergs suivis par le satellite Éole. *Comptes Rendus Hebdomadaires des Séances de l'Académie de Sciences (Paris)*, Série B, 278 (14): 667—70.

VINJE, T., 1977: Drift av Trolltunga i Weddellhavet. *Norsk Polarinstitutt Årbok* 1975: 213.

— 1977: Sea ice studies in the Spitsbergen — Greenland area. *Landsat Report E77-10206 National Technical Information Service*. Springfield.

Snow accumulation and snow stratigraphy on Riiser-Larsenisen, Dronning Maud Land, Antarctica*

BY KJELL REPP

Abstract

The western part of Riiser-Larsenisen is fairly flat, with small undulations difficult to detect. Outstanding features are an ice dome of 200 metres elevation and a long, narrow depression parallel to the edge of the ice shelf. Snow stratigraphy and density were measured in nine pits, the deepest 4.5 metres. Mean accumulation of all pits for the year 1976 was 588 mm in water equivalent, which is higher than earlier investigations. Five snow cores to depths of 11 to 15 metres were collected for laboratory analyses.

Introduction

The 1976/77 Norwegian Antarctic Expedition is described by Orheim (1977). This paper will deal with the snow studies carried out by the author in the period 19 January — 10 February 1977. The primary aim of these studies was to get information on the accumulation pattern, as a pilot project for more extensive investigations on the 1978/79 expedition. Shortness of time forced us to concentrate the work on a rather small area.

Riiser-Larsenisen is a rather unknown area. Only brief studies were done previously by Lunde on the 1968/69 Norwegian Expedition (Liestøl, pers. comm.) (see Fig. 1). At Maudheim, 230 kilometres farther east, extensive glaciological investigations were conducted during the Norwegian-British-Swedish Antarctic Expedition 1949—52. Even further east, glaciological work was carried out around Norway Station by Den Norske Antarktisekspedisjon, 1956—60.

Morphology and climatology

The area investigated is located around 16° 30' West, extending from the coast to Vestfjella, 120 kilometres from the sea. The ice shelf is fairly flat.

* Publication No. 12 of the Norwegian Antarctic Research Expeditions (1976/77).

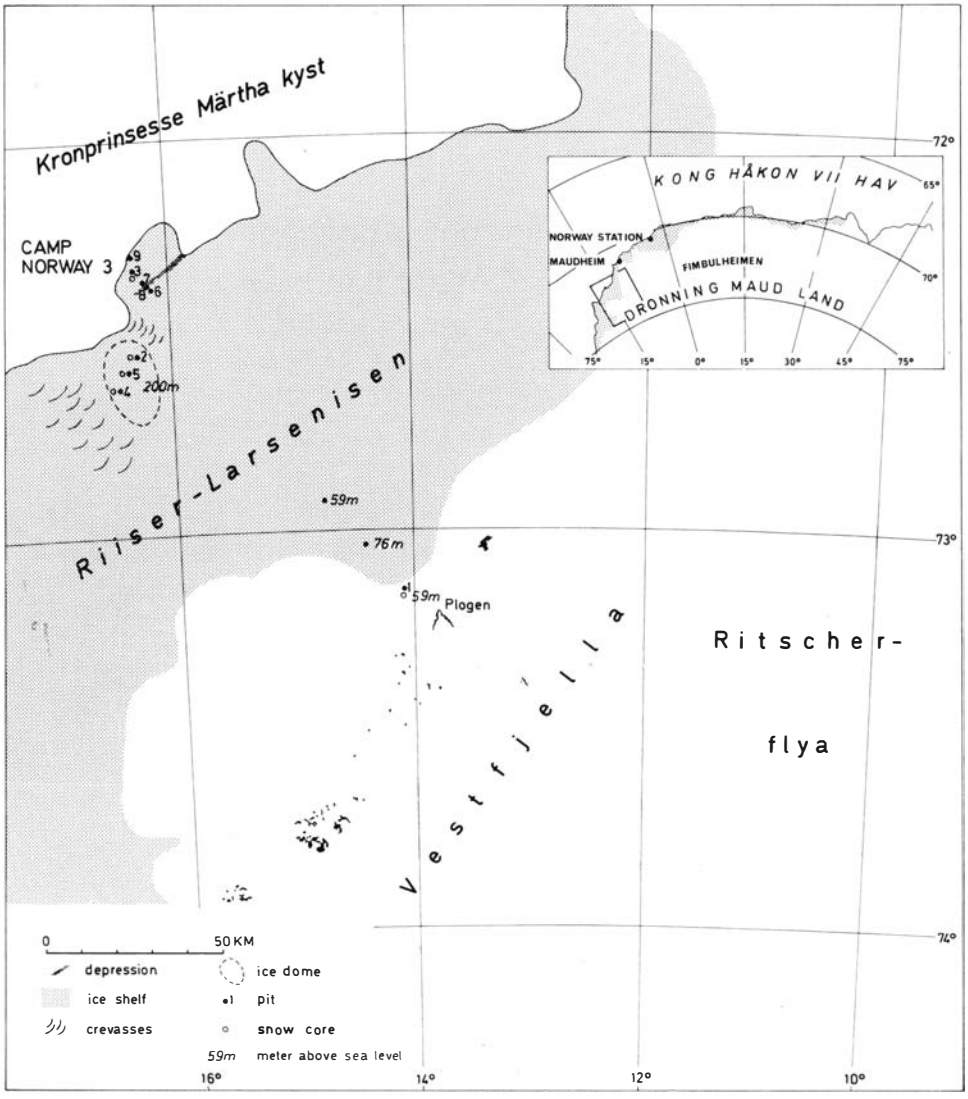

Fig. 1. *Location map.*

Undulations are common, although they may often be hard to detect without instrumental levelling. Camp Norway 3, three kilometres from the coast, was 35 metres above sea level (measured by two aneroid barometres). 15 kilometres inland the gentle surface was partly broken by a 2.5 kilometres wide shallow depression, running in the direction ENE—WSW. Fig. 1 indicates the borders of the ice shelf and includes some elevations, most of them readings from aneroid barometres. The elevations of the inner part were surveyed by Gjessing (unpublished), and are more reliable.

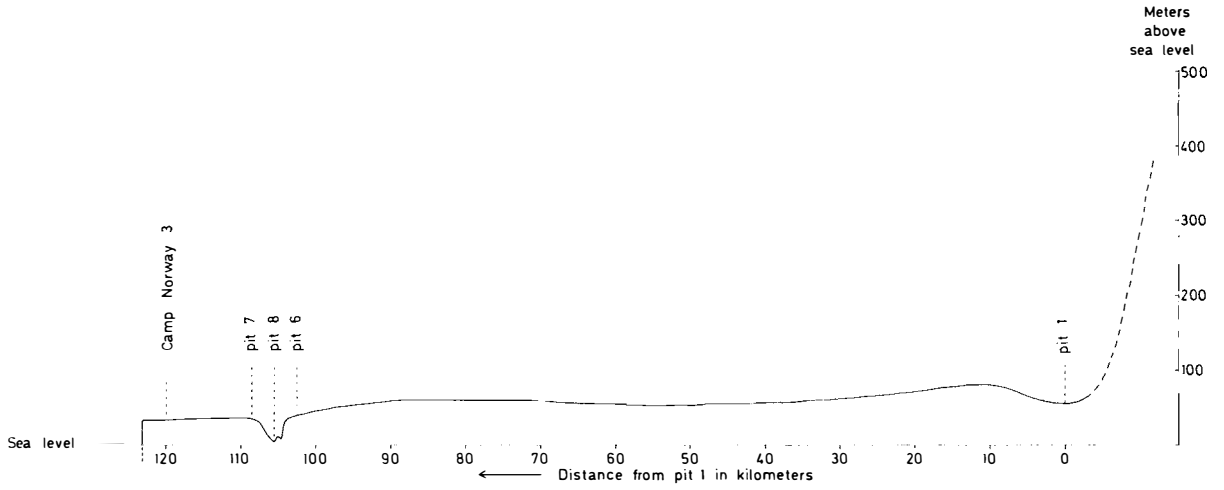

Fig. 2. *Surface profile along the traverse route from Camp Norway 3 to pit 1.*

The most outstanding feature of the studied part of the ice shelf is an ice dome, situated 20—30 kilometres southeast from Camp Norway 3 at an elevation of approximately 200 metres above sea level. There are few crevasses. Only on the northern and southern sides of the ice dome are some crevasses formed by the ice streams. Fig. 2 shows a profile of the ice surface from Camp Norway 3 along the traverse route to Vestfjella.

The predominant wind direction is from the eastnortheast (T. Vinje, pers. comm.). The size and density of sastrugi are variable; their maximum heights are 0.2 m on the eastern side of the ice dome.

Technique

Nine pits were dug to determine the annual net accumulation (Fig. 1). They varied in depth from 2 to 4.5 metres. It was hoped that the stratigraphy and density measurements would reveal the annual layers, with the summer surface being represented by a coarse-grained, highly metamorphosed layer (Schytt 1958). The density measurements were made as described by Lunde (1961) with an accuracy of about $\pm$ 0.015 g/cm^3.

Results and discussion

Figs. 3 to 11B present the stratigraphy, snow density, and cumulative water equivalent of the pits. Ice layers and ice lenses are shown by black lines, indicating the thickness of the layers. The grain diametre of the snow and firn is indicated by the diametre of the circles. Heavy dots indicate very dense (and often windpacked) snow. A brief description is given on each section. A more detailed description is available at Norsk Polarinstitutt. (For localization of the pits, see Fig. 1.)

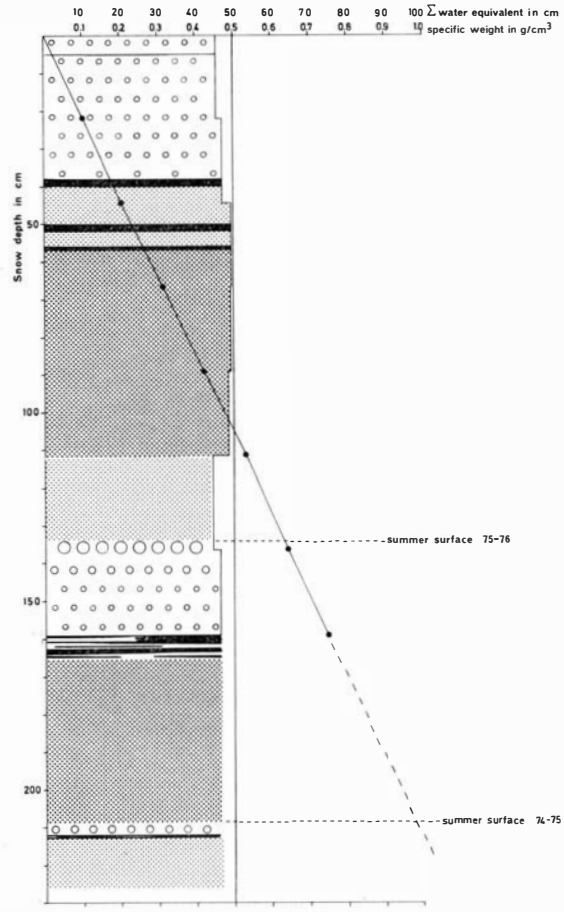

Fig. 3. *Pit 1. The hinge zone of the ice shelf.*
0 — 38 cm: Coarse-grained firn with a very thin ice layer near the top. The firn was partly wet and soaked with melt water.
57 —112 cm: Wind-packed, fine-grained snow with no signs of refrozen melt water.
133—159 cm: Very coarse-grained firn. Ice pellets.
159—165 cm: Several ice layers, locally reaching a thickness of 6 cm.
Summer surfaces at 133 and 208 cm.

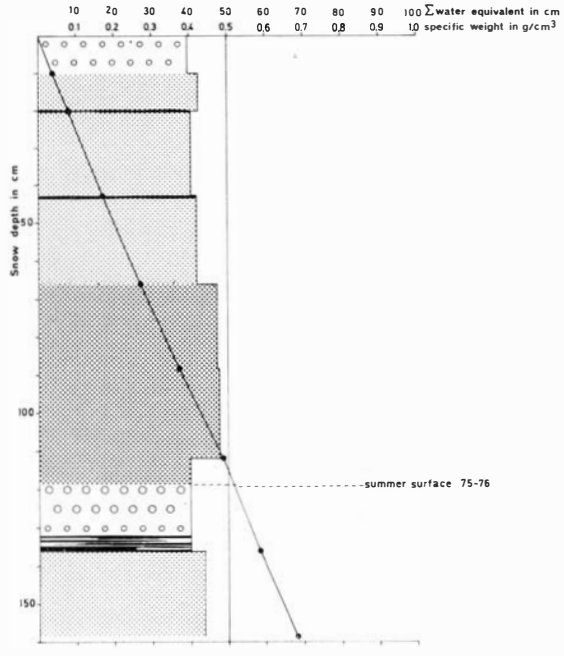

Fig. 4. *Pit 2. Eastern slope of the ice dome.*
118—136 cm: Coarse-grained firn with ice pellets. Last 4 cm several ice layers, varying from 0.2 cm to 1 cm thickness.
Summer surface at 118 cm.

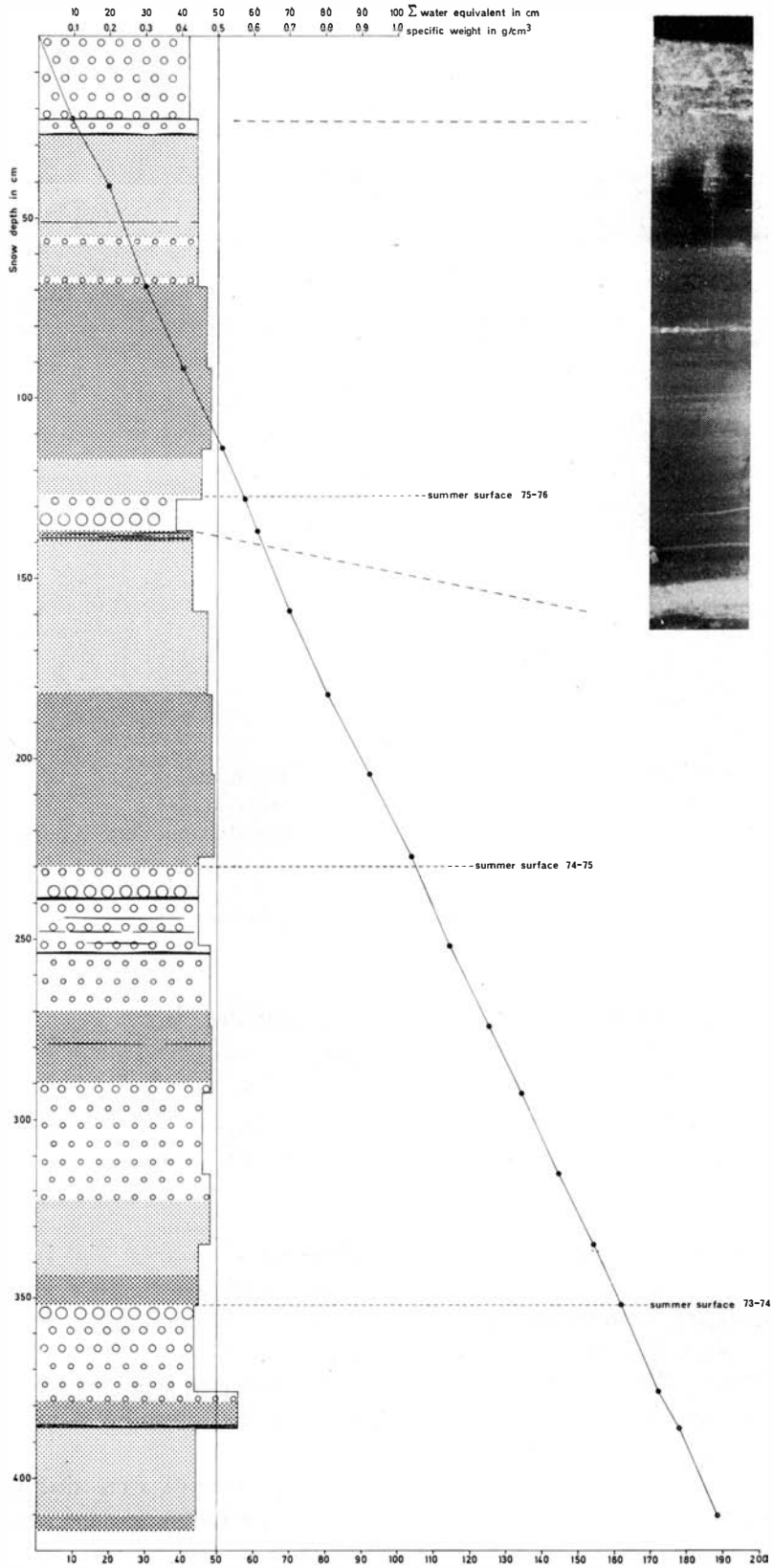

Fig. 5. *Pit 3. Camp Norway 3.*

0 — 27 cm: Very coarse-grained firn, soaked with melt water.

126—137 cm: Very coarse-grained, small ice pellets.

230—270 cm: Very coarse-grained. Slightly finer towards the bottom Numerous ice pellets. Ice layers at 238 cm, 244 cm, 248 cm, and 253 cm.

352—379 cm: Very coarse-grained firn, finer and increasing density towards the bottom. *Summer surfaces at 126 cm, 230 cm, and 352 cm.*

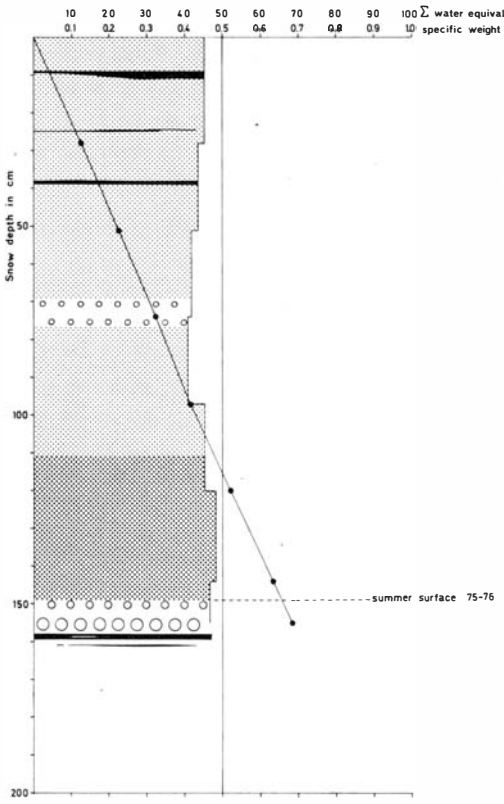

Fig. 6. *Pit 4. Southwestern slope of the ice dome.*
149—161 cm: Very coarse-grained firn. No ice pellets. Ice layers (2—15 mm) at the bottom.
Summer surface at 149 cm.

Table 1.
Annual accumulation in water equivalent in mm.

	Pit number								
Year	1	2	3	4	5	6	7	8	9
1976	633	515	570	655	665	408	572	730	549
1975	349		480			370	518		384
1974			567						

Pit 1 was located at the hinge zone between the ice shelf and the inland ice. Pits 2, 4, and 5 are respectively from the northeastern slope, the southwestern slope, and near the top of the ice dome. At Camp Norway 3 two parallel pits were dug, and the separating thin wall was photographed by transmitted light (pit 3). Three pits, 6, 7, and 8, were dug at the above mentioned east-west running depression, respectively on the southern side, on the northern side, and in the centre.

Table 1 summarizes the accumulation values. All pits were dug between 19 January and 9 February, and the precipitation in this period was negligible.

The horizontal variability of accumulation is the result of relationships between topography, on a large as well as a small scale, wind velocity, and

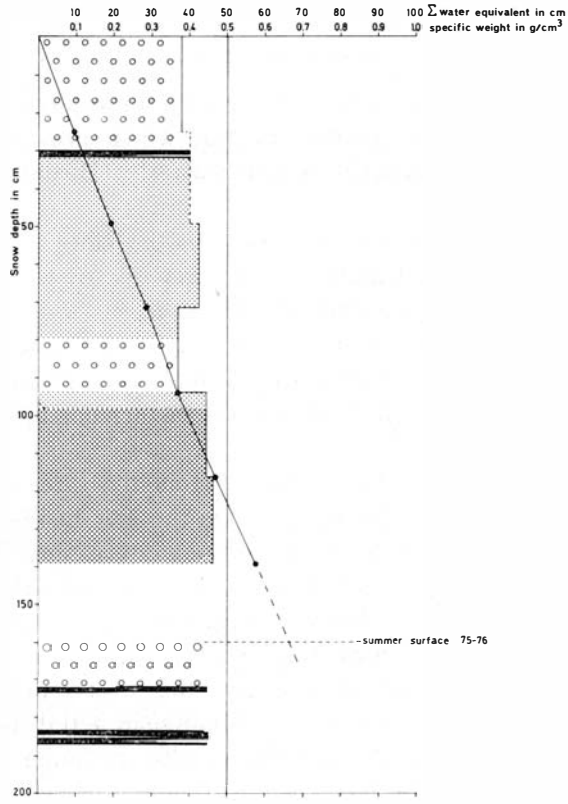

Fig. 7. *Pit 5. Top of the ice dome. Due to shortness of time, the stratigraphy of this pit was not sufficiently analysed. However, last summer surface was found at 160 cm. Between this and the summer layer of 1976/77 no layers were saturated and no ice layers could be traced. Below 160 cm was found 12 cm of coarse-grained firn with numerous ice pellets, and below this two thick ice layers (10—40 mm) at 172 cm and 183 cm.*

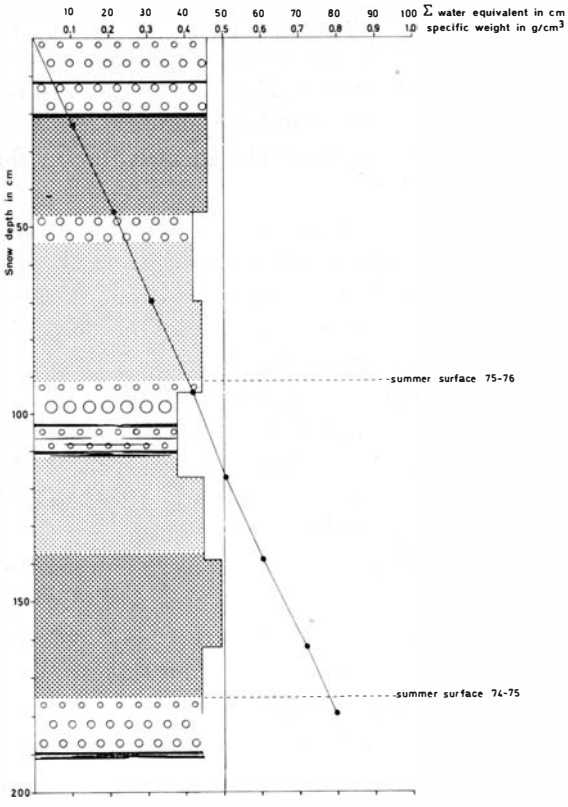

Fig. 8. *Pit 6. Southern side of the depression.*

91 —111 cm: Very coarse-grained firn. An abundance of ice pellets. Numerous ice layers between 102 cm and 111 cm.

175—191 cm: Coarse-grained firn with an ice layer (10—20 mm) at the bottom.

Summer surfaces at 91 cm and 175 cm.

turbulence. Riiser-Larsenisen lies in an area affected by a cyclonic wind system broadly similar to that which prevails at Maudheim where all high winds are easterly or northeasterly (Hisdal 1958). The bulk of the precipitation is probably due to those winds.

The accumulation at pit 1 is probably affected by drift snow swept from the interior. Katabatic winds remove snow from the glacier slopes near Plogen, where the glacier surface drops from 500—600 metres elevation to 50 metres elevation at pit 1. The katabatic winds affect the accumulation pattern only over short distances. Visual observation of the stratigraphy in two shallow pits 17 and 35 kilometres further northwest showed a significant accumulation decrease.

The accumulation values from the three pits at the ice dome are closely related to the topography. On the east-facing slope accumulation is much less than on the top and the southwestern side. The eastern slope with frequent sastrugi bears witness of strong northeasterly winds, which erode and carry the snow to the leeward side. The heavier accumulation at the top is probably due to orographic precipitation.

Pit 3 is assumed to give the most representative accumulation value at Riiser-Larsenisen as it is situated in a flat, uniform area of considerable extension. The most variable results are found for pits 6, 7, and 8, lying within very short distance from each other. However, the regime at each pit is related to the topography. The centre of the depression receives most accumulation (pit 8). The depression is clearly visible on the air photos from 1951. Extending strain and subsidence of the depression may compensate for the greater accumulation. The accumulation value on the northern side (pit 7) equals that of pit 3. On the southern side erosive winds may explain the very low accumulation rate. The mean value of the pits, 570 mm, is, however, the same as for pit 3.

Pit 9 differs slightly from pit 3. The decrease is probably due to its short distance from the ice front. Northeasterly winds may have an erosive effect near the front of the ice shelf (Swithinbank 1957).

The three years of accumulation noted in pit 3 give a mean value of 539 mm. The comparable figure from pit measurements for the years 1935—51 at Maudheim is 365 mm (Schytt 1958), and from stake measurements in 1951, 375 mm (Swithinbank 1957). At Norway Station the mean accumulation was 484 mm for the ten-year period 1940—49, while it was 506.3 mm for the period 1950—59 (Lunde 1961). The height of five masts above the snow surface at Maudheim measured in 1952 and remeasured in 1960, showed a mean annual accumulation of 420 mm (Swithinbank 1962).

The analysis of the snow cores will possibly provide more detailed data of the accumulation for the past 10—15 years. The accumulation pattern will be established from accumulation stakes put into the ice shelf during the field season. One line of stakes runs between the edge of the ice shelf and Vestfjella, and some were established on the ice dome. These stakes will be remeasured during the 1978/79 expedition.

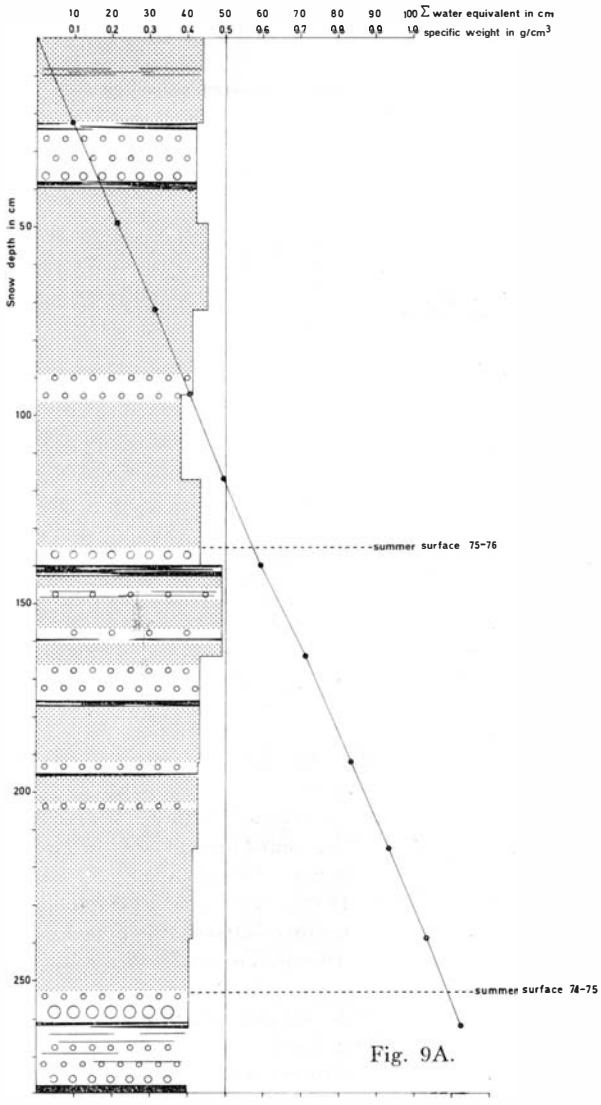

Fig. 9A.

Fig. 9B.

Fig. 9C.

Fig. 9A. *Pit 7. Northern side of the depression.*

135—140 cm: Very coarse-grained firn. Ice pellets.

140—143 cm: Several ice layers of varying thicknesses.

143—196 cm: Fine-grained snow. Looser layers in connection with ice crusts and ice layers at 146 cm, 156 cm, 166 cm, and 192 cm. This section is illustrated in Fig. 9B.

253—280 cm: Very coarse-grained firn. Ice layer (2—15 mm) at 261 cm. Thin ice laminae between 262 cm and 271 cm. Near the bottom of the pit, at 278 cm, a thick ice layer (25 mm) had developed (Fig. 9C).

Summer surfaces at 135 cm and 253 cm.

Fig. 9B. *The summer section between 143 cm and 185 cm See Fig. 9A.*

Fig. 9C. *The thick ice layer at the bottom of pit 7.*

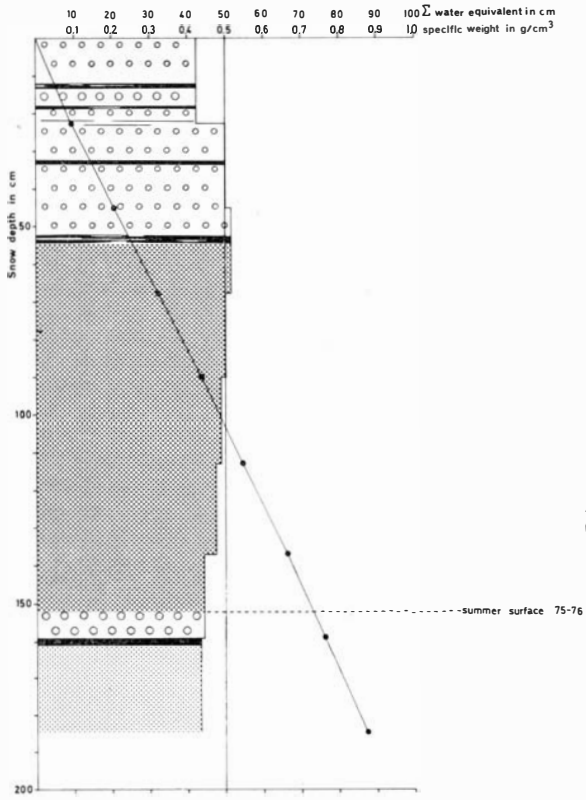

Fig. 10. *Pit. 8. Centre of the depression.*

0 — 54 cm: Uniform, coarse firn. An abundance of ice pellets. Ice layers (10—20 mm) at 12 cm, 18 cm, 32 cm, and 52 cm. Thin ice laminae between 21 cm and 23 cm. This section was soaked with melt water.

152—161 cm: Coarse-grained firn. A few ice pellets.

Summer surface at 152 cm.

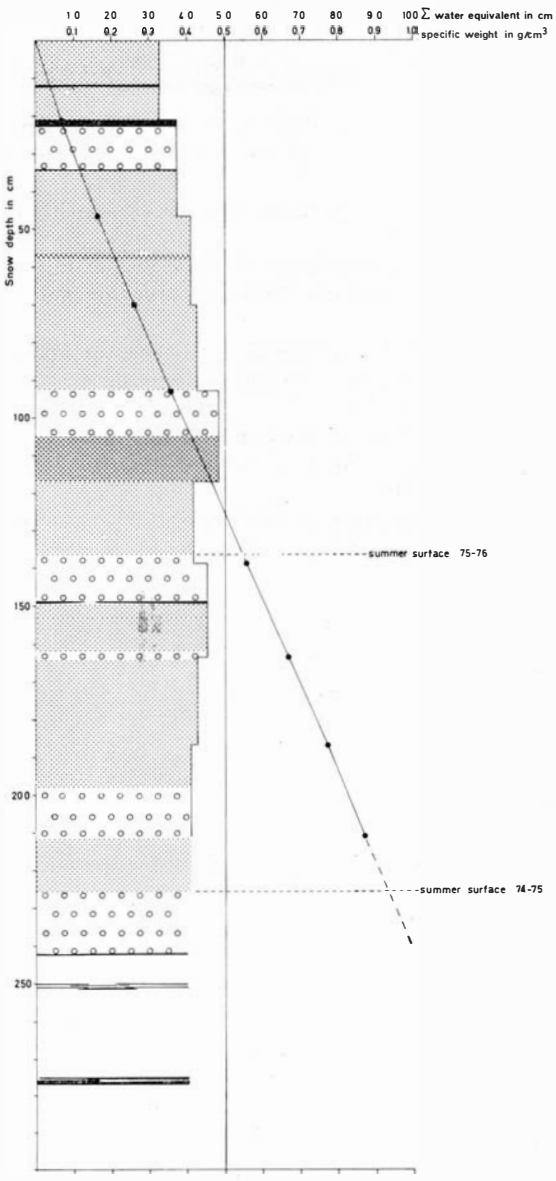

Fig. 11A. *Pit 9. North of Camp Norway 3.*

34 —92 cm: Homogenous, fine-grained snow. A denser layer, probably a wind crust at 57 cm.

137—149 cm: Coarse-grained firn, with a thin ice layer at the bottom. Probably a summer horizon.

226—277 cm: Very coarse-grained firn. A few ice pellets and several ice layers of varying thicknesses (2—20 mm).

Summer surfaces at 137 cm and 226 cm. This pit wall is shown in Fig. 11B.

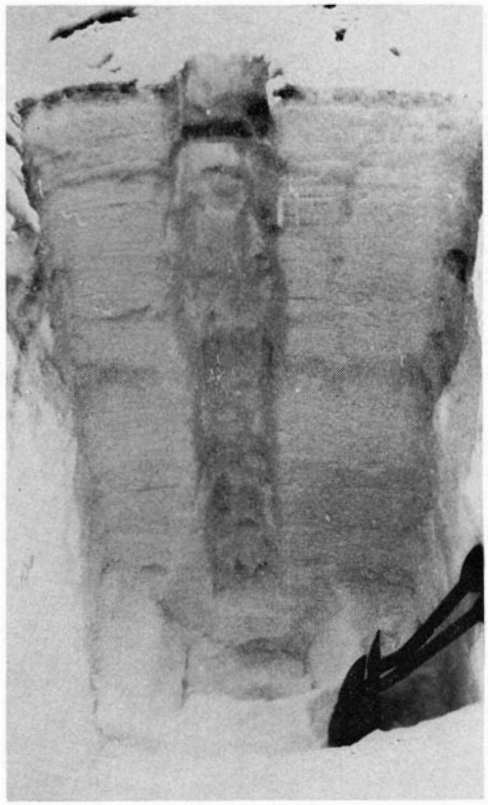

Fig. 11B. *This pit wall shows the two years accumulation described in Fig. 11A.*

References

HISDAL, V., 1958: Surface observations. — B. Wind. *Norwegian — British — Swedish Antarctic Expedition, 1949—52. Scientific Results I* (I) part 2 B: 65—122.

LUNDE, T., 1961: On the snow accumulation in Dronning Maud Land. Den Norske Antarktisekspedisjon, 1956—60, Scientific Results No. 1. *Norsk Polarinstitutt Skrifter* Nr. 123.

ORHEIM, O., 1977: Preliminary report of the 1976/77 Norwegian Antarctic Research Expedition. *Norsk Polarinstitutt Årbok* 1976: 327—332.

SCHYTT, V., 1958: Glaciology. — A. Snow Studies at Maudheim. B. Snow Studies Inland. *Norwegian — British — Swedish Antarctic Expedition, 1949—52. Scientific Results* IV (II).

SWITHINBANK, CH., 1957: Glaciology. — B. The Regime of the Ice Shelves at Maudheim as shown by Stake Measurements. *Norwegian — British — Swedish Antarctic Expedition, 1949—52. Scientific Results* III (I): 1—76.

— 1959: Glaciology. — E. The Regime of the Ice Sheet of Western Dronning Maud Land as shown by Stake Measurements. *Norwegian — British — Swedish Antarctic Expedition, 1949—52. Scientific Results* III (I): 97—144.

— 1962: Maudheim revisited: The morphology and regime of the Ice Shelf, 1950—1960. *Norsk Polarinstitutt Årbok* 1960: 28—31.

Paleomagnetism and morphology of lava(s) at Cape Meteor*, Bouvetøya**

BY REIDAR LØVLIE[1] AND HARALD FURNES[2]

Abstract

At Cape Meteor a shallow marine lava delta consisting of basic lava units and hyaloclastites are overlain by flatlying massive/aa type flow units. The junction between the lava delta and overlying flow, defining the sea at the time of formation, is presently situated at a maximum of 15 m above sea level. Palaeomagnetic investigation of a thick, massive flow unit of the lava delta, revealed the presence of a stable, tightly grouped remanent magnetization defining a virtual pole position that is significantly different from the present geomagnetic south pole. Assuming a constant westward drift of the geomagnetic field of 0.06°/year this lava has a minimum age of around $2 \cdot 10^3$ years. Thus the maximum rate of uplift of Bouvetøya at Cape Meteor appears to have been ca. 0.75 cm/year.

Introduction

Bouvetøya is an ice covered (95%), volcanically active island situated on the Mid-Atlantic Ridge at 54° 26' S, 3° 24' E. Previous palaeomagnetic information from the island (Snape and Retief 1971) has only been based on three oriented hand samples, two from Larsøya and one from Westwind Beach (Fig. 1). The samples were normally magnetized and in good agreement with the present axial geomagnetic field direction. From this result Snape and Retief suggested a maximum age for the lavas of less than 700,000 years.

During a short visit to the Blacksand Beach in February 1977 (Fig. 1), nine oriented drill cores were collected with the intention of utilizing the se-

* No official place-name guide has yet been made for Bouvetøya. Geographical names are thus somewhat inconsistently used. Names used in this article will problably have the following future forms: Westwind Beach — Nyrøysa, Westwind-stranda; Blacksand Beach — Svartsandstranda; All Cape combinations — Kapp ...

** Publication No. 10 of the Norwegian Antarctic Research Expeditions. (1976/77).

[1] Geofysisk institutt, avd. C., Allegt. 70, N-5014 Bergen, Norway.

[2] Geologisk institutt, avd. A, Allegt. 41, N-5014 Bergen, Norway.

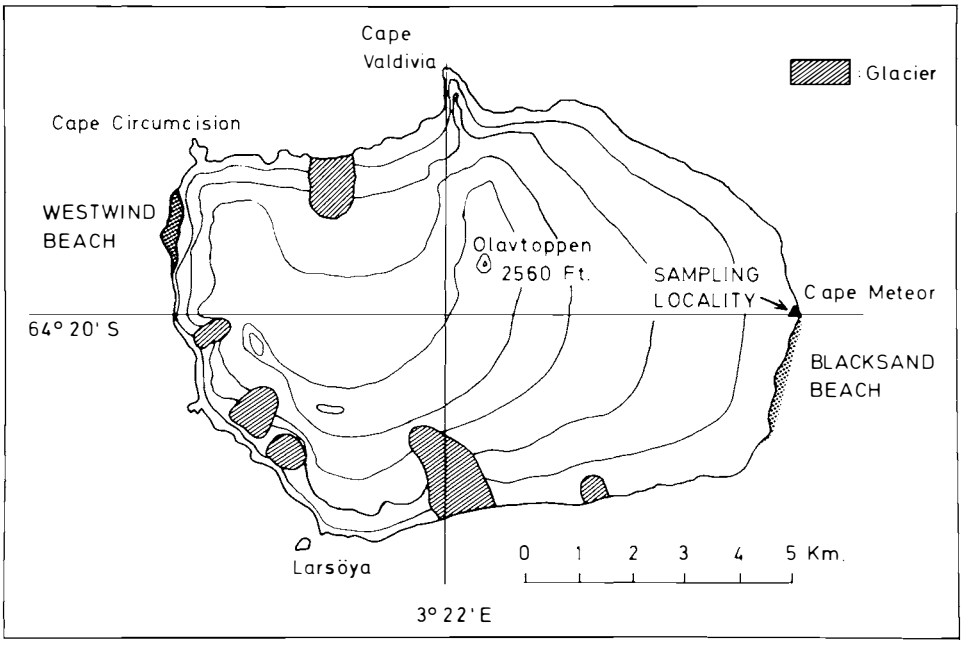

Fig. 1. *Topographic map of Bouvetøya showing the sampling locality at Cape Meteor.*

cular variation of the geomagnetic field for dating purposes. All the samples were taken from a massive flow unit in an uplifted shallow marine hyaloclastite deposit of basic composition. The sampling area covered some 50 m^2 and the cores were obtained employing a portable gasoline powered diamond drill (inner diameter: 19 mm). Azimuthal orientation was made by magnetic compass compensated for the southern hemisphere.

Geological relationships at the Blacksand Beach

The stratigraphically lowest rock is a massive, slightly vesicular basic lava, of which a thickness of 5 m is exposed. Above this lava is a 3 m thick bed of fine to coarse grained volcaniclastic rocks. It consists of vesicular and angular fragments of sideromelane (strongly altered to palagonite and zeolites), and may represent a reworked hyaloclastite. The main rock unit at Cape Meteor is a hyaloclastite/massive lava deposit which again is overlain by a large number of massive to transitional aa basic flow units (Fig. 2). The hyaloclastite/massive lava deposit characteristically has a pronounced foreset structure which is defined by a parallel orientation of elongated lava bodies of various sizes. In some cases these lava bodies can be seen to be in direct continuity with the overlying massive/aa type subaerial flow units (Figs. 2, 3). The 'hyaloclastite' is a poorly sorted breccia consisting of irregular fragments of vesicular basic lava and it reaches a maximum exposed thickness of

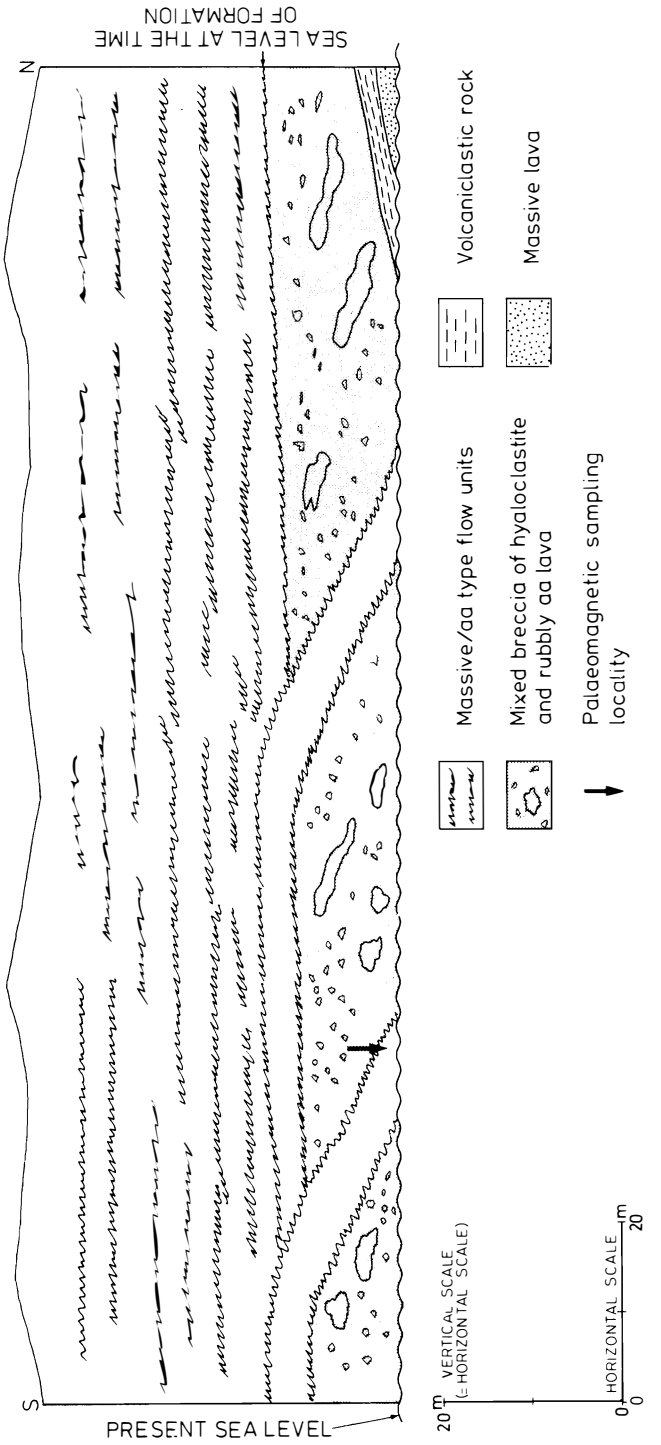

Fig. 2. *Generalized sketch of the rock sequence at Cape Meteor.*

Fig. 3. *Junction between 'hyaloclastite' (lower part of photograph) and overlying massive flow units. Note how the lowest flow unit bends down into the 'hyaloclastite'. (Compare with midpart of Fig. 2, which schematically illustrates the same feature.)*

about 15 m. Pillow bodies with a ragged outline (Fig. 4) exist in a very limited amount. From the structure and physical properties of the lava flow above the volcaniclastic bed (cf. Fig. 2), it seems most plausible that it flowed from land into a shallow sea, the depth of which can be equated with the thickness of the 'hyaloclastite' breccia.

It is well known that the formation of a true hyaloclastite requires a subaquatic environment to give a rapid quenching and brecciation of the lava. In the deposit dealt with here, a great deal of the fragments are not glassy, and indeed they look more like rubbly lava fragments of a subaerial aa lava. However, the presence of a rather high proportion of palagonitized sideromelane fragments, the presence of some poorly developed pillow lava, and the foreset structure of the deposit, all give evidence for deposition in a subaquatic (probably submarine) environment. Such deltas are quite common and have been described from many places by a number of authors (e.g. Fuller 1931; Waters 1960; Jones 1968; Jones and Nelson 1970; Moore et al. 1973; Furnes and Fridleifsson 1974; Furnes and Sturt 1976). The character of the components of such volcanic deltas varies considerably, reflecting the physical properties of the lava when it reached the sea. In some deposits pillow lava is the main component (Furnes and Fridleifsson 1974), whereas in the deposit dealt with here massive irregular lumps of lava is the most common component. This is certainly related to the viscosity of the flow when it enters the sea, i.e. in low viscosity lava, smooth-surfaces pillows and hyaloclastite will

fig. 4. *Pillowy body sitting in a poorly sorted 'hyaloclastite'. On the top part of the photograph is the massive lava that overlies the 'hyaloclastite'.*

dominate, whereas in the case of high-viscosity lava irregular lava lumps with structures characteristic of subaerial lava will be the dominant component.

It is emphasized that the massive/aa type lava is cogenetic with the breccia deposit. This has important implications since the transition from inclined foreset bedded breccia to flatlying massive lava records the sea level at the time the lava flowed into the sea (Fuller 1931; Waters 1960; Jones 1968; Jones and Nelson 1970; Moore et al. 1973; Furnes and Friedleifsson 1974; Furnes and Sturt 1976). This shows that the sequence has been uplifted about 15 m since deposition.

Anisotropy of magnetic susceptibility (AMS)

The reversible magnetic susceptibility (K) is a symmetric, second-order tensor which may be expressed as a susceptibility ellipsoid. The shape of the ellipsoid depends on the preferred orientation of the ferromagnetic minerals reflecting the magnetic fabric (Graham 1954) in a rock. The shape of the susceptibility ellipsoid may be described by chosen ratios of the values of the principal susceptibilities, the orientation by the direction of the maximum (K_1), the intermediate (K_{11}) and the minimum (K_{111}) susceptibility axis. The anisotropy factor $P = K_1/K_{111}$ reflects the degree of preferred orientation of magnetic minerals. The linear-parallel and planar-parallel orienta-

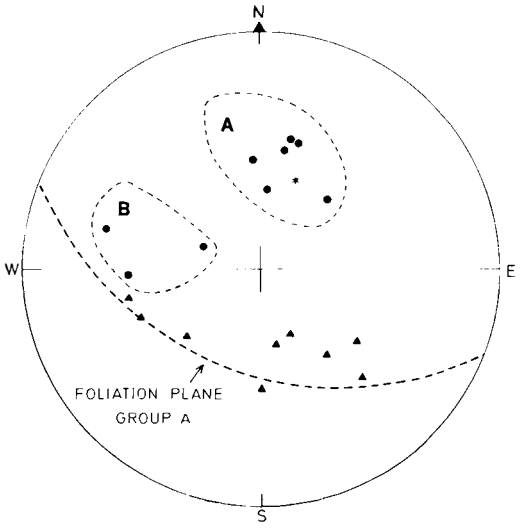

Fig. 5. *Stereographic projection of K_1 (filled triangles) and K_{111} (filled circles) directions of the AMS-ellipsoid. Star represents mean direction of K_{111}-axis of group A from which the stippled foliation plane is constructed.*

tion of ferromagnetic minerals may be expressed by $L = K_1/K_{11}$ and $F = K_{11}/K_{111}$ respectively. If the ratio between F and L ($E = (K_{11})^2/(K_1K_{111})$) is greater than unity an oblate fabric is dominating, as opposed to the situation for $E < 1$ when a prolate fabric is the most developed. The AMS was determined in one cylinder (height: 19 mm) from each drill core and the results are presented in Table 1. The anisotropy factor (P) ranges between 1.4—2.6% and with one exception (B6—A2), the linear-parallel orientation (L) dominates over the foliation parameter F also reflected by E-values less than one.

The directions of the principle minimum and maximum susceptibility axes are plotted in Fig. 5. The distribution of the minimum-axis may be divided into two groups, the most numerous one (group A) define a foliation plane dipping some 40° towards NNE. The axis of maximum susceptibility is also confined to this plane, with an elongated azimuthal distribution covering 90° or arc. While the direction of the K_{111} axis in igneous rocks has been found

Table 1.
AMS-results. (For definition of the parameters (P, L, F, E.), see text.)

Specimen	P	L	F	E
B1—A2	1.0234	1.0050	1.0183	1.0131
B2—A1	1.0141	1.0055	1.0086	1.0031
B3—A3	1.0157	1.0019	1.0137	1.0118
B4—A2	1.0253	1.0004	1.0249	1.0245
B5—A2	1.0224	1.0049	1.0174	1.0125
B6—A2	1.0147	1.0115	1.0031	0.9917
B7—A1	1.0143	1.0061	1.0082	1.0021
B8—A2	1.0263	1.0095	1.0166	1.0071
B9—A2	1.0254	1.0094	1.0159	1.0065

to be normal to the flow plane (Khan 1962) the orientation of the K_1-axis is still a matter of dispute, K_1 is either parallel with or perpendicular to the direction of flow. The geological setting of the sampled lava flow suggests a general direction of flow from S to N, hence the distribution of K_1-axis is interpreted to be aligned in the direction of flow. The fairly steeply dipping foliation plane implies that the sampled area represents a section of a lava which flowed rather steep down towards NNE.

Magnetic properties

The dominating ore minerals in seven polished sections are euhedral grains ($< 50\ \mu$) of titanomagnetite and ilmenite, the latter occurring both as separate grains and as lamellas within cubic titanomagnetite grains. The amount of ilmenite lamellas varies within each section corresponding to titanomagnetite phases in high temperature oxidation classes I—III (Ade-Hall et al. 1971), averaging class II.

Saturation magnetization (J_s) versus temperature (T) curves were determined for each sample, seven of which revealed a single Curie temperature (T_c) between 560° and 590° indicative of almost pure magnetite. Two samples show highly irreversible J_s-T curves with an initial T_c in the 300° to 400° range, transforming to a single T_c around 580°C associated with a 10% and 100% increase in J_s upon cooling from 700°C. These samples probably contain cation deficient spinels (O'Reilly et al. 1971) inverting to almost pure magnetite upon heating.

The intensity of natural remanent magnetization (J_m) and the reversible magnetic susceptibility ($\varkappa$) of cylindrical specimens (19 mm x 19 mm) cut from each drill core was determined by a slow speed spinner magnetometer (Molyneux 1971) and a commercial AC-bridge respectively. NRM intensities ranged between $3.5—10.10^{-3}\ \mu$G and the Q'_n-factor ($= J_m/\varkappa$) varied between 2 and 8. All nine specimens were stepwise demagnetized in progressively increasing AF-fields up to 1200 Oe. Median destructive fields that range from 225 to 430 Oe are associated with stable magnetization over the entire range of demagnetization. The directions are tightly grouped with a normal polarity and the mean direction (corrected for an estimated declination of $\div 22°$, IGRF 1965.0 (IAGA Bulletin No. 29)), precision parameter (k) and radii of the 95 per cent cone of significance (α_{95}) are as follows:

D_{mean}	I_{mean}	k	α_{95}
327.6°	-78.6°	299	3.9°

The small scatter ($\alpha_{95} = 3.9°$), high precision and absence of directional trends upon demagnetization suggest that the mean direction represents a spot-reading of the geomagnetic field acquired during the emplacement of the lava flow. The position of the corresponding virtual geomagnetic south pole is situated at (δ_p, δ_m being errors in latitude, longitude of the determined pole):

68.9°S 219.9°E δ_p : 6.9°, δ_m : 7.4°

This pole position, however, is statistically different from the present position of the geomagnetic south pole deduced from the 1965.0 IGRF-values of D and I:

70.5°S 123.5°E

The discrepancy, which is mainly one of longitude, is likely to reflect either secular variation or dipole wobble of the axial geomagnetic field.

Conclusions

The normal polarity of the stable remanent magnetization of the investigated lava flow in conjunction with the assumed Pleistocene age of Bouvetøya (Tuzo Wilson 1963) suggest a maximum age of around 700,000 years (Brunhes normal epoch) for the island. The lack of directional trends upon progressive AF-demagnetization along with the small directional scatter may suggest that the paleomagnetic record represents a spot-reading of the geomagnetic field at the time the lava cooled. Assuming a westward drift of the geomagnetic field of the order 0.06°/years (Rikitake 1966), the clockwise, longitudinal difference of around 100° between the present geomagnetic south pole (70°S, 124°E) and the virtual palaeomagnetic pole (69°S, 220°E) tentatively infers a minimum age of around $2 \cdot 10^3$ years for the lava.

Since the geological relationships indicate that the sequence has been uplifted about 15 m since its formation, the inferred minimum age indicate a maximum rate of uplift of ca. 0.75 cm/year.

The rock magnetic fabric in the lava, represented by AMS-ellipsoids, suggest that the maximum susceptibility-axis is aligned parallel with the direction of flow.

Acknowledgement

We are grateful to Dr. W. Lowrie for computer processing of the AMS-data, and to Dr. K. M. Storetvedt for critical evaluation of the manuscript.

References

ADE-HALL, J. M., H. C. PALMER, and T. H. HUBBARD, 1971: The Magnetic and Opaque Petrological Response of Basalts to Regional Hydrothermal Alteration. *Geophys. J.R. astr. Soc.* 24: 137—174.

FULLER, R. E., 1931: The aqueous chilling of basaltic lava on the Columbia River Plateau. *Am. J. Sci.* 21: 281—300.

FURNES, H., and I. B. FRIDLEIFSSON, 1974: Tidal effects on the formation of pillow lava/hyaloclastite deltas. *Geology* 2: 381—384.

FURNES, H., and B. A. STURT, 1976: Beach/shallow marine hyaloclastite deposits and their geological significance — an example from Gran Canaria. *J. Geol.* 84: 439—453.

GRAHAM, J. W., 1954: Magnetic susceptibility anisotropy, an unexploited petrofabric element (Abstr.) *Bull. Geol. Soc. Am.* 65: 1257—1258.

JONES, J. G., 1968: Intraglacial volcanoes of the Laugarvatn retion, south-west Iceland — *I. Quart. J. Geol. Soc. Lond.* 124: 197—211.

JONES, J. G., and P. H. H. NELSON, 1970: The flow of basalt from air into water — its structural expression and stratigraphic significance. *Geol. Mag.* 107: 13—21.

KHAN, M. A., 1962: The anisotropy of magnetic susceptibility of some igneous and metamorphic rocks. *J. Geophys. Res.* 67: 2873.

LEATON, B. R., and D. R. BARRACLOUGH, 1971: Grid Values of the IGRF 1965. *IAGA Bulletin* No. 29.

MOLYNEUX, L., 1971: A complete result magnetometer for measuring the remanent magnetization of rocks. *Geophys. J.R. astr. Soc.* 24: 429—433.

MOORE, J. G., R. L. PHILLIPS, R. W. GRIGG, D. W. PETERSON and D. A. SWANSON, 1973: Flow of lava into the sea, 1969—1971, Kilanea Volcano, Hawaii. *Bull. Geol. Soc. Am.* 84: 537—546.

O'REILLEY, W., and P. W. READMAN, 1971: The preparation and unmixing of cation deficient titanomagnetites. *Zeitschrift für Geofysik* 37: 321—327.

RIKITAKE, T., 1966: Electromagnetism and the Earth's Interior. *Developments in Solid Earth Geophysics* 2.

SNAPE, C., and J. A. RETIEF, 1971: Palaeomagnetic study of some recent lavas. Marion and Prince Edward Islands. *Report of the South African Biological and Geological Expedition, 1965—1966, Cape Town, Balkema,* 1971: 63—71.

TUZO WILSON, J., 1963: Evidence from islands on the spreading of ocean floors. *Nature* 197: 536—538.

WATERS, A. C., 1960: Determining direction of flow in basalts. *Am. J. Sci.* 258, ser. A: 350—366.

An eruptional model for recent lava flow on Bouvetøya, South Atlantic Ocean*

BY HARALD FURNES[1] AND REIDAR LØVLIE[2]

Abstract

A recent trachytic flow at Bouvetøya, South Atlantic Ocean, shows time-related differences in its structural development. During the first phase of eruption, a domal body, encrusted by obsidian, formed. During the final stage of eruption, block lava resulted when slow-moving, viscous lava issued from cracks in the central, partly broken-up, domal body. This different structural development is believed to be related to a change in the environmental conditions during the eruption, and it is suggested that the eruption started subglacially and terminated subaerially.

Introduction

During the Norwegian Antarctic Research Expedition 1976/77, good weather permitted landing on Bouvetøya (54° 26' S, 3° 24' E) and a visit to the Westwind beach[3], a low platform on the northwestern coast.

Except for some rocky cliffs and beaches, Bouvetøya is an ice-covered volcanically active island, situated on the Mid-Atlantic Ridge, close to the triple junction between the Antarctic, African and South American Plates (Johnson et al. 1973) in the South Atlantic Ocean. It covers an area of approximately 50 km². The physiography and structure of the island have been described by Holtedahl (1929), and some aspects of the geology are outlined by Baker (1967) and Baker and Tomblin (1964). The age of the island is probably less than 1 m.y. (Snape 1971; Verwoerd et al. 1976). Geochemically the lavas range from basic through intermediate to peralkaline silicic rocks of a transitional series (Imsland et al. 1977).

* Publication No. 3 of the Norwegian Antarctic Research Expeditions. (1976/77).

[1] Geologisk institutt, avd. A, Allégaten 41, N-5014 Bergen, Norway.

[2] Geofysisk institutt, avd. C, University of Bergen, N-5014 Bergen, Norway.

[3] No official place-name guide has been made for Bouvetøya. Geographical names are thus somewhat inconsistently used. Names used in this article will probably have the following future forms: Westwind Beach — Nyrøysa, Westwind-stranda; Blacksand Beach — Svartsandstranda; All Cape combinations — Kapp . . .

Between February 1, 1955, and January 1, 1958, a small eruption of trachytic lava supposedly occurred at the Westwind beach (Baker and Tomblin 1964). Later, Baker (1974) found that the name *benmorite* is more appropriate for the lava. Prior to the present landing, this locality had been visited many times, and different opinions have been expressed as to the origin of this particular volcanic rock. Baker and Tomblin (1964) described the flow as a partly flowbanded block lava, in places forming well-developed tumuli, typical features of a subaerial lava flow. Fumarolic activity was also observed at the southern end of the Westwind beach, by Baker and Tomblin (1964), and during our visit a previously unreported fossil fumarole was observed. Lunde (1965) interpreted the structure of the flow as representing giant broken pillows, and thus to be the result of a submarine eruption. None of these authors, however, could find any indication of a crater. The interpretation of the Westwind beach as being volcanic in origin was later challenged by Winsnes (1966), considering the deposit to represent a recent scree, and Verwoerd (1972) and Verwoerd et al. (1976) considering it to have resulted from an avalanche.

In this account we propose another model for the development of the volcanic rocks of the Westwind beach, which we believe to be of both subglacial and subaerial volcanic origin.

General features of the Westwind beach

The physiography of the Westwind beach has been thoroughly described by Baker and Tomblin (1964) and Baker (1967), and only the features that are important for the later interpretation are summarized below.

In general the low platform of the Westwind beach consists of three components. These are:

1. A sandy beach containing abundant well rounded cobbles and boulders of lava and pyroclastics. This beach, rising about 2 m above sea level, occupies the northern and southern parts of the platform (the Westwind beach).
2. Situated upon this sandy and bouldery beach is a poorly sorted deposit, containing big angular blocks of different volcanic material. The maximum thickness of this deposit, is about 15 m, but it diminishes rapidly to the north and south.
3. Resting on the above described deposits is the lava flow, as will be described below.

Structures of the flow

Two main features of the lava can be recognized. They are:

(1): Remnants of an approximately circular dome-like body with a minimum diameter of 30 m. This body is composed of an obsidian rim, about 0.5—1 m thick, followed inward by a zone of highly vesicular, flowbanded

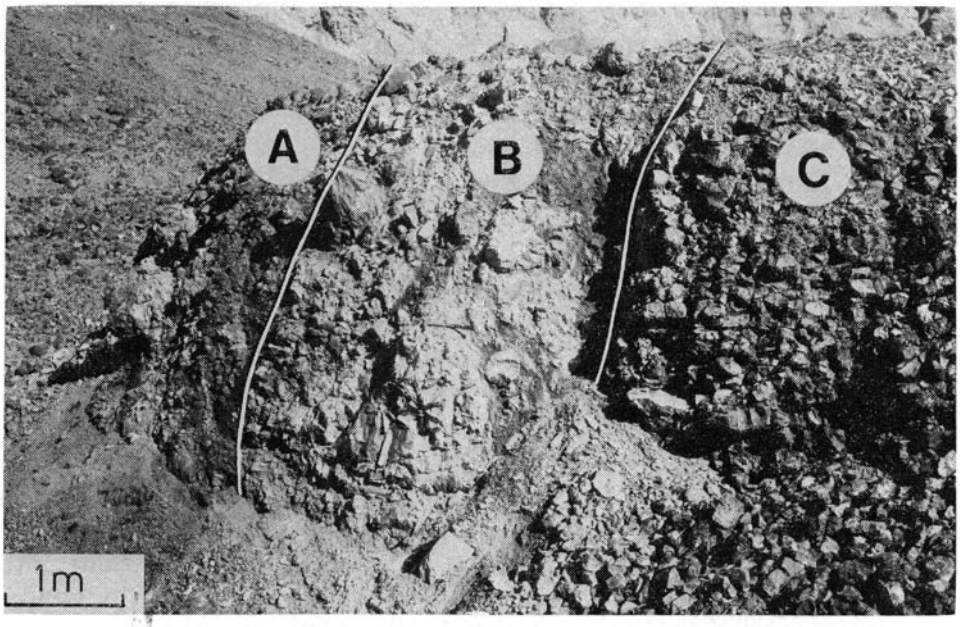

Fig. 1. *Part of the lava dome showing black obsidian (A), flowfolded and flowbanded, highly vesicular lava (B), and columnar jointed, massive trachyte (C). Scale is shown by hammer in the central part of the photo.*

and flowfolded lava (approximately 1—2 m thick), and a central part of predominantly crystalline, columnar jointed lava (Fig. 1). The domal structure of the flow was also mentioned by Baker (1967), writing that it «originated during a minor volcanic eruption involving the emplacement of a trachyte dome». The outer part of this body has an irregular network of vertical to subhorizontal cracks with widths up to 1 m.

(2): The circular body is surrounded by hummocky block lava with a reddened slaggy top. In places there are solidified contracts between the block lava and the dome-like body, demonstrating that they are cogenetic.

Blocks of older lava and pyroclastics are in places associated with the new lava.

Discussion

Observations made during our visit, confirm the volcanic origin of the Westwind beach. Employing a fluxgate magnetometer, the magnetic polarity of twelve samples of block lava at different sites showed the same magnetic polarity, strongly suggesting that the block lava has remained in situ since the eruption. Thus the two depositional origins suggested by Winsnes (1966), and Verwoerd et al. (1976), are rejected. Neither do we agree with the interpretation forwarded by Lunde (1965) since no proper pillows or fragments of pillows were observed; a lava of such a composition would probably

not have the physical properties necessary for forming pillow lava in the strict sence of the term. Furthermore, the lava is resting on, and to the west piled against, a poorly sorted deposit containing big angular blocks of older volcanic rocks in a structureless matrix of sand and mud (Fig. 2). If the eruption started under the sea, it implies that the chaotic sediment which the lava rests on, is a shoreline deposit. In no way does the deposit resemble a deposit of such an origin, and it is considered most likely that it represents either a subaerial debris flow, or a terminal moraine. The description given by Baker and Tomblin (1964) is partly in accordance with our observations.

The structural relationships and physical properties of the lava as described, and its association with probable moraine and other foreign material, suggests that the eruption started under a cover of ice. During the initial stage of the eruption, the encrusting skin of obsidian formed by the quenching of the lava in melt water (Fig. 2A). The obsidian layer would, for a certain length of time, prevent gases from escaping from the magma, which, adjacent to the obsidian cover would become flowbanded and flowfoliated. During growth of such an obsidian/magma blob, the obsidian layer would intermittently crack, allowing new lava to be exposed to the ice and water (Fig. 2B). Thus the process of build-up and sudden release of gas pressure would be periodically repeated as long as there was water available to quench the lava, and the extrusion rate and/or gas pressure was sufficiently high to break the obsidian skin (Furnes et al. in prep.).

The existence of a former ice-cap covering the Westwind beach has been argued against (Winsnes 1966). However, older maps (e.g. Aagaard 1944) show the existence of a former glacier (named Horntvedts bre) in the vicinity of the Westwind beach. Although the precise location varies on different maps, the most likely place is above the Westwind beach, as proposed by Verwoerd et al. (1976). According to old maps from the Norwegia Expedition 1927—28, the movement of Horntvedts bre was towards the north, and it may thus be unlikely that it covered the Westwind beach. However, Verwoerd et al. (1976) assumed that ice avalanches charged with lava fragments originating at the edge of Horntvedts bre, account for the origin of the deposit. In fact, such a mechanism of providing an ice cover over the Westwind beach might have been more likely than the former presence of a glacier. However, whether the Westwind beach was covered by a glacier or an accumulation of fallen-down ice blocks, does not make any difference to the proposed eruptional model which only requires the initial presence of an aqueous environment above sea level. This would most likely be provided by the melting of an ice cover.

The ice must have covered an area of approximately 300 x 200 m. If it had a thickness of about 15—20 m, a conservative estimate of the heat released from the trachyte (or benmorite) magma during cooling, sufficient to melt the ice, would require a magma body of about 10^4 m^3. Simultaneously, foreign material carried by the ice was dropped and became intermixed with the new lava.

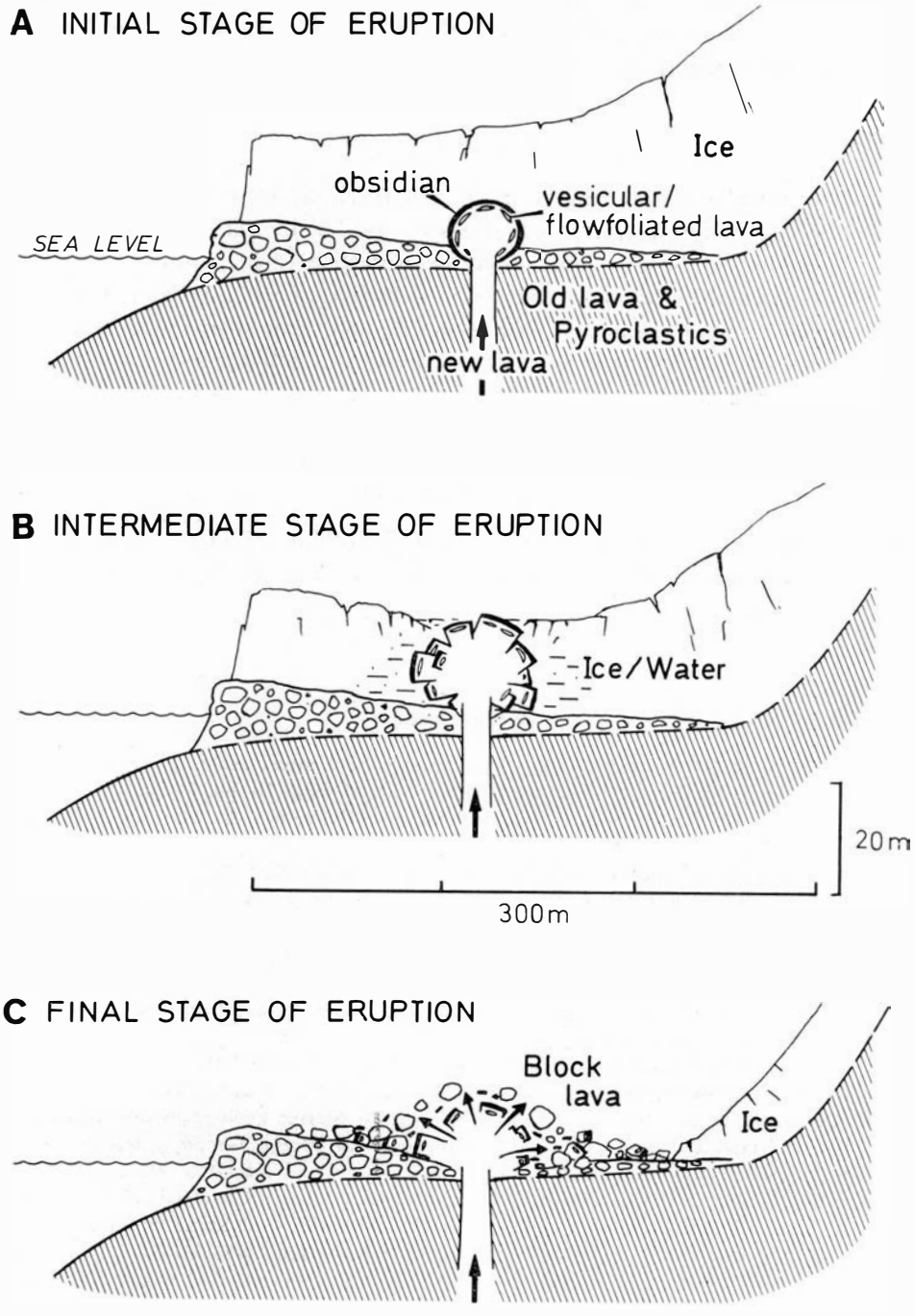

Fig. 2. *Cartoon depicting successive stages of the structural development of the lava during the trachyte eruption on the Westwind beach. The deposit on which the new lava rests is either a subaerial debris flow or a terminal moraine (see text).*

The eruption could then proceed in a subaerial environment, and the viscous lava that issued from the open cracks of the blob-like body, would travel slowly as a block lava flow (Fig. 2C).

Conclusions

The structural relationships of the recent trachytic flow on Bouvetøya indicate that the eruption started subglacially and terminated subaerially. During the subglacial phase a domal body, consisting of lithic, columnar jointed trachyte encrusted by obsidian, was formed during a quiet injection of magma into a glacier tongue. Heat released from this body was sufficient to melt the ice. At this stage the domal build-up stopped, and subsequently the lava issued from cracks in the dome to form a typical subaerial block lava.

Acknowledgements

We thank I. B. Fridleifsson, P. E. Baker, B. Robins, A. Hjelle, and O. Orheim for reading an early draft of the manuscript, and M. Adachi for making the illustrations.

References

AAGAARD, B., 1944: Antarktis 1502—1944. Oppdagelser, naturforhold og suverenitetsforhold. *Norges Svalbard- og Ishavsundersøkelser Meddelelser* Nr. 60. 308 pp.

BAKER, P. E., 1967: Historical and geological notes on Bouvetøya. *Br. Antarct. Surv. Bull.* 13: 71—84.

— 1974: Peralkaline and volcanic rocks of oceanic islands. *Bull. Volcanol.* 38: 737—754.

BAKER, P. E., and J. F. TOMBLIN 1964: A recent volcanic eruption on Bouvetøya, South Atlantic Ocean. *Nature* 203: 1056—1057.

FURNES, H., I. B. FRIDLEIFSSON, and F. B. ATKINS, (in prep): Subglacial volcanics. On the formation of acid hyaloclastites.

HOLTEDAHL, O., 1929: On the geology and physiography of some Antarctic and sub-Antarctic islands. *Scient. Results Norw. Antarct. Exped.* No. 3.

IMSLAND, P., J. G. LARSEN, T. PRESTVIK, and E. M. SIGMOND, 1977: The geology and petrology of Bouvetøya, South Atlantic Ocean. *Lithos* 10: 213—234.

JOHNSON, G. L., R. N. HEY, and A. LOWRIE, 1973: Marine geology in the environs of Bouvet Island and the south Atlantic triple junction. *Marine Geophys. Res.* 2: 23—36.

LUNDE, T., 1965: Fra et besøk på Bouvetøya. *Norsk Polarinst. Årbok* 1963: 197—203.

SNAPE, C., 1971: Palaeomagnetism of three samples of lava from Bouvet Island: In: *Marion and Prince Edward Islands* (Eds. E. M. VAN ZINDEREN BAKKER Sr., J. M. WINTERBOTTOM and R. A. DYER), Cape Town, A.A. Balkema: 69—71.

VERWOERD, W. J., 1972: Islands on the mid-ocean ridge between Africa and Antarctica. (Abst.). *EOS Trans. Am. Geophys. Union* 53: 168—170.

VERWOERD, W. J., A. J. ERLAND, and E. J. D. KABLE, 1976: Geology and geochemistry of Bouvet Island. In: *Proc. of the Symp. on «Andean and Antarctic Volcanology Problems» (Santiago, Chile, Sept. 1974)* (Ed. O. GONZALES FERRAN): 203—237.

WINSNES, T. S., 1966: Besøk på Bouvetøya i 1958 og 1966. *Norsk Polarinst. Årbok* 1965: 143—149.

Weather and tide observations at Bouvetøya*

BY TORGNY E. VINJE

Introduction

Weather observations from the Bouvetøya area are sparse and have mostly been limited to the summer and autumn periods of the years when large scale whaling still went on. The island, 6 by 9 km in extension, is situated at 54.4°S and 3.3°E, supposedly near the general track of the low pressure systems passing round Antarctica.

An automatic station using the Nimbus-6 Random Access Measurement System (RAMS) was left at the island on 23 February 1977 during a short visit by members of the Norwegian Antarctic Research Expedition 1976—77. The station was placed on the western side of the island on a 30—40 m high platform (Fig. 1) formed between 1956 and 1958 by a combination of volcanic activity and rock sliding (Baker et al. 1964). This area, called Nyrøysa, is the proposed site for the operation of a manned radiosonde station during January and February 1979. Thus the automatic station served both the purpose of obtaining an observation series from this desolate ocean area, and to collect local data for the planning of the manned station.

We also plan to establish long term sea level measurements at Bouvetøya in 1979, using an automatic ARGOS station. To obtain information on the tidal amplitude, a tide gauge was anchored for 25 hours at the lee side of the island during the visit in 1977.

Instruments

By kind permission of the US National Aeronautic and Space Administration (NASA) we have used the Nimbus-6 data collecting system for ice drift experiments in the Arctic (Vinje and Steinbakke 1976). To take advantage of the experience gained from these experiments the same type of capsule was

* Publication No. 11 of the Norwegian Antarctic Research Expeditions. (1976/77).

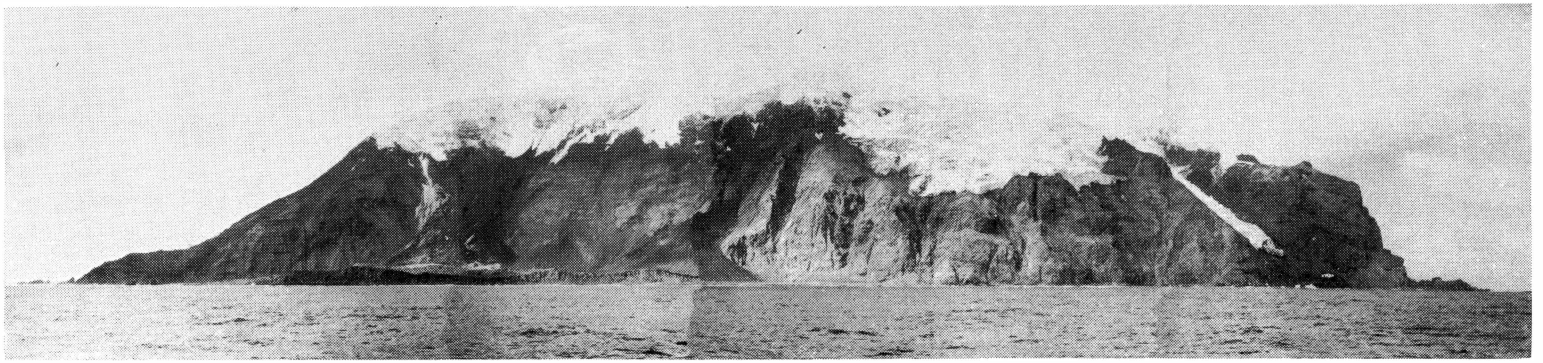

Fig. 1. *Bouvetøya seen from the west. To the left, Nyrøysa, the level area where the automatic station is placed.*

Table I
Monthly means of pressure (mb) and temperature (°C) 28 m above sea level at Bouvetøya

	1977										1978					
Month	MAR	APR	MAY	JUN	JUL	AUG	SEP	OCT	NOV	DEC	JAN	FEB	MAR	APR	MAY	JUN
Pressure	989.9	993.9	995.0	993.4	987.3	993.3	988.0	988.3	987.9	982.9	988.6	990.2	987.8	997.1	990.3	1000.1
standard dev.		15.9	12.6	13.8	14.2	12.9	14.8	10.5	12.9	8.9	10.1	14.0	12.3	11.5	12.5	9.9
Temperature	2.8	1.2	0.2	—1.3	—2.4	—2.5	—2.0	—1.8	0.1	1.1	2.1	2.2	1.6	1.6	—1.1	—1.7
standard dev.		1.3	1.4	1.4	1.6	1.7	2.1	2.3	1.4	1.9	1.7	2.4	1.5	2.0	1.8	1.8
Number of obs.	114	147	136	161	137	112	125	153	166	171	181	170	177	185	173	88

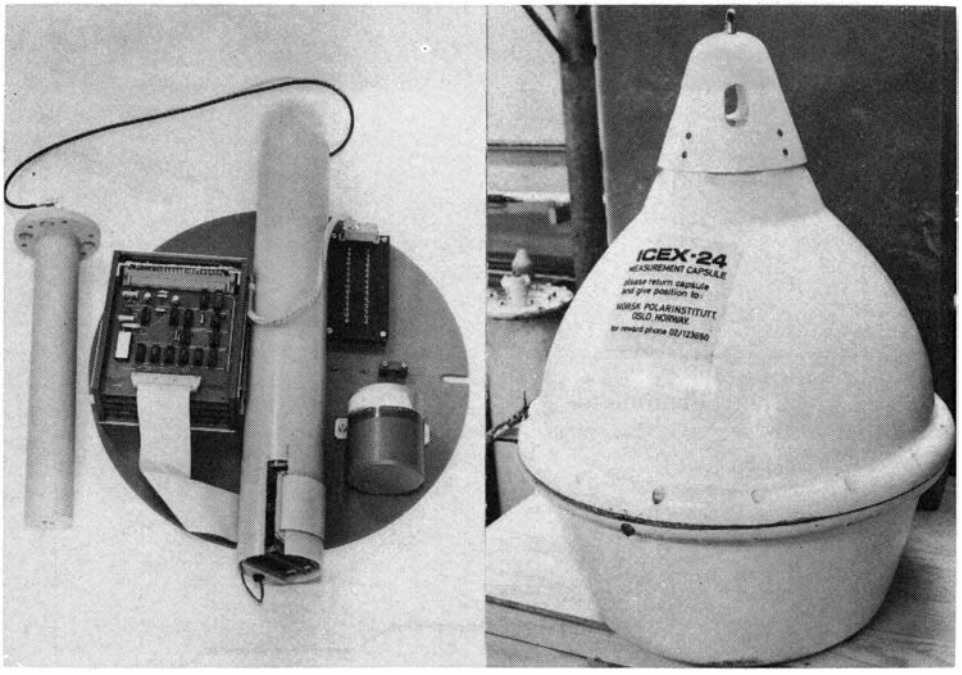

Fig. 2. *The automatic station placed at Bouvetøya. The station has been manufactured by Chr. Michelsens Institute.*

used at Bouvetøya (Fig. 2). This transmitted air pressure, air temperature, the one minute average wind speed, and «housekeeping» data.

The air pressure was measured with an aneroid barometer and a linear displacement transducer with a range of 900 to 1028 mb with temperature compensation. The sensor resolution is better than 0.1 mb, while the system resolution is 0.4 mb.

The air temperature was measured with a radiation shielded termistor, range — 20° to + 20°C with a system resolution of 0.2°C. The bottom and internal temperatures were measured with a similar device. The wind speed, which had a resolution of 0.2 m sec^{-1}, was measured with a cup anemometer designed by the constructor of the automatic station, Chr. Michelsens Institute, Bergen. The American Electronic Laboratory delivered the buoy terminal transmitter.

The battery voltage range is 11.9 to 18.5 V and lithium batteries, Enernacell Model 660-5, have been used.

Tests of the sensors were made during January and February 1977 when the automatic station was activated on the Riiser-Larsenisen in Antarctica. Of particular interest was the accuracy of the air pressure observations. A series of readings on a precision aneroid barometer were made and compared with the values obtained via Nimbus-6. Fig. 3 shows that there is a good agreement between the two series. Some of the differences may be

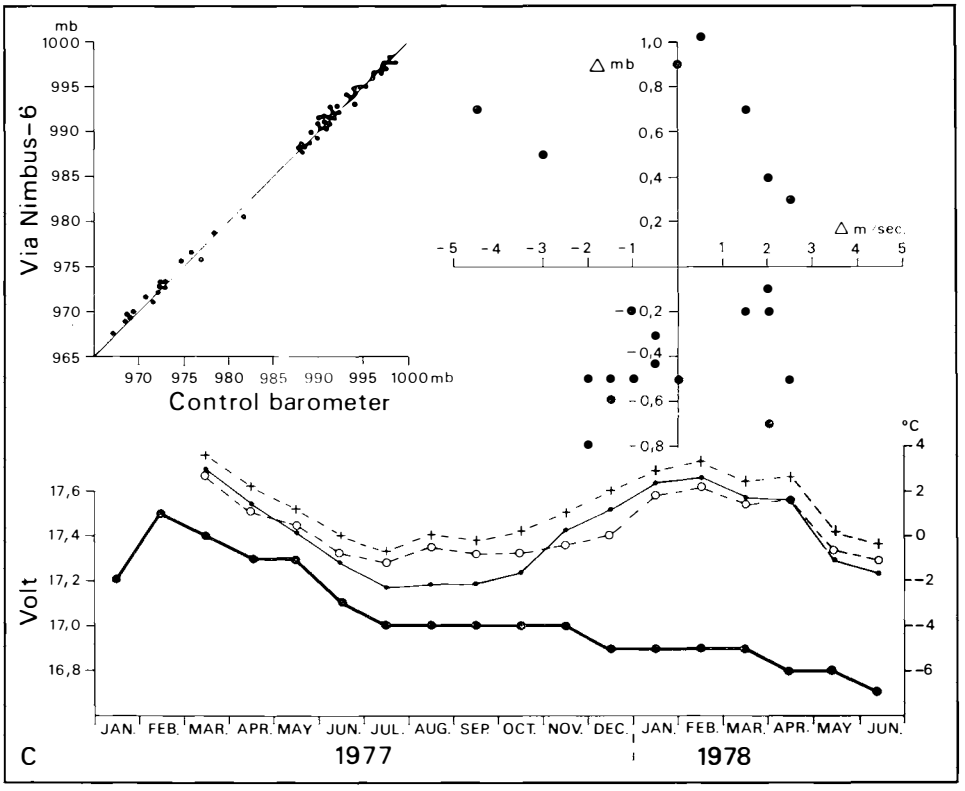

Fig. 3. *Top left: Comparison between a control barometer read in situ and pressure observations via Nimbus-6. Top right: Comparison between change in wind speed and effect on the pressure reading. Lower graph: Variation of the battery voltage and the variation of the monthly mean of air temperature (●), earth surface temperature (○), and temperature at the barometer in the measuring capsule (+).*

caused by up to half an hour time differences between the reading obtained via Nimbus and the visual one. The difference between the means of the two series is less than 0.1 mb. We also checked whether variations in the wind speed influenced the pressure reading. Assuming the air pressure constant during the 15 minutes passage-time of the satellite we have compared the change in pressure reading (△mb) from the 15 min average in the course of one minute with the corresponding change in the average wind speed (△m/sec). Fig. 3 shows that there can be considerable variation in the pressure reading from minute to minute during gusty conditions. There seems, however, not to be any systematic effect of the wind speed on the pressure readings.

The automatic station was equipped with batteries for about 82 weeks. Since the activation of the station in January 1977 the variation in the voltage has been as expected (Fig. 3). The station still sends its messages at the end of August 1978.

Meteorological observations

Nyrøysa, the site of the automatic station, is on its eastern side bordered by 700—800 m high, very steep mountain sides. Its western boundary is in the form of 20—30 m high coastal cliffs. The station was located 28 m above the sea level, and because of the topography only the air pressure and temperature observations are presumed representative for the island as a whole.

The annual course of the air pressure and the air temperature is shown in Fig. 4 and Table 1. The air pressure has a relatively small annual variation,

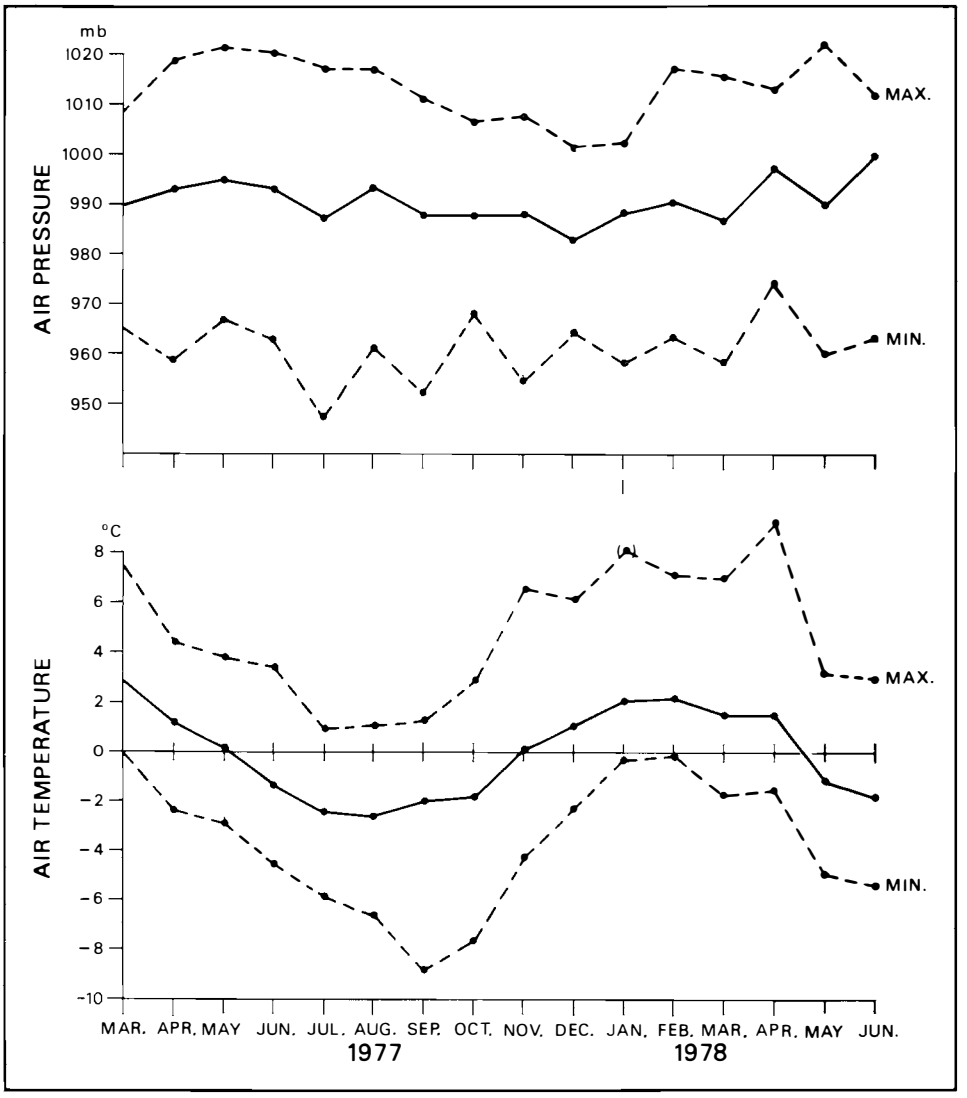

Fig. 4. *Monthly mean, maximum, and minimum of air pressure and temperature at Bouvetøya at 28 m above sea level. The maximum temperature observed in January 1978 (●) is probably too high because of radiation error in calm weather. The absolute maximum, 9.3°C, observed in April 1978 was recorded under conditions with gale force winds.*

which is similar to that observed at Orcadas (60° 44' S — 44° 44' W) (Orvig 1970). At Bouvetøya there is an indication of a flat maximum in the period March — August and a flat minimum in the period September — February. From the long series at Orcadas a maximum is found around June — August and at South Georgia a maximum is found in September (Pepper 1954). There is no indication of a double wave in the annual pressure variation as has been observed to be very pronounced in the Graham Land area (Meinardus 1938) at Maudheim (Hisdal 1956) and at Norway Station/ SANAE (Taljaard et al. 1977). The last mentioned series represents a period of 15 years (1960—1975). However, studying only a two-year period (1958—1959) at the same station (Vinje 1965), such an annual variation could not be seen. A longer series from Bouvetøya is therefore necessary to obtain reliable information in this respect.

The monthly mean pressure at Bouvetøya reduced to sea surface and the pressure read from numerical hemispherical analyses (Schulze 1978) have been compared in Table II.

Table II

Monthly mean surface pressure (mb) as observed at Bouvetøya (B) and as read from numerical analyses (NA) during 1977

	Mar	Apr	May	Jun	Jul	Aug	Sep	Oct	Nov	Dec
N A	998	999	1002	998	995	1002	1000	1000	996	996
B	993	996	998	996	990	996	991	991	991	986
Diff.	5	3	4	2	5	6	9	9	5	10

The comparison shows that the numerical analyses systematically overestimate the pressure by 2 to 10 mb.

The square root of the mean of the monthly variance is 16.1 mb (Table 1). This is considerably higher than that observed at Maudheim (9.8) but more in accordance with figures found for example for Londonderry (55.0°N — 7.3°N) (Hisdal 1956). This seems reasonable because of the relative positions of the station with respect to the west wind belts.

The absolute minimum and maximum pressures were 947.4 and 1021.1 mb. When reducing the Bouvetøya average for July and January to the sea level we obtain 991.4 and 990.1 mb, respectively. This is close to the estimated averages, 994 and 993 mb, given on the maps drawn by Taljaard et al. (1969).

The small annual variation (Fig. 4) of the monthly air temperature is typical for a maritime station. The drift ice was relatively far away from the island during 1977, and there is indication of a «temperature barrier» around ÷2°C, in analogy to that Hisdal (1960) found for 0°C over the ice shelf during summer time. The January and July monthly averages, 2.1 and ÷2.4°C, are fairly close to the monthly averages given by Taljaard et al. (1969), 2.0 and ÷3.0°C.

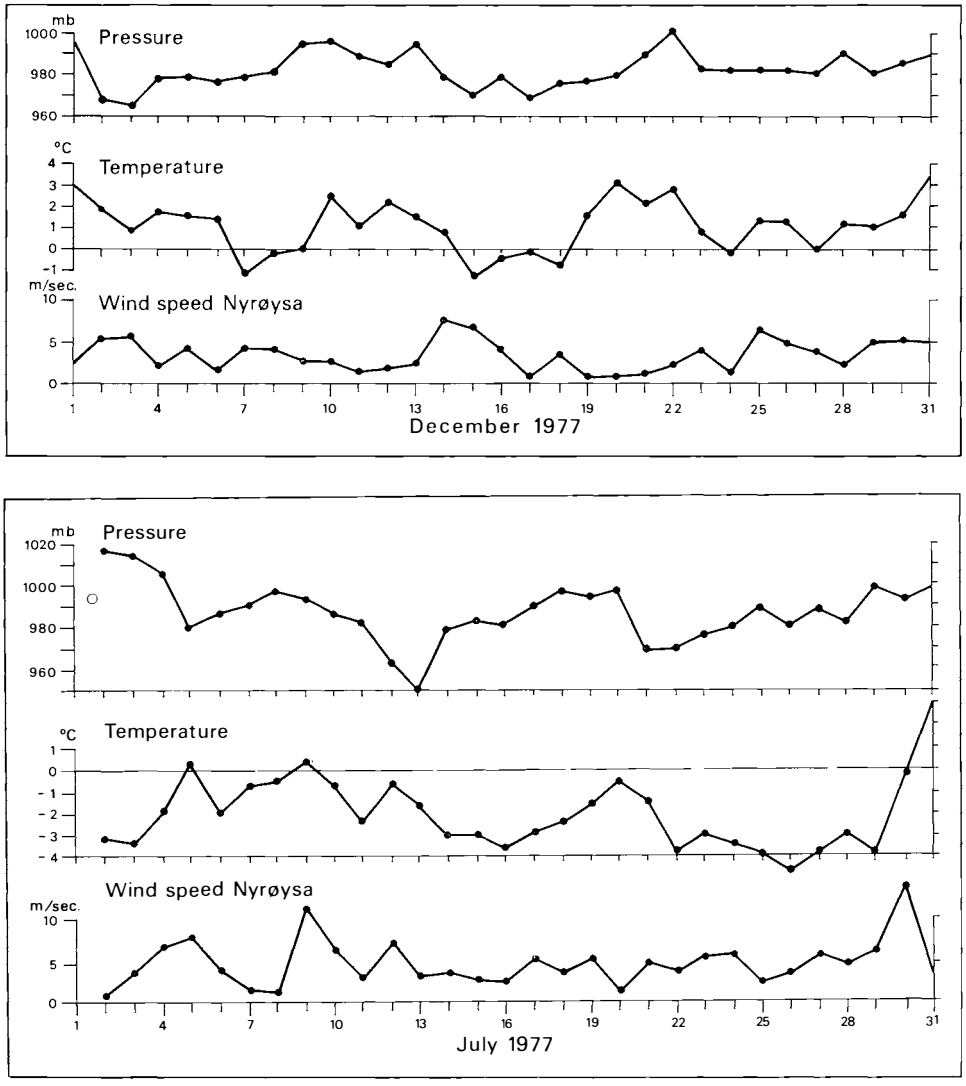

Fig. 5. *Daily means of pressure, temperature, and wind speed at Nyrøysa, Bouvetøya, for July and December 1977.*

The wind conditions at Nyrøysa are illustrated in Fig. 5. It is presumed that the strongest wind is observed in the front or back of a low, because for the corresponding wind directions, NW and SW, the wind can sweep over the level area, parallel with the steep mountain side. The small value of the average wind speed (Fig. 6) indicates that Nyrøysa is very well screened against winds from other directions. The one minute average wind speed at Nyrøysa reached 20 kts during only 3.3% of the time in January and February 1978, and only during 7.6% of the period July and August 1977.

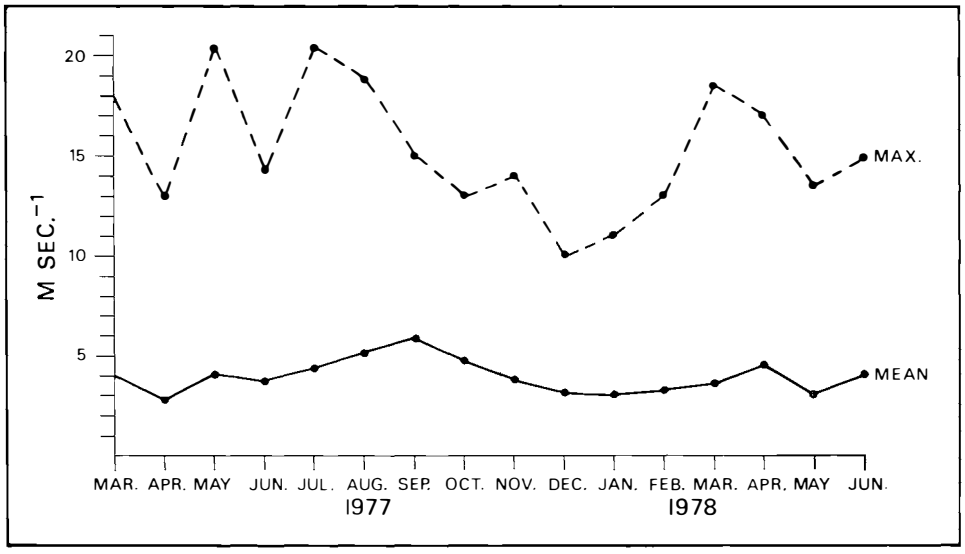

Fig. 6. *Observed wind speed at Nyrøysa.*

The temperature observations in Fig. 3 show that the ground temperature is higher than the air temperature from mid May to mid November 1977. This suggests that there has been a snow cover on Nyrøysa during this period.

Tide measurements

A film recording tide gauge, General Oceanics model 3040, was anchored at a depth of about 10 m on the eastern side of the island. Fifteen pictures per hour were taken of a precision Bourdon tube gauge with super 8 mm film. The hourly averages have been plotted in Fig. 7. There are two daily maxima, and a harmonic analysis gives an amplitude of the semidiurnal wave of 0.14 m. There is also an indication of swells with a frequency of 5.4 per hour and an amplitude of 0.07 m.

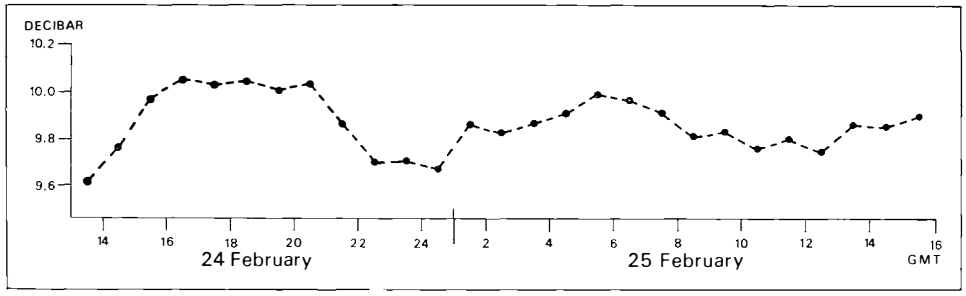

Fig. 7. *The hourly averages of the sea level at Bouvetøya given in decibar as observed during 24 and 25 February 1977.*

Acknowledgements

We are much obliged to NASA for making it possible to perform the meteorological studies. The continuous flow of data has been impressive. We are also grateful to the Norwegian Meteorological Institute for its cooperation during planning and data processing. Thanks are extended to Mr J. Snuggerud for his cooperation during the field work and to Mr. Ø. Finnekåsa who did the processing of the data. Mr. A. Foldvik analysed the tide observations. The automatic Nimbus-6 station was funded by the Norwegian Committee for GARP.

References

BAKER, P. E. and J. F. TOMBLIN, 1964: A recent volcanic eruption on Bouvetøya, South Atlantic Ocean. *Nature* 203 (4949).

HISDAL, V., O. AMBLE, and N. J. SCHUMACHER, 1956: Surface observations. Air pressure. *Norw. — Br. — Sw. Ant. Exp. 1949—52. Sc. Res.* 1. Oslo.

HISDAL, V., 1960: Surface observations. Temperature. *Norw. — Br. — Sw. Ant. Exp. 1949-52. Sc. Res.* 1. Oslo.

MAINARDUS, W., 1938: Klimakunde der Antarktis. *Handbuch der Klimatologie* (W. KÖPPEN and R. GEIGER) 4(V). Gebr. Bomtraeger, Berlin.

ORVIG, S. (editor), 1970: *Climates of the Polar Regions.* Elsevier Publishing Company, Amsterdam.

PEPPER, J., 1954: *The Meteorology of The Falkland Islands and Dependencies 1944—1950.* Hodgson and Son, London.

SCHULZE, G. C., 1978: Discussion of Numerical Hemispherical Analysis. *News Letter* Nr. 336—345. Weather Bureau, Pretoria.

TALJAARD, J. J., H. VAN LOON, H. L. CRUTCHER, and R. L. JEUNE, 1969: *Climate of the Upper Air; Part 1. Southern Hemisphere, 1. Sea Level Pressure and Selected Heights, Temperatures and Dewpoints.* U.S. Gov. Printing Office, Washington D.C. NAVAIR 50-16-55.

TALJAARD, J. L., and T. I. POTGIETER, 1977: Surface temperature and sea-level pressure at Norway Station and SANAE. *S.Afr. Jr. of Ant. Res.* 6 Pretoria.

VINJE, T. E., 1965: Climatological tables for Norway Station. Den norsk Ant. eksp. 1956—60. Sc.res. No. 8, *Norsk Polarinstitutt Årbok* 1963: 181—183. Oslo.

VINJE, T. E., and P. STEINBAKKE, 1976: Nimbus-6 located automatic stations in the Svalbard waters in 1975. *Norsk Polarinstitutt Årbok* 1975: 109—117. Oslo.

Harald Lyche & Co. A.s